ANL-7501

ANL-7501
ANL-7501
ANL-7501
ANL-7501
ANL-7501
ANL-7501
ANL-7501
ANL-7501
ANL-7501
ANL-7501
ANL-7501
ANL-7501
ANL-7501
ANL-7501
ANL-7501
ANL-7501
ANL-7501
ANL-7501

The facilities of Argonne National Laboratory are owned by the United States Government. Under the terms of a contract (W-31-109-Eng-38) between the U. S. Atomic Energy Commission, Argonne Universities Association and The University of Chicago, the University

The facilities of Argonne National Laboratory are owned by the United States Government. Under the terms of a contract (W-31-109-Eng-38) between the U. S. Atomic Energy Commission, Argonne Universities Association and The University of Chicago, the University

The facilities of Argonne National Laboratory are owned by the United States Government. Under the terms of a contract (W-31-109-Eng-38) between the U. S. Atomic Energy Commission, Argonne Universities Association and The University of Chicago, the University

The facilities of Argonne National Laboratory are owned by the United States Government. Under the terms of a contract (W-31-109-Eng-38) between the U. S. Atomic Energy Commission, Argonne Universities Association and The University of Chicago, the University

The facilities of Argonne National Laboratory are owned by the United States Government. Under the terms of a contract (W-31-109-Eng-38) between the U. S. Atomic Energy Commission, Argonne Universities Association and The University of Chicago, the University

The facilities of Argonne National Laboratory are owned by the United States Government. Under the terms of a contract (W-31-109-Eng-38) between the U. S. Atomic Energy Commission, Argonne Universities Association and The University of Chicago, the University

The facilities of Argonne National Laboratory are owned by the United States Government. Under the terms of a contract (W-31-109-Eng-38) between the U. S. Atomic Energy Commission, Argonne Universities Association and The University of Chicago, the University

The facilities of Argonne National Laboratory are owned by the United States Government. Under the terms of a contract (W-31-109-Eng-38) between the U. S. Atomic Energy Commission, Argonne Universities Association and The University of Chicago, the University

The facilities of Argonne National Laboratory are owned by the United States Government. Under the terms of a contract (W-31-109-Eng-38) between the U. S. Atomic Energy Commission, Argonne Universities Association and The University of Chicago, the University

The facilities of Argonne National Laboratory are owned by the United States Government. Under the terms of a contract (W-31-109-Eng-38) between the U. S. Atomic Energy Commission, Argonne Universities Association and The University of Chicago, the University

The facilities of Argonne National Laboratory are owned by the United States Government. Under the terms of a contract (W-31-109-Eng-38) between the U. S. Atomic Energy Commission, Argonne Universities Association and The University of Chicago, the University

ANL-7501
Chemistry

ARGONNE NATIONAL LABORATORY
9700 South Cass Avenue
Argonne, Illinois 60439

NUCLEAR MAGNETIC RESONANCE SPECTRA IN BINARY MIXTURES OF INORGANIC FLUORIDES

by

Lesley L. Williams

Chemistry Division

Based on a thesis submitted in partial fulfillment
of the requirements for the degree of
Doctor of Philosophy (Chemistry)
at The University of Wisconsin

August 1968

TABLE OF CONTENTS

	Page
ABSTRACT	9
CHAPTER I. INTRODUCTION	10
CHAPTER II. VACUUM LINE FEATURES	12
A. General Description	12
B. Pressure Gauges and Their Applications	13
C. Special Metal Equipment	14
D. Special Kel-F Apparatus	16
CHAPTER III. PREPARATION OF CHEMICALS AND NMR SAMPLES	21
A. Notes on Seasoning of Equipment	21
B. Synthesis and Purification of the Fluorides	23
C. Preparation of NMR Samples	28
D. Concentration Calculations	32
CHAPTER IV. NMR MEASUREMENT TECHNIQUES	34
A. Synopsis of Instrument Usage	34
B. A56/60A Instrument at ANL	34
C. Modified HA-60 at UW	36
D. Saturation Study of IF_7 and IOF_5	37
E. Calibration of H_1	37
CHAPTER V. EXPERIMENTAL RESULTS	40
A. General Data Treatment	40
B. Computer Programs for Fitting IOF_5 Spectra	41
C. Chemical Shifts	42
D. Line Half-widths	49
E. Spin-Spin Coupling Constants	53
F. Longitudinal Relaxation Times in IF_7 and IOF_5	55
G. Samples of Solid IOF_5-IF_5 Mixtures	64

TABLE OF CONTENTS

Page

CHAPTER VI. RELAXATION MECHANISMS IN LIQUID IF_7 AND IOF_5 68

A. Relaxation of the ^{127}I Nucleus 68

B. Fluorine Relaxation 71

C. Conclusions and Interpretation of Narrowing in IOF_5 77

CHAPTER VII. SUMMARY 80

A. General 80

B. IOF_5 Solutions and Molecular Rotation 80

C. Line Widths in Three AB_4 Spin Systems 82

D. HF Spectra in Dilute Solution 83

APPENDIXES

I. Saturation Data 85

II. Nuclear Properties 87

ACKNOWLEDGMENTS 88

REFERENCES 89

LIST OF FIGURES

No.	Title	Page
1.	Sketch of the Vacuum Line, including the Main Pumping System, the Kel-F Working Manifold, and the Metal Working Manifold	12
2.	Photo of Three-stage Cold Trap (triple-trap) Used to Isolate Working Manifolds from Main Pumping System	13
3.	Photo of Several Welded Nickel Cans Used for Reactions and Storage	15
4.	Photo of Nickel Test-tube Type of Container, Assembled and Disassembled	15
5.	Photo of an Assembled 10-cm Nickel IR Cell	16
6.	Drawing of an All-Kel-F Valve, Disassembled	17
7.	Photo of a Cross, a Tee, and a "y" Machined from Kel-F and Useful in the Assembly of All-Kel-F Manifolds and Equipment	17
8.	Photo of an All-Kel-F Test-tube Type Container, Assembled and Disassembled	18
9.	Photo of an All-Kel-F NMR Tube Assembly, Assembled and Disassembled	18
10.	Photo of Kel-F Tubing Sealer in Operation	19
11.	Photo of a Typical NMR Sample, before and after Insertion into a Standard 5-mm-OD Glass Spinner Tube with an Airtight Polyethylene Cap	19
12.	Photo of a Spinnable Valve (Assembled and Disassembled), a Small Cylindrically Symmetric Kel-F Valve Which Was Designed To Be Sealed to Small Kel-F NMR Sample Tubing, Inserted into a 5-mm Glass Spinner Tube, and Spun in a Standard Spinner Assembly	20
13.	Photo of the Combination of Nickel IR Cell and Large Kel-F Bottle Used to Monitor the Reaction of IF_7 with Quartz Wool to Produce IOF_5	27
14.	Photo of the Temperature Bath Used to Equilibrate NMR Samples before Taking Spectra	35
15.	Typical ^{19}F NMR Spectrum of IOF_5 Dissolved in IF_5 with Matching Computed Stick Spectrum and Matching Computed Spectral Envelope Curve	42

LIST OF FIGURES

No.	Title	Page
16.	Chemical Shifts for IOF_5 in HF-IOF_5, IOF_5-BrF_5, and IOF_5-IF_5 Solutions	44
17.	^{19}F Chemical Shift for WF_6 in IOF_5-WF_6 Solutions and HF Proton Chemical Shift at 20 ± 1°C	45
18.	HF Fluorine Chemical Shift in HF-BrF_5 and HF-IOF_5 Solutions	46
19.	BrF_5 Chemical Shifts in HF-BrF_5 and IOF_5-BrF_5 Solutions	47
20.	IF_5 Chemical Shifts in IOF_5-IF_5 and IF_5-IF_7 Solutions	48
21.	IOF_5 Fitted Half-width $\Delta\nu_F$ in Pure IOF_5 as a Function of Temperature and in IOF_5-BrF_5 and IOF_5-IF_5 Solutions	49
22.	WF_6 Line Half-width $\Delta\nu$ in IOF_5-WF_6 Solutions as a Function of Temperature and HF Proton and Fluorine Line Half-width in HF-BrF_5 Solutions	51
23.	BrF_5 Line Half-widths in HF-BrF_5 and IOF_5-BrF_5 Solutions	52
24.	IF_5 Line Half-widths in IOF_5-IF_5 and IF_5-IF_7 Solutions	52
25.	Fluorine Spin-Spin Coupling Constant of the BrF_5 Doublet in HF-BrF_5 and IOF_5-BrF_5 Solutions and of the IF_5 Doublet in IOF_5-IF_5 and IF_5-IF_7 Solutions	53
26.	Melting-point Data, Spectral-area Ratios, and Partial Phase Diagram for the IOF_5-IF_5 Mixture System	65

LIST OF TABLES

No.	Title	Page
I.	Inorganic Fluorides and Binary Mixtures Chosen for Solvent-effect Study	11
II.	Liquid-phase Concentrations for NMR Samples Containing One Liquid Phase and No HF, after Correction for Ideal-solution Vapor Pressures at 25°C	32
III.	Concentrations for NMR Samples Containing HF	33
IV.	Extrapolated Chemical Shifts for IOF_5	43
V.	Liquid-to-Solid Chemical Shifts for WF_6 at -3.5 ± 1°C	45
VI.	Extrapolated Chemical Shifts for IF_7, WF_6, and HF Fluorine	45
VII.	Extrapolated Chemical Shifts for BrF_5 and IF_5	48
VIII.	Extrapolated Intrinsic Half-widths for the ν_B-band Multiplet Components for IOF_5	50
IX.	Extrapolated Half-widths for IF_7, WF_6, and Pure HF	50
X.	Extrapolated Half-widths for BrF_5 and IF_5	53
XI.	Extrapolated J_{FF} and Calculated RATIO Values for BrF_5 and IF_5 in Solution	54
XII.	Fitted J_{FF} for IOF_5 in Solution	54
XIII.	Longitudinal Relaxation Times T_1 in Pure IF_7 from a Saturation Study	61
XIV.	Longitudinal Relaxation Times T_1 for the IOF_5 ν_B Band in Several Liquid Samples at 29 ± 2°C, from a Saturation Study	62
XV.	Longitudinal Relaxation Times T_1 for the IOF_5 ν_B Band in Several Samples at -12 ± 2°C from a Saturation Study	63
XVI.	Longitudinal Relaxation Times T_1 for the IOF_5 and IF_5 ν_A Bands in Several Samples at 29 ± 2°C from a Saturation Study	63
XVII.	Half-widths of IOF_5 and IF_5 ν_B (doublet) Bands in IOF_5-IF_5 Mixtures in the Solid-sample Temperature Range	67
XVIII.	Parameters for the ^{127}I Relaxation in IF_7 and IOF_5	69
XIX.	Calculated Contributions to $(1/T_1)_F$ and $(1/T_2)_F$ for IF_7 and IOF_5	72

LIST OF TABLES

No.	Title	Page
XX.	Quantities Used in Theoretical Calculations of Relaxation Rates	75
XXI.	Comparison of Calculated Relaxation Times with Experimental Relaxation Times	77
XXII.	Line Widths in Three AB_4 Spin Systems	82
XXIII.	Peak Height as a Function of RF Field Strength for Pure IF_7	85
XXIV.	Peak Height as a Function of RF Field Strength for IOF_5 in Various Samples	86
XXV.	Some Useful Nuclear Properties	87

NUCLEAR MAGNETIC RESONANCE SPECTRA IN BINARY MIXTURES OF INORGANIC FLUORIDES

by

Lesley L. Williams

ABSTRACT

The effects of solvent, concentration, and temperature on the chemical shifts, line widths, and spin-spin coupling constants are reported for eight binary liquid inorganic fluoride mixtures from their high-resolution ^{19}F and ^{1}H nuclear magnetic resonance (NMR) spectra. The mixture systems studied were: IOF_5-WF_6, IOF_5-IF_7, IOF_5-IF_5, IOF_5-BrF_5, IF_5-IF_7, HF-IF_7, HF-IOF_5, and HF-BrF_5. Samples were prepared by vacuum techniques in sealed Kel-F tubes which were then inserted into standard 5-mm spinner tubes.

All line-width data for IOF_5 were obtained by fitting NMR traces with curves computed from the standard equations for an AB_4 spin system under the assumption that all transitions had a Lorentzian shape function of the same width. A solvent effect for the IOF_5 line width was found in liquid IF_5 and BrF_5 solutions. For IOF_5 dilute in IF_5 at -15°C, the line width was reduced tenfold, revealing the second-order AB_4 pattern and yielding a fluorine coupling constant of $J_{FF} = 284 \pm 5$ Hz. A similar solvent effect was not observed for IF_7 in the solutions examined, nor for IOF_5 in three other solvents.

Longitudinal relaxation times of the order of 1 sec were obtained for IF_7, IOF_5, and IOF_5 dilute in IF_5 from saturated peak-height data by an adaptation of the Bloembergen, Purcell, and Pound* procedure. Analysis by conventional relaxation theory of the transverse and longitudinal relaxation rates in these samples indicates that the rapid transverse fluorine relaxation rate is due to coupling with the quadrupolar ^{127}I nucleus, and that the spin-rotation interaction mechanism is the dominant source of longitudinal fluorine relaxation in the pure liquids.

The narrowing of IOF_5 lines in IF_5 solvent is thus associated with an increase in the correlation time for molecular reorientation and, in accordance with Hubbard's theory,** a corresponding decrease in the correlation time for fluctuations in the angular momentum. This result is interpreted in terms of reduced rotational freedom for IOF_5 in mixtures with IF_5 and BrF_5.

*N. Bloembergen, E. M Purcell, and R. V. Pound, Phys. Rev. 73, 679 (1948).

**P. S. Hubbard, Phys. Rev. 131, 1155 (1963).

For the most part, other changes reported here in chemical shifts, coupling constants, and line widths with concentration and temperature are relatively small and gradual, giving little indication of specific interaction, with the exception of HF dilute in BrF_5.

In contrast to HF dilute in IOF_5, the dilute HF fluorine line in BrF_5 solution is shifted away from the HF monomer fluorine resonance,* and the proton and fluorine lines are both appreciably broadened. Consistent with previous NMR and conductivity measurements of the HF-BrF_5 system, it is suggested that a limited degree of proton transfer occurs in these solutions according to the equation

$$BrF_5 + (HF)_{n+1} \rightleftharpoons HBrF_5^+ + (H_nF_{n+1})^- .$$

A limited amount of data on solid samples is also included. Linewidth results indicate that molecular rotation may be present in solid IF_7, solid IOF_5, and solid IOF_5-IF_5 mixtures. In the latter system, some evidence is given for the existence of solid solutions of limited solubility.

Samples were prepared at Argonne National Laboratory, and the NMR measurements were made there and at The University of Wisconsin.

CHAPTER I

INTRODUCTION

The field of nuclear magnetic resonance (NMR) spectroscopy approaches its first quarter-century mark in a remarkably sophisticated state, both experimentally and theoretically. One of the more difficult areas of NMR research, particularly theoretically, has been and surely will continue to be the area of solvent effects in liquid mixtures. As a perusal of recent reviews of this topic reveals, however, attention has been directed almost exclusively towards the experimental and theoretical characterization of solvent effects in the proton NMR spectra of aqueous and organic solutions.[1,2]

The work presented in this thesis is concerned with solvent effects in the ^{19}F NMR spectra of inorganic fluorides and was undertaken primarily in an attempt to discern the origin of a solvent effect reported a few years ago for IOF_5.

Two of the three independent publications which announced the discovery of IOF_5 in 1963[3-5] included IOF_5 NMR results, but the line widths observed for IOF_5 multiplets in liquid samples were not consistent. Alexakos, Cornwell, and Pierce[4] reported an unresolved AB_4-type spectrum

*D. K. Hindermann and C. D. Cornwell, J. Chem. Phys. 48, 2017 (1968).

for pure IOF_5 and for IOF_5 dissolved in IF_7, whereas Gillespie and Quail[3] recorded a resolved AB_4 pattern for IOF_5 dissolved in IF_5. A year later, Bartlett, Beaton, Reeves, and Wells[6] had confirmed these findings, noting that the mixing of one part IF_5 with two parts IOF_5 reduced the IOF_5 multiplet line widths by a factor of two or more, from about 470 to 170 Hz in the case of the equatorial fluorines.

Table I lists the inorganic fluorides studied in the present work and indicates the eight binary mixtures chosen, five of which contain IOF_5. The effects of solvent, concentration, and temperature on ^{19}F and ^{1}H chemical shifts, line widths, and coupling constants were determined for all the mixture components in an effort to define the nature and magnitude of the solvent effects common to this general class of compounds, as well as to IOF_5 in particular.

TABLE I. Inorganic Fluorides and Binary Mixtures Chosen for Solvent-effect Study. The eight mixture systems are indicated with an "X."

Study of Component A	Dissolved in Component B					
	WF_6	IF_7	IOF_5	IF_5	BrF_5	HF
WF_6	-		X			
IF_7		-	X	X		X
IOF_5	X	X	-	X	X	X
IF_5		X	X	-		
BrF_5			X		-	X
HF		X	X		X	-

At room temperature, each of the fluorides selected exists as a volatile, diamagnetic liquid which, with the important exception of HF and possibly IF_5, would be described as nonassociated. The fluorides are listed in Table I in the order of increasing molecular polarity, and they range on either side of IOF_5 from spherical and nonpolar to distinctly polar. The NMR spectra of the pure liquids are known and span a wide range of chemical shifts, line widths, and multiplet patterns.

It was anticipated that many, though hopefully not all, of the fluorides in this set could be mixed without chemical reaction, complex formation, or extensive ionization. Complications such as these, while of welcome interest in themselves, tend to obscure the effects of the weaker interactions which presumably account for the narrowing of the IOF_5 spectra.

The reactive substances involved in this study can be handled by what have now become fairly standard vacuum techniques in inorganic fluoride chemistry.[9b] However, in view of the necessity of obtaining samples of good purity, the apparatus and procedures applied here, which

made extensive use of metal and polychlorotrifluoroethylene (Kel-F) equipment, will be described in some detail.

CHAPTER II

VACUUM LINE FEATURES

A. General Description

A large-diameter high-speed metal pumping system located in the ANL Chemistry Division was made available for the course of this research. It consisted of a 10-cm oil diffusion pump with a two-stage rotary forepump, two 10-cm gate valves, a steel cold-finger trap with an automatic liquid nitrogen-filling system, and a long, 10-cm welded steel manifold equipped with heaters for degassing, a mass spectrometer for residual gas analysis, and four 1-in.-diam ports for the connection of working manifolds. The 10-cm manifold routinely maintained a vacuum of 10^{-7} Torr or better, and was protected from mechanical and human failures by an integrated system of monitoring and controlling devices described in detail by Sheft and Lind.[7]

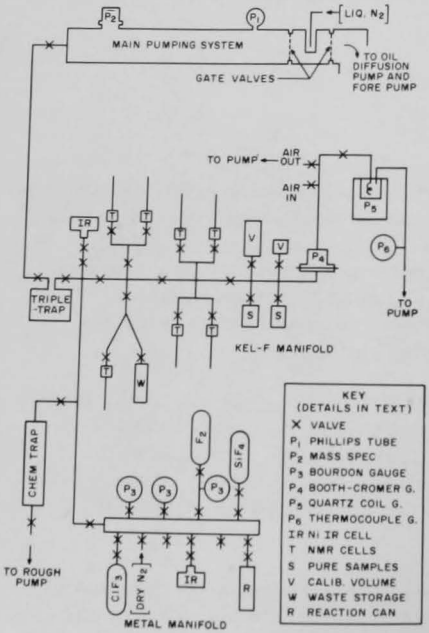

Fig. 1. Sketch of the Vacuum Line, Including the Main Pumping System, the Kel-F Working Manifold, and the Metal Working Manifold

Figure 1 is a sketch of the entire vacuum line, including the working manifolds described below. A working manifold attached to the main pumping system was customarily isolated by a three-stage cold trap constructed from four Hoke (411 Series) valves and three replaceable Kel-F "test tubes" attached to the trap framework with large flare fittings (see Fig. 2). A covered, wide-mouthed silvered glass Dewar of 3-l capacity maintained the triple-trap at liquid nitrogen temperature overnight when filled initially to the level of the flare fittings. A mechanical pump preceded by a chemical trap (consisting essentially of a 1-ft section of 2-in.-diam brass pipe packed with soda lime) was available for roughing out the working manifolds.

A metal working manifold suitable for the synthetic and purification procedures described in Ch. III was assembled from a welded nickel body (volume of 330 ± 10 cc)

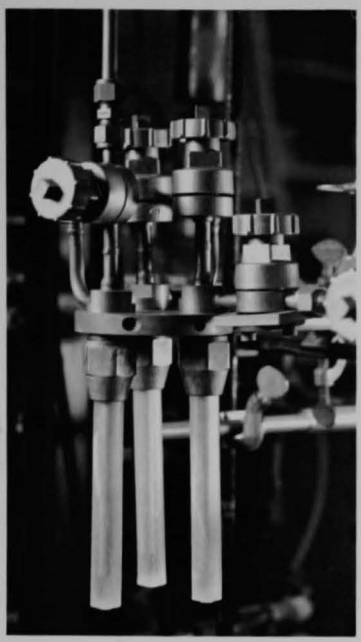

121-3468

Fig. 2. Photo of Three-stage Cold Trap (triple-trap) Used to Isolate Working Manifolds from Main Pumping System

and Hoke (411 Series) valves. Equipment was attached at each of the several ports primarily with Monel or stainless steel Swagelok fittings, chosen for their versatility and dependability; a variety of ferrule materials was available, including Teflon front ferrules for attaching glass or plastic equipment; a dry film lubricant (such as "Fluoro-Glide") was applied to the metal Swagelok threads to prevent galling. Pressure gauges included in this manifold are described in Sect. IIB. Sources of F_2, ClF_3, SiF_4, and dry nitrogen gas were connected to the line for the duration of the project.

For the preparation of NMR samples by the method described in Sect. IIIC, an all-Kel-F working manifold was assembled and attached to the main pumping system. The wide variety of equipment which can presently be fashioned from good-quality Kel-F is described in more detail in Sect. IID and was, of course, an important factor in making an all-Kel-F line possible. Constructed from 1/4-in.-OD Kel-F tubing, valves, tees, Y's, and crosses, it featured several separate sections, a small total volume (30 cc), and places for attaching up to six Kel-F NMR sample tube assemblies (see Fig. 1). This line gave very satisfactory performance, both mechanically and chemically.

During routine use of the working manifolds, pressure in the extremities of the lines was $\sim 10^{-5}$ Torr. Better evacuation was probably inhibited by the small-diameter tubing (of 3/8- or 1/4-in. OD) and orifices prevalent in these manifolds.

B. Pressure Gauges and Their Applications

The various types of pressure gauges installed in the working manifolds and main pumping system are listed below with a brief description of their function.

1. Helium leak detectors were extensively used for checking vacuum lines and equipment.

2. An Aero-Vac (model AVA-1) mass spectrometer for residual gas analysis mounted in the far end of the 10-cm pumping manifold was occasionally used to check for small leaks in the working manifolds by observing the ratios of N_2:O_2:CO_2:H_2O present.

3. A metal cold-cathode (Phillips) gauge (CVC-PHG06) was attached to the 10-cm pumping manifold near the cold-finger trap with a 1/2-in. stainless steel Swagelok union. It was part of the monitor and control safety circuit and routinely indicated 10^{-7} Torr or less. It was frequently consulted as it was sensitive to very small leaks and abnormal outgassing in the working manifolds.

A similar Phillips gauge was used to determine the pressures present in the working manifolds during routine operations.

4. Two Monel Bourdon gauges (operating in the ranges 0-1500 and 0-4000 Torr) protected by Hoke valves were attached to the metal manifold and used during the transfer of large amounts of F_2 and other gases. Another Monel Bourdon gauge (of range 0-500 psig) was used to monitor pressures in the connecting line to a tank of F_2.

5. For accurate measurements of sample pressure in this system, a Booth-Cromer diaphragm pressure gauge modified as described by I. Sheft[8] was chosen. In the present application, a Texas Instruments Co. model 141 fused-quartz Bourdon gauge was used to measure the air pressure on the back side of the diaphragm; air was admitted or removed from the back side through Ideal needle valves; the balance point was detected with a vacuum-tube voltmeter set on the x0.01 V scale; the reference side of the Bourdon gauge was maintained at <0.010 Torr by a mechanical pump. Pressures could be measured to ± 0.01 Torr with this equipment, although that degree of accuracy was seldom required in the following procedures. The Booth-Cromer gauge could be attached to either the metal or the Kel-F working manifold. It is shown attached to the Kel-F manifold in Fig. 1.

6. A thermocouple gauge was used to monitor the exhaust pressure of the 10-cm oil diffusion pump. Another thermocouple gauge monitored the zero-pressure reference side of the Texas Instruments Co. fused-quartz Bourdon gauge.

C. Special Metal Equipment

Welded nickel cans in a variety of sizes and weights were available. Several are shown in Fig. 3, ranging in size from 1500 to 135 cc, and in weight down to as little as 200 g (with valve). The larger cans were suitable for high-pressure fluorination reactions and hence were generally fitted with Monel Autoclave Engineers, Inc. valves as shown. The smallest can was designed to make accurate weighing (± 0.1 mg) possible. Also useful for

storage or reactions were wide-mouthed nickel test-tube-shaped containers connected to valves with copper-gasketed flare fittings (see Fig. 4).

121-2265

Fig. 3. Photo of Several Welded Nickel Cans Used for Reactions and Storage

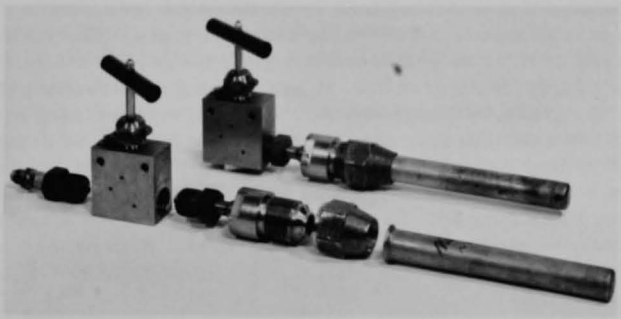

121-2256

Fig. 4. Photo of Nickel Test-tube Type of Container, Assembled and Disassembled

Infrared (IR) spectra of corrosive gases were conveniently obtained in the 10-cm gas sample cell (of 65-cc volume) shown in Fig. 5 (see also Fig. 8, Ch. III). The cell was assembled from a welded nickel body (of 1.035-in.-ID), windows (of 1.250-in. OD), compression flanges with silver knife edges, a sidearm for sample storage, and a high-pressure valve. For

121-2251

Fig. 5. Photo of an Assembled 10-cm Nickel IR Cell

the course of this investigation, AgCl windows were quite adequate, and these were protected from moist air by Drierite held in place with a sheet of Parafilm (Minnesota Mining and Metallurgy Co.), as can be noted in Fig. 8.

D. Special Kel-F Apparatus

The most generally suitable material for the handling and storage of reactive fluorides at moderate or low pressures and ordinary or lower temperatures is probably Kel-F. Chemically, it is fairly inert and very amenable to seasoning, although it is porous to helium and has a tendency to "absorb" quantities of certain relatively nonpolar substances. (In ^{19}F NMR work, Kel-F does have the distinct disadvantage of becoming somewhat porous on exposure to liquid CCl_3F for a few hours.) Mechanically, high-quality Kel-F is very workable, as is amply demonstrated here and elsewhere[9] in the variety of equipment fashioned from it. Kel-F also has the highly desirable property of not being completely opaque; thin layers may be almost as clear as glass.

Extruded Kel-F tubing free from flaws such as bubbles and small holes is now available in a very wide range of sizes. The tubing can be readily flared or bent by gently warming the tools with a torch before inserting the tubing. With practice, it can be worked directly over a flame somewhat like glass, although the working temperature range, centered at about 250°C, is considerably narrower; capillaries can be drawn in this way. Small tubing can be heat sealed by simply pinching, by heating under vacuum, or by setting in holes drilled in the top of a thermostated hot plate until a bottom has formed. Larger tubing can be shaped when hot by using Teflon, metal, or glass as a mold or a mandrel. With proper temperature control and a little mechanical pressure, vacuum-tight Kel-F to Kel-F joints can be made.

An essential element in the progress of fluorine chemistry at ANL has been the development of a Kel-F valve.[10] Shown in Fig. 6, it has a one-piece Kel-F body, a threaded Kel-F stem with a Teflon O-ring seat, and a Teflon gasket under the packing nut. Mechanical support and sturdy threads for 1/4-in. flare connections are provided by split sections of brass or galvanized aluminum. This valve is durable and has given dependable service under as much as 10-atm pressure.

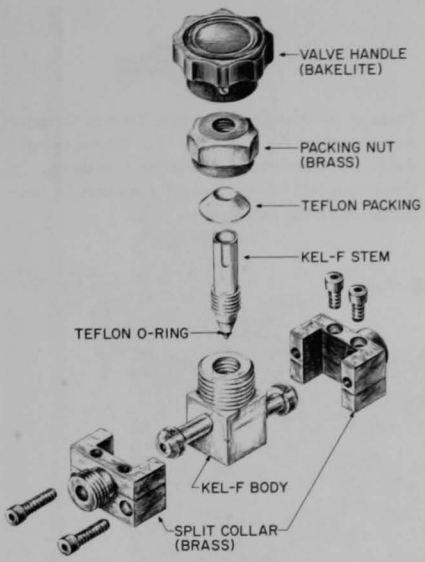

120-9409

Fig. 6. Drawing of an All-Kel-F Valve, Disassembled

Tubing, valves, and other machined fittings such as those shown in Fig. 7 can be readily assembled with flare joints to make vacuum lines (e.g., see Fig. 1) and other apparatus in which the contents are exposed only to Kel-F surfaces.

Large and small "all-Kel-F" containers are also available, made from a Kel-F valve, an adapter section, and a Kel-F tube, and connected by Kel-F to Kel-F flare joints. A small bottle (28 cc) made from an injection-molded Kel-F test tube is shown in Fig. 8; a larger bottle (of 120-cc volume) can be seen in Fig. 13.

An all-Kel-F assembly suitable for the preparation of small NMR samples is shown in Fig. 9. The Kel-F valve and 1/4-in.-OD tubing are connected to a small-diameter (~0.150-in. OD) sample tube by a Swagelok-type union containing special one-piece ferrules machined from high-density Kel-F; small flat washers are used behind the smaller ferrule to keep it from lodging in the nut. When over-tightening is avoided, the unions and even the ferrules can be used many times over.

The small-diameter NMR tubing was cut from a long stock piece, and the rounded bottom was formed by fusing one end of the tube in a shallow hole drilled in the aluminum top of a variable-temperature hot plate set at about 400°C; the inner contour of the bottom was simultaneously shaped with a long thin brass rod.

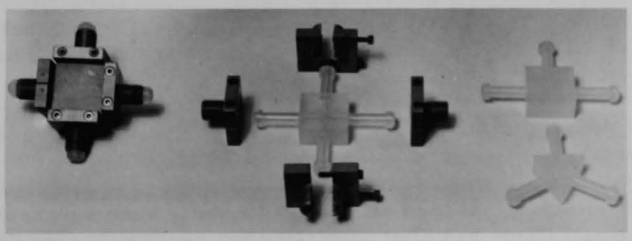

121-2267

Fig. 7. Photo of a Cross, a Tee, and a "y" Machined from Kel-F and Useful in the Assembly of All-Kel-F Manifolds and Equipment

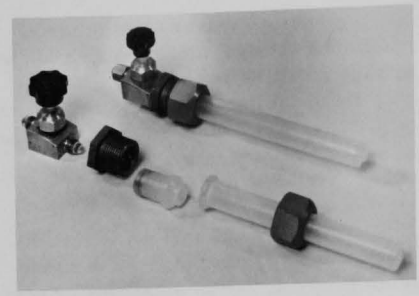

Fig. 8

Photo of an All-Kel-F Test-tube Type of Container, Assembled and Disassembled. The hidden end of the Kel-F adapter section contains a recessed, threaded metal bushing and 45° flare seat for connection with the Kel-F valve.

121-2258

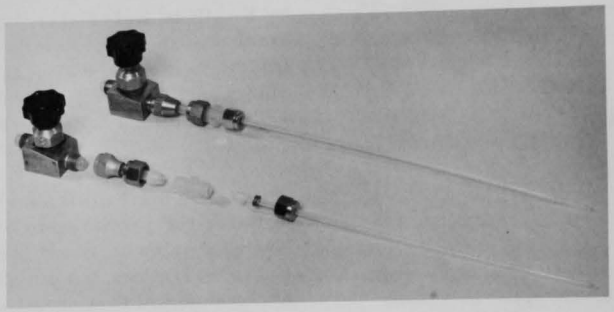

121-2249

Fig. 9. Photo of an All-Kel-F NMR Tube Assembly, Assembled and Disassembled

For the purpose of sealing off the resulting NMR sample, a Kel-F tubing sealer designed at ANL was routinely used. Shown in operation in Fig. 10, it was made from an insulated aluminum block, was heated by a capsule heater controlled by an adjustable thermostat, and had two spring-loaded wedge-shaped copper jaws for pinching off the tubing inserted down the center of the aluminum block. After proper adjustment of the thermostat for the OD (up to 1/4 in.) and wall thickness of the tubing to be sealed, the sealer would reliably and quickly produce a thick and strong wedge-shaped seal of slightly greater width than the original tubing diameter. A typical Kel-F NMR sample and 5-mm glass spinner tube are shown in Fig. 11.

For the preparation of the NMR samples the sealer proved to have two disadvantages: it required an excessive length of empty tubing above the seal area, and it demanded at least three hands to operate. A simpler and much smaller ring-shaped sealer has recently been successfully used at ANL;[11] a small flame has also been tried for sealing, but the failure rate was generally much higher.

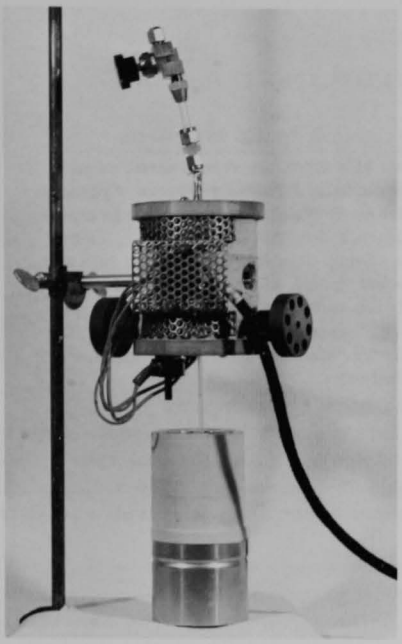

210-1124

Fig. 10. Photo of Kel-F Tubing Sealer in Operation

Recently also, a small cylindrically symmetric and spinnable Kel-F valve, henceforth called a "spinner valve," has been developed which, when attached to an NMR sample tube, can be inserted into a 5-mm glass spinner tube and spun in standard spinner assemblies, thus allowing for easy modification or retrieval of samples. The spinner valve design is shown, assembled and disassembled, in Fig. 12. The valve body is to be heat sealed to a 6-in. length of small-diameter Kel-F NMR sample tubing. Small holes drilled down the center of the valve stem and through the stem just above the Teflon O-ring comprise one "side" of the valve. A Teflon gasket is used under the aluminum packing nut.

The top portion of the stem can be attached to a vacuum manifold by a 1/4-in. Swagelok fitting containing a Kel-F ferrule. After filling the tube with an NMR sample, the valve is closed by rotating the valve body with respect to the stem. Without the Swagelok fittings and the split-ring "handle," both of which should be removed during spinning, the design shown weighs 10 g.

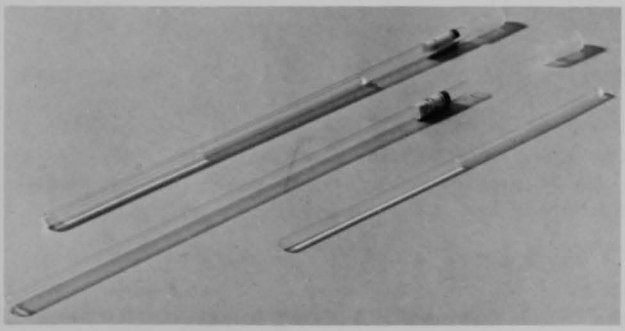

121-2242

Fig. 11. Photo of a Typical NMR Sample, before and after Insertion into a Standard 5-mm-OD Glass Spinner Tube with an Airtight Polyethylene Cap

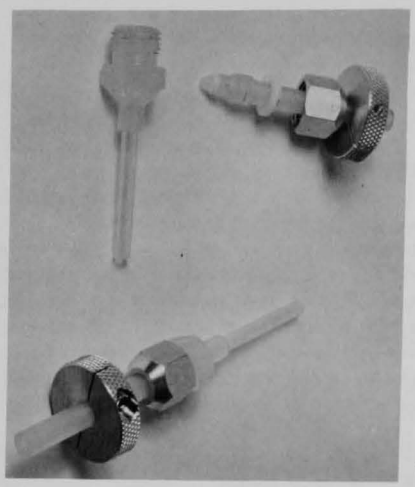

Fig. 12

Photo of a Spinnable Valve (assembled and disassembled), A Small Cylindrically Symmetric Kel-F Valve Which Was Designed To Be Sealed to Small Kel-F NMR Sample Tubing, Inserted into a 5-mm Glass Spinner Tube, and Spun in a Standard Spinner Assembly. Upper left: valve body and section for attaching NMR sample tubing. Upper right: valve stem, packing, and split-ring "handle." Lower left: Assembled spinner valve.

121-3467

CHAPTER III

PREPARATION OF CHEMICALS AND NMR SAMPLES

A. Notes on Seasoning of Equipment

The successful handling of corrosive fluorides in any vacuum line depends heavily on an appropriate chemical seasoning or passivation of all inner surfaces, which will then allow certain desired procedures to be completed without contamination of the sample(s) in question and without appreciable loss of the sample(s) through adsorption on or reaction with the walls of the apparatus. It is, of course, essential to work in a vacuum system free of even small leaks.

Metal equipment is used extensively in fluorine chemistry because proper "fluorination" of the metal produces a thin, nonreactive surface film which is nonporous enough to prevent further corrosion. Polymerized fluorinated alkenes, such as Kel-F or Teflon, are extensively used because they are intrinsically impervious to further fluorination.

Cleaning. The chemical seasoning of surfaces is often made substantially easier by beginning with physically clean apparatus. For the work described in this chapter, routine laboratory cleaning of the equipment was usually adequate. Dilute nitric acid was effective in cleaning up used nickel vessels, IR cells, and other metal pieces; new nickel vessels, valves, and Swagelok fittings were washed with clean acetone or benzene to remove surface grease and oil. Copper gaskets were annealed and cleaned by being heated to red heat in a flame and then plunged into a small quantity of 95% ethyl alcohol. All Kel-F pieces including tubing were thoroughly washed with clean acetone before use; this step proved particularly efficient in removing potentially reactive surface films from the small, NMR sample tubing.

All equipment was given a final rinse with clean acetone, assembled, leak tested, and then pumped out further on a working manifold for at least 24 hr to remove as much of the adsorbed H_2O and CO_2 as possible. The volume of air pumped through the line at this time was kept to a minimum in order to reduce the detrimental effects of readsorption and/or reaction of moist air in the previously degassed and seasoned portions of the manifold.

Seasoning Procedures. The passivating treatment chosen in a particular application will depend in general on the material of which the apparatus is constructed, on the nature of the substances to which the apparatus will later be exposed, and on the details of the exposure itself (e.g., duration and temperature). Several generally useful seasoning procedures are outlined in the following; variations used for specific applications are detailed in Sect. IIIB and IIIC.

Reduction followed by fluorination is a very reliable way to passivate those metal surfaces which can be heated to red heat. This method was used extensively to season nickel reaction and storage vessels. About 400 Torr of hydrogen gas was admitted to an evacuated nickel can and preseasoned-metal working manifold. With the valves between can and manifold open, the can was heated to red heat with a torch. (A hydrogen flame for this purpose is not only faster than a gas flame, but has the attractive feature of leaving the equipment surfaces clean (reduced) and bright.)

When necessary, nearby valves (especially Hoke valves of the 411 type) were cooled by wrapping them in wet asbestos. The pressure could be monitored on a Bourdon gauge. When the metal had cooled, the pressure was observed to drop back to the original value or lower. While still slightly warm, the hydrogen gas was removed through the chemical trap and the line pumped on for at least an hour. Then about 400 Torr of F_2 gas was admitted, and the heating, cooling, and evacuation steps repeated. The can and line were then pumped on at least overnight.

Since the metal working manifold with its many closely spaced Hoke valves could not be heated to red heat, this manifold had to be seasoned by other methods. After thorough degassing by repeated warming with a torch, the manifold was exposed to 700 Torr ClF_3 for several hours (or overnight). About two days of pumping was then required before degassing became undetectable.

This same manifold was also successfully reseasoned by admitting 400 Torr F_2 gas and heating quite strongly with a torch. The seasoning of the metal manifold was, of course, revitalized during the routine reduction and fluorination of vessels attached to it.

All of the Kel-F equipment was seasoned with ClF_3. A half-hour exposure at 400 Torr followed by two days of pumping was generally sufficient; longer exposures tended to allow the ClF_3 to penetrate the Kel-F too far, occasionally producing degassing or surface reaction problems during later use.

Nickel IR cells with AgCl windows could also be adequately seasoned with ClF_3. The cell was filled with 400 Torr of ClF_3 for up to 15 min, followed by two days of pumping. For use with particularly aggressive substances (e.g., IF_7 or XeF_6), the ClF_3 seasoning was repeated. The seasoned windows seemed to withstand attack by fluorides best when care was taken to degas the cell <u>very</u> well before the first exposure to ClF_3.

Quartz glass equipment was usually "seasoned" by baking overnight at 400°C under vacuum, which tended to remove surface-held water to an

extent which prevented the formation of HF during later use. Beyond this baking out, a few minutes of exposure to some HF-free reactive substance such as F_2 (warm), ClF_3, or IF_7, followed by pumping, was often used to provide some form of chemical seasoning.

Flushing. In addition to formal seasoning procedures such as those described above, there was a final treatment of all apparatus to further insure the "clean" handling of chemicals. Just prior to the actual transfer of a particular substance, the pertinent equipment was flushed at least once with a gas sample of the substance. The advisability of this step has its origin in the basic spongelike nature of all surfaces, fluorinated or otherwise. This final flush was intended to saturate the remaining active sites (physical adsorption sites as well as chemical reaction sites) as much as possible with the substance to be transferred.

B. Synthesis and Purification of the Fluorides

A description is given below of the original source and final purity of the following substances: F_2, HF, IF_5, WF_6, BrF_5, IF_7, and IOF_5.

In addition to crude purity checks on the final stock sample of these substances, such as the color and apparent viscosity of a condensed phase, the IR spectrum of a gas-phase sample of each of these fluorides (except HF) was examined in order to detect and possibly identify the impurities present. For this purpose, a well-seasoned 10-cm nickel IR cell with AgCl windows (see Fig. 5) was filled to a pressure of several hundred Torr (when possible) of the sample to be investigated. All IR spectra were run with a Beckman Model IR-12 Spectrophotometer against an evacuated reference cell from 350 to 4000 cm^{-1}. Background and low-temperature spectra were readily obtained by condensing the sample in the cell sidearm with baths of various temperatures. After as brief a time as possible in the IR cell, the sample was removed to prevent attack on the AgCl windows and either discarded or used to season some portion of the manifold.

It was found that as little as one Torr of HF, a common impurity, could be detected by observing its characteristic monomer band at 3800 cm^{-1}. Much smaller traces of CO_2 were readily detected from bands at 667 and 2350 cm^{-1}. Less-common impurities were identified as often as possible, although no quantitative estimates were attempted.

F_2. The fluorine used in this work was obtained from the ANL Chemical Engineering Division, where it had been redistilled from commercial sources to a purity of 99.99%. Subsequent IR spectra of samples at about 2 atm pressure showed the absence of all detectable impurities except a very small trace of CF_4.

The steel tank containing 0.5 lb F_2 at 410 psi had been fitted with an Autoclave Engineers, Inc., high-pressure Monel valve with Teflon stem packing, which gave trouble-free service for over two years. The tank was attached to the metal manifold with 1/4-in.-OD copper tubing; for safety and monitoring purposes, the top of the F_2 tank was covered with a metal shield, and a Monel Bourdon gauge (ranging from 0 to 500 psig) was included in the copper connecting section.

HF. High-purity anhydrous HF (conductivity: $\sim 1 \times 10^{-6}$ mho)[12] stored in large Kel-F bottles was kindly supplied by L. Quarterman.

IF_5. A 20-g sample of IF_5 purified by H. Selig and stored in a large Kel-F bottle was obtained. A trace of HF was detected in the IR spectrum.[13]

WF_6. A 25-g sample of WF_6 was distilled from an Allied Chemical and Dye Corp. lecture bottle into a seasoned nickel weighing can. A very small amount of noncondensable gas was pumped off at liquid nitrogen temperature; twice, the sample was warmed to room temperature, recondensed at dry ice temperature (where the vapor pressure is ~0.5 Torr) and pumped on, through a liquid nitrogen trap, for 10 min; only a very small amount of white solid was collected by the liquid nitrogen trap. The sample was next allowed to warm slowly and an initial fraction of perhaps 0.5 g was discarded. An IR spectrum of 200 Torr of the resulting WF_6 sample showed no traces of HF, CO_2, or other clearly detectable impurities. It was noted that published IR spectra for WF_6 are of such poor resolution that they are quite unsuitable for comparison with spectra produced by modern instruments.[14,15]

BrF_5. Two impure, highly colored samples of BrF_5, surely containing Br_2, BrF, and BrF_3, and probably containing HF, were purified by refluorination over NaF pellets.

A wide-mouthed welded nickel can of 400-cc volume with a copper-gasketed compression seal and a Hoke 413 inlet valve on the top was filled loosely with new NaF pellets, sealed, leak tested, and placed on a metal vacuum manifold. The can was strongly heated with a torch for 30 min under vacuum and then cooled. About 60 cc of the impure BrF_5 was distilled into the can, which was then pressurized with 2 atm fluorine. The fluorine was replenished several times during the day to maintain about 2 atm pressure. After about 6 hr, the can and contents were heated strongly with a torch and allowed to cool slowly. The fluorine was replenished and left for another hour. After removal of the fluorine at dry ice temperature, about 50 cc of colorless, low-viscosity BrF_5 was distilled into two seasoned, small Kel-F bottles, where it was further degassed.

An IR spectrum[13] of about 150 Torr of this BrF_5 showed no trace of HF or CO_2, and no other detectable impurities. Presumably, HF and certain other impurities were effectively retained by the NaF pellets.

IF_7. High-purity IF_7 was readily prepared by the reaction of KI and excess F_2:[16,17]

$$KI + 12F_2 \xrightarrow[2\ hr]{270°C} IF_7 + KF + 8F_2.$$

This method, when used as described below, reliably gave better than 90% yield of very pure IF_7, requiring no additional purification step. The reaction chosen avoided the moisture problems usually encountered in the fluorination of I_2 crystals and had the added advantage of producing KF in amounts which would readily absorb any small amounts of HF or IF_5 present.

A total of 50 g of IF_7 was prepared in several batches. The batch size was limited by the fluorine pressure in the reaction vessel, which for safety reasons was not to exceed 40 atm at the higher temperature, calculated before any reaction occurred. The reagent-grade KI was ground to a fine grain with an agate mortar and pestle, weighed into stoppered bottles, and dried in a 160°C oven for several days just before use. Weight loss was generally negligible, as KI is not particularly deliquescent. However, routine precautions against moisture inclusion were believed to be important in minimizing the amount of IOF_5 formed in the reaction.

For a 30-g yield of IF_7, a weighed amount of KI (19.2 ± 0.1 g) was funneled as quickly as possible into a well-seasoned, 1500-cc, welded nickel reaction can. A high-pressure Monel Autoclave Engineers, Inc., valve was attached. The can was leak tested and returned to the vacuum line, where it was pumped on with heating overnight.

The appropriate amount (1.35 moles) of high-purity F_2 was distilled by successive transfers from a known ballast volume into the reaction can held at liquid nitrogen temperature. The first additions of fluorine were almost completely absorbed, indicating either reaction even at liquid nitrogen temperature or solution formation. The expected vapor pressure of pure fluorine is ~300 Torr at -195°C and ~1000 Torr at -185°C (liquid oxygen temperature).

The reaction can and contents were allowed to warm naturally to room temperature and were then held at 270 ± 10°C for 2 hr by a band heater (or a furnace) placed around the can, controlled in this case by a thermocouple connected to a regulator. The can was allowed to cool naturally to room temperature and was then immersed for at least 20 min in liquid nitrogen before any F_2 was removed. The nitrogen bath was replaced

by a liquid oxygen bath, and the excess F_2 was distilled into a large, high-pressure welded nickel storage can held at liquid nitrogen temperature. The expected amount of F_2 was indeed recovered and proved suitable for use in later IF_7 syntheses, provided small initial and final fractions were discarded. When the residual pressure in the reaction vessel dropped below 300 Torr, the liquid oxygen bath was replaced by liquid nitrogen, and the remaining F_2 was pumped away by the rough, and eventually, the good pumping systems. This process often took several hours and suggested again the existence of a liquid F_2 solution.

After F_2 removal, the products were warmed to dry ice temperature, at which a pressure head of only 2 Torr was usually observed, corresponding to the expected vapor pressure of IF_7. As a precaution, however, the first few 2-Torr samples were used for seasoning and discarded. The bulk of the product was then slowly transferred at low temperature and pressure (5 Torr) to a seasoned, welded nickel storage can immersed in liquid nitrogen. When the transfer pressure dropped below ~1 Torr, the two cans were shut. The reaction vessel was warmed to room temperature where it generally showed only a very few Torr pressure when opened to the metal manifold.

The product IF_7 was degassed by thawing and freezing a few times. Initial IR spectra[18,19] of several batches sometimes showed very small amounts of HF, CO_2, CF_4, SiF_4, and SO_2F_2, which were easily removed by discarding several large (manifold volume) vapor pressure heads at some low temperature (e.g., dry ice temperature). The final combined sample showed no traces of any impurities.

<u>IOF_5</u>. The IOF_5 used in this work was prepared by reacting IF_7 with quartz wool:[16,17]

$$2IF_7 + SiO_2 \xrightarrow{\text{catalyst ?}} 2IOF_5 + SiF_4.$$

Under suitable conditions to be described below, this reaction went to completion, giving a high yield of IOF_5 which could be readily purified by simple distillation. Beaton, using apparently minor variations of this method, has had less success in causing complete conversion;[20] attempts at a direct hydrolysis of IF_7 have also generally resulted in mixtures of IF_7 and IOF_5, thus necessitating special separation procedures.[5,20,21]

The reaction of IF_7 with SiO_2 was found to go to completion only if significant amounts of water were adsorbed on the quartz wool, thus lending further support to the cyclic reaction scheme involving HF proposed by Alexakos, Cornwell, and Pierce.[4] To prepare the quartz wool for the reaction (quartz is preferable to Pyrex because of its lower boron content), it was placed overnight in a 600°C oven to remove organic impurities and was then placed on a rack over distilled water in a closed container for at least two weeks to promote readsorption of water.

A large Kel-F bottle (of 120-cc volume) was packed loosely with a slight excess of quartz wool (~2 g) and assembled with a Kel-F valve. In order to prevent water loss, the bottle was placed in a liquid nitrogen bath while being evacuated. An appropriate amount of pure IF_7 (~10 g; for purity see above), designed to produce less than 10 atm total pressure of SiF_4 and IOF_5 at completion of the reaction, was condensed into the bottle and was allowed to warm to room temperature.

In order to monitor the progress of the reaction, the Kel-F bottle was attached to a 10-cm nickel IR cell in such a way that an IR spectrum could still be run with the bottle attached (see Fig. 13). The Kel-F valve could be opened to the small volume between the bottle and the IR cell, and the gases trapped in this volume were then expanded into the IR cell, where relative changes in absorption-band intensities were noted. Such changes were clearest if the bulk of the SiF_4 formed was removed first, as described below.[22]

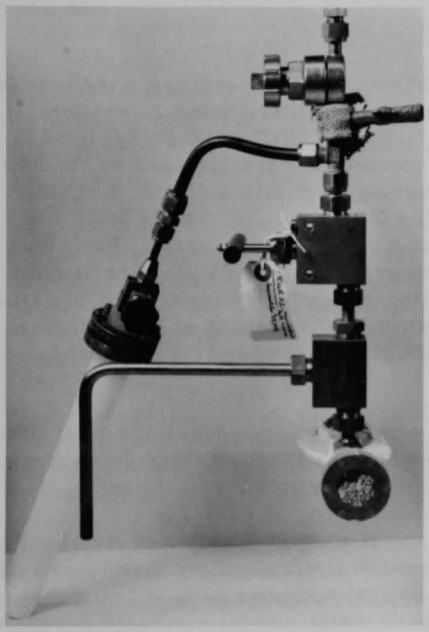

121-2263

Fig. 13. Photo of the Combination of Nickel IR Cell and Large Kel-F Bottle Used to Monitor the Reaction of IF_7 with Quartz Wool to Produce IOF_5

The reaction generally reached completion in less than two days; if it stopped before completion, the IF_7-IOF_5 mixture was removed to temporary storage, the remaining quartz wool was replaced with a fresh "wet" sample, and the reaction was tried again.

Several batches were run with ~1 g NaF in the bottom of the bottle, with no clear effect on the completion rate. The batch which was completed in the shortest time contained quartz wool which was neither cleaned nor dried; there were substantially more impurities in the products of this run.

The SiF_4 formed was removed by cooling the bottle (attached to the vacuum line) first in a liquid nitrogen bath and then in a -100°C bath (a slush of 1 part chloroform and 2 parts trichloroethylene), and allowing the SiF_4 to expand into the manifold several times. The temperature and method were chosen to minimize the loss of IOF_5 which has a vapor pressure of ~0.5 Torr at -100°C. This method also served to remove small amounts of volatile impurities such as CO_2 and CF_4.

At the completion of the reaction and following SiF_4 removal, the IOF_5 was distilled into a seasoned nickel storage can containing 0.5 g NaF, which had been activated by heating it in the can under 400 Torr F_2. When necessary, the IOF_5 was further purified by discarding a few low-temperature vapor pressure heads expanded into the metal manifold.

An IR spectrum of the final combined sample of 25 g showed no trace of CO_2, HF, SiF_4, IF_5, or any other detectable impurity. All the IOF_5 IR spectra showed the complete absence of the 640-cm^{-1} band reported by Smith and Begun;[21] this band was probably due to IF_5 impurity as has also been suggested by other investigators.[23]

C. Preparation of NMR Samples

Introduction. Several liquid NMR samples, covering a wide concentration range, were prepared for each of eight binary-mixture systems: IOF_5-WF_6, IOF_5-IF_7, IOF_5-IF_5, IOF_5-BrF_5, HF-IOF_5, HF-BrF_5, HF-IF_7, and IF_5-IF_7. In general, desired concentrations were obtained by condensing a large, known gas volume of each component into a small, weighed Kel-F NMR tube assembly (see Fig. 9) and then sealing off the NMR tube while the contents were frozen at liquid nitrogen temperature. For solutions containing IF_5, which has a vapor pressure of only 20 Torr at room temperature, and for solutions containing HF, which shows large deviations from ideal gas behavior, an approximation to the amount of liquid desired was obtained directly by filling the NMR tube assembly to a precalculated level.

All samples except one were contained in sealed Kel-F tubes. Details of their preparation are described below. Final mixture concentrations, given in Sect. IIID, were usually known to better than ±1 m/o.

First Weighing. Two sizes of small-diameter extruded Kel-F tubing were available, both fitting inside 5-mm-OD NMR glass spinner tubes. The tubing of larger size had quite thin walls and a volume almost twice that of the smaller tubing, which had fairly heavy walls. Sample pressure, possible corrosion (particularly with IF_7), and NMR spectral intensity were factors considered in choosing between the two sizes for a particular sample.

The various sections of a Kel-F NMR tube assembly, weighing ~140 g and described in Sect. IID (see Fig. 9), were given a final rinse with acetone, assembled, leak tested, and weighed (evacuated) to the nearest 0.1 mg on an analytical balance. Care was taken to discharge static electricity from the long Kel-F tube, which protruded during weighing into a closed cardboard extension of the standard balance housing.

Seasoning. A calibrated volume can, pure samples of the components of a mixture, and up to six weighed NMR tube assemblies were attached to

the Kel-F manifold, pumped on overnight, seasoned with ClF_3, and then pumped out for two days. Several seasonings of the line and tubes with the vapor of the fluorides to be used were always required, followed again by thorough pumping.

In the cases of HF and BrF_5, for which very slight impurities cause intense coloration of the liquid phase, all tubes were repeatedly seasoned for several hours with several centimeters of liquid, until a colorless liquid phase was attained; impure BrF_5 seasoning liquid was pumped out; impure HF seasoning liquid had to be poured out by inverting the tube assembly on a flexible section of the Kel-F line, to prevent leaving a nonvolatile residue in the tube.

Seasoning of the tubes with liquid IOF_5, WF_6, and IF_7, while desirable, was not included, as it was discovered that Kel-F tubing saturated with these relatively nonpolar substances turned into a porous, fibrous white material when warmed even slightly for sealing.

Sample Transfer. Gas transfers for the preparation of six samples took about 3 hr; the first mixture component was transferred to the NMR tubes in several consecutive transfers; the line was flushed twice with the second component before its transfer was begun. Two calibrated volumes were used (a 28.0 ± 0.5-cc Kel-F bottle and a 134 ± 1-cc nickel weighing can, each calibrated with both CCl_4 liquid and SiF_4 gas) in order to keep the measured gas-sample pressures between 50 and 400 Torr.

To obtain a pure gas sample for seasoning or for transfer to an NMR tube, the stored pure sample was cooled slightly, opened to the manifold, and allowed to warm until it exerted the desired vapor pressure in the line and calibrated volume can. The desired pressure was conveniently preset on the Modified Booth-Cromer gauge (described in Sect. IIB) by admitting air manually at that pressure to the back side of the gauge diaphragm. After a final balancing of the pressures on either side of the diaphragm, the air pressure could be read to the nearest 0.08 Torr on the Texas Instruments Co. gauge.

To use this gas sample for an NMR mixture, the valve on the calibrated volume can was shut (with care being taken not to warm the apparatus, since this would disturb the pressure), the line was briefly evacuated, the ambient laboratory temperature was noted, the pressure gauge zeroes were rechecked, and the gas sample in the calibrated volume can was condensed into one of the NMR tubes with liquid nitrogen. At the end of the transfer, residual gas pressure was measured and, when appreciable, included in concentration calculations; the NMR tube-assembly valve was then closed, the residual gas was checked for noncondensables, and the line was evacuated briefly before the next pure gas sample was measured out.

Because of the small diameter of the Kel-F tubing, a transfer sometimes took 5 min to reach a reasonable completion; at the "end" of a transfer, residual gas pressure in the small Kel-F manifold and calibrated volume can was generally less than 2 Torr, decreasing as more transfers of that mixture component were made. For this reason, the transfers at higher pressure were made first. It was also found that brief pumping (no more than 5 min) between transfer operations put the Kel-F manifold in the best condition for efficient transfers with minimal degassing problems.

Sealing and Weighing. Tubes were sealed immediately after filling with the Kel-F tubing sealer described in Sect. IID (see Fig. 10), with care being taken to keep the sample frozen in the bottom of the tube at all times. As soon as the lower, freshly sealed portion of the Kel-F tubing was released from the jaws of the sealer, the hot sealed area was gently pushed into a cylindrical shape which would surely allow the sample tube to slip into standard, 5-mm-OD glass NMR spinner tubing (of 0.164-in. ID). To achieve this shape, a pair of warm needle-nosed pliers with a 0.160-in.-diam hole drilled between the jaws was used. When the seal was completely cool, the sample was allowed to warm up (in a hood). None of the seals ruptured at the higher pressures (exceeding 5 atm in some cases) attained during NMR experiments.

The resulting NMR sample was a tube about 12 cm in length containing at least 5 cm of liquid and weighing about 2 g (see Fig. 11). By weighing both portions of the original NMR tube assembly, the total weight of the liquid sample (0.5-1.0 g) could be determined. If both components of a mixture had been obtained by transfer of a measured amount of gas sample, this weight served only as a check of the calculated bulk concentrations. For solutions containing HF or BrF_5, however, this weight was needed to determine the amount of these liquids originally condensed into the tubes. Although individual weighings could be made to the nearest 0.1 mg, the final calculated liquid weights were assigned an uncertainty of ±2 mg, consistent with variations observed in samples containing known amounts of liquid.

After the weighing, each sample tube was placed in a labeled, 5-mm-OD glass NMR spinner tube with an airtight polyethylene cap, as shown in Fig. 11, and stored at dry ice temperature.

Pure IF_7 in Quartz Glass. In order to obtain a greater NMR signal intensity for IF_7 than was provided by samples sealed in small Kel-F tubes, a 5-mm NMR sample of pure IF_7 was prepared.

A 5-mm-OD quartz glass precision NMR spinner tube (Wilmad Glass Co., Inc.) was attached to a short piece of 1/4-in.-OD quartz glass tubing and a constriction for sealing was placed in the spinner tube. The tube was attached to the vacuum manifold by a 1/4-in. Monel Swagelok union with a Teflon front ferrule and baked overnight at 400°C with pumping;

during baking, the Swagelok joint was cooled with an airstream. The tube was seasoned twice with IF_7 vapor, pumped out, and then gently flamed. About 2 g of pure IF_7 were distilled into the tube, which was then sealed and stored at dry ice temperature. Only a very slight etching of the quartz was observed when the sample was liquified for the first time. No impurities were ever observed in the NMR spectra of this sample.

Quality and Aging of Samples. Each of the 48 samples prepared was initially colorless, even at dry ice temperature, except for two mixtures of IF_5 in IF_7, which were a very pale yellow when solid, perhaps from insufficient seasoning of the Kel-F. No impurities or other peculiarities were detected in the initial NMR spectra of any of the 48 samples, even after extensive searches on many samples.

Spectra were recorded over a total period of a year, but in general only for samples prepared within the preceding six months. All samples were stored at dry ice temperature and examined about once a month for signs of aging, which were very few during the first six months after preparation. Two samples had a slow leak at the seal, but were retained for the purpose of elucidating the effects of such a leak on their respective NMR spectra. Any other sample showing chemical or physical deterioration was eliminated from later studies unless it could be shown that the spectra remained unaffected.

Some perspective on the aging behavior of samples of inorganic fluorides in Kel-F NMR tubes is given by a description of the forms of deterioration observed in only a few of the samples after prolonged storage.

The most frequent aging problem occurred in samples containing HF. With few exceptions, a slight etching of the inner walls of the glass spinner tube became visible after six to twelve months of storage. The accompanying weight loss was usually very small (~1 mg).

After a year, two samples of IOF_5 in IF_7 were noted to have suffered corrosion of the Kel-F along with a small weight loss (2 mg). The Kel-F showed a number of very small lengthwise cracks containing a white substance. This same type of corrosion was observed in an independent sample of pure IF_7 in Kel-F which had been allowed to sit at room temperature for about six months.

Two samples developed distinct impurity peaks. About 1% IF_5 was detectable in the NMR spectrum of the pure IOF_5 sample after 12 months. After about 8 months an unidentified peak appeared at approximately the center of the broad doublet spectrum of the sample of pure IF_7 stored in Kel-F. This peak was also reported by Bartlett *et al.*[6] for a sample of IF_7 in a Teflon cell.

Three samples containing BrF_5 developed a pale yellow coloration after about 6 months.

Although it had been expected that some of the more nonpolar fluorides would be slowly absorbed by the Kel-F tubing even at dry ice temperature, no measurable effect on the liquid levels was ever noted.

D. Concentration Calculations

The number of moles of each mixture component in a sample tube was calculated and then assigned a maximum possible experimental uncertainty based on the following sources of error: uncertainty in the measured gas pressures; uncertainty in the volume of the calibrated volume can; uncertainty in the ambient laboratory temperature; uncertainty in the NMR tube-assembly weight, if used to calculate a total liquid sample weight.

For all solutions having only one liquid phase, except those containing HF, vapor pressure corrections to the bulk m/o concentrations were made by assuming ideal solution behavior (Raoult's law) and ideal gas behavior. Corrections were calculated as the actual number of moles of a component which would be found in the vapor space (estimated for each tube individually) over an ideal solution of a certain mole fraction at 25°C. The values used for the vapor pressures at 25°C of pure components are found in Refs. 5, 16, 20, 24, and 25.

An uncertainty of ±25% was then assigned to each correction to allow for possible deviations from ideal behavior. The uncertainties in the concentrations given in Table II for these solutions are the sums of the

TABLE II. Liquid-phase Concentrations for NMR Samples Containing One Liquid Phase and No HF, after Correction for Ideal-solution Vapor Pressures at 25°C

Contents A-B	A (m/o)		Contents A-B	A (m/o)	
IOF_5	100	(1)[a]	BrF_5	100	(2)
WF_6	100	(1)	IOF_5-BrF_5	8.2 ± 0.3	
IOF_5-WF_6	16.4 ± 0.3		IOF_5-BrF_5	19.8 ± 0.3	
IOF_5-WF_6	49.9 ± 0.1		IOF_5-BrF_5	29.8 ± 0.3	
IOF_5-WF_6	82.3 ± 0.4		IOF_5-BrF_5	49.7 ± 0.3	
IF_5	100	(2)	IOF_5-BrF_5	75.0 ± 0.5	
IOF_5-IF_5	9.8 ± 0.3		IF_7	100	(2)
IOF_5-IF_5	12.2 ± 0.5		IOF_5-IF_7	4.8 ± 0.5	
IOF_5-IF_5	17.6 ± 0.2	(L)[b]	IOF_5-IF_7	24.8 ± 0.4	
IOF_5-IF_5	26.5 ± 0.3		IOF_5-IF_7	49.6 ± 0.4	
IOF_5-IF_5	37.8 ± 0.5		IOF_5-IF_7	74.4 ± 0.5	
IOF_5-IF_5	53.8 ± 0.5		IOF_5-IF_7	94.7 ± 0.7	
IOF_5-IF_5	57.7 ± 0.4		IF_5-IF_7	37.1 ± 0.4	
IOF_5-IF_5	75.1 ± 0.5		IF_5-IF_7	72.0 ± 0.5	
IOF_5-IF_5	91.7 ± 0.8				

[a]The number in parentheses indicates the number of samples of this concentration prepared.

[b]The "L" indicates a sample which began leaking slowly at the seal after three months.

experimental and vapor-pressure-correction uncertainties at 25°C. Because of the generally small magnitude of the corrections (~0.2 m/o), no attempt was made to calculate corrections at lower temperatures, where they would in general be even smaller.

Samples which exhibited two liquid phases at all temperatures are denoted by a † in Table III. For these cases no vapor pressure corrections to the bulk concentrations were made, since concentrations within each liquid phase were not known.

TABLE III. Concentrations for NMR Samples Containing HF

Contents	HF (m/o) Bulk	Maximum Liquid Phase	Minimum Liquid Phase
HF (3)[a]	100		
$HF-IF_7$ †	9.1 ± 0.4		
$HF-IF_7$ †[b]	88.9 ± 2.0		
$HF-IOF_5$	6.2 ± 1.0	6.2	3.3
$HF-IOF_5$	15.4 ± 1.0	15.2	13.6
$HF-IOF_5$ (†)[c]	26.7 ± 1.8	27.0	26.8
$HF-IOF_5$ (†)	50.5 ± 2.0	50.9	50.4
$HF-IOF_5$ (†)	75.1 ± 3.1	75.2	75.1
$HF-BrF_5$	10.8 ± 0.3	10.8	10.0
$HF-BrF_5$	26.3 ± 0.2	26.3	25.7
$HF-BrF_5$	50.2 ± 0.2	50.0	49.6
$HF-BrF_5$ (L)[d]	73.0 ± 3.5	72.9	72.8
$HF-BrF_5$	86.0 ± 3.3	86.4	86.3
$HF-BrF_5$	93.5 ± 3.3	93.5	93.4

[a]The number in parentheses indicates the number of samples of this concentration prepared.
[b]This symbol denotes a sample exhibiting two liquid phases at all temperatures studied.
[c]This symbol in parentheses denotes a sample having two liquid phases at some of the temperatures studied.
[d]The "L" indicates a sample having slow leak at seal.

Concentration calculations for solutions containing HF and only one liquid phase are summarized in Table III and were made in the following manner. The bulk concentrations in mole percent were first corrected for the amount of both components in the vapor phase at 25°C on the basis of ideal solution and ideal gas behavior. These values were considered an upper limit for the concentration of HF in the liquid phase at 25°C and appear in Column 3. A lower limit for the concentration of HF in the liquid phase was then estimated (see Column 4) by assuming that the HF component exerted its full room-temperature vapor pressure (920 Torr with an association factor of 3.5)[9a] while the second component was treated again as part of an ideal solution system.

CHAPTER IV

NMR MEASUREMENT TECHNIQUES

A. Synopsis of Instrument Usage

Two NMR spectrometers were employed during the course of this project, one located in the Argonne National Laboratory Chemistry Division and the other at The University of Wisconsin (UW). Most of the results reported in Ch. V were obtained with the ANL instrument. The UW spectrometer, because of its greater sweep width and radiofrequency power range, was used for the saturation study described in Sect. IVD and for all the IF_7 spectra obtained. The IF_7-IOF_5 system was run exclusively at UW; ^{19}F spectra in the HF-IOF_5 system were obtained with both instruments.

B. A56/60A Instrument at ANL

A Varian A56/60A NMR Spectrometer with a Varian V-4341 NMR Variable Temperature Accessory, and a Hewlett Packard Model 200 CDR Wide Range Oscillator with a Hewlett Packard Model 5212A Electronic Counter for sideband measurements, were used to obtain most of the ^{19}F spectra and all of the proton spectra described in Ch. V. The frequency-offset range of the spectrometer in the fluorine mode was easily expanded from the standard 19 to 32 kHz by installing thirteen additional crystals in the frequency-synthesizer section.

The substitution method of obtaining a ^{19}F "zero" reference line was employed, with a separate sample of CCl_3F (Matheson Co.) sealed in a 5-mm-OD glass spinner tube. Since it has been demonstrated that Kel-F exposed to liquid CCl_3F becomes slightly porous, the otherwise convenient method of using an annular CCl_3F reference sample in each glass-and-Kel-F NMR sample (see Fig. 11) was avoided. No direct attempts were made to determine bulk susceptibility corrections, except in the HF-BrF_5 system, for which an annular CCl_3F reference was used during the last run only, with negligible effect (<1 Hz) on the chemical shifts. A sample of pure HF (liquid) provided a reference line for the proton spectra obtained, again by the substitution method.

Sweep widths and frequency offsets were calibrated by the use of standard sidebanding technique with the CCl_3F sample. Care was taken to correct for the shifts induced by the relatively high oscillator amplitudes needed to produce the sidebands of higher frequency.

Temperatures were measured by switching the instrument to the proton mode, inserting a methanol sample, waiting about 10 min for temperature stabilization, and recording the chemical shift between the two methanol proton sites. Because of the rather large temperature gradient

set up along the length of the glass spinner tube, some uncertainty in the actual temperature of the spinning liquid samples was present, particularly in those samples having longer Kel-F tubes and/or longer liquid columns. For this reason, spinning was not always used when recording very wide lines (e.g., unresolved IOF_5 spectra).

Chemical shifts in Hz from CCl_3F (or in Hz from pure HF proton) were computed in most cases by combining sample and reference line positions, offset calibrations, and sweep-width calibrations. In a few cases (e.g., WF_6), a chemical shift was determined more directly by placing one or more CCl_3F sidebands near the recorded resonance and interpolating. Sweep-width calibrations were determined daily and after any large temperature change.

On a given work day, a selected set of chemically related samples was removed from cold storage, a temperature was chosen, spectrometer calibrations were made, and one particular resonance line was recorded from each of the samples run in succession. This method was chosen to provide maximum accuracy in determining changes of chemical shift and line width with solvent and concentration at a given temperature.

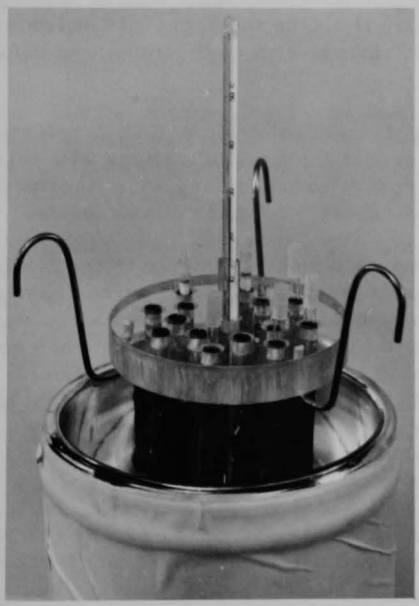

121-2243

Fig. 14. Photo of the Temperature Bath Used to Equilibrate NMR Samples before Taking Spectra

In order to minimize equilibration time of the samples in the probe, all of the samples (CCl_3F, CH_3OH, and mixtures) were placed in a constant temperature bath of appropriate temperature. A convenient bath which also keeps the sample tubes dry is shown in Fig. 14. It was made from several 7-in. lengths of 1/4-in.-OD copper tubing crimp-sealed at the bottom and force-fitted into a Lucite plate suspended in a large Dewar by three S-hooks. Water, ice and salt, and CCl_2F_2 (b.p.: -28°C) were used for baths from +35 to -35°C.

For a few samples in each mixture, system, a search was made over the full frequency range (-14 to +18 kHz from CCl_3F) for unexpected resonances arising from impurities or other sources such as rapid exchange. As is noted in Ch. V, no rapid exchange phenomena were

detected in the present studies; the few impurities which eventually showed up are noted in Sect. IIID.

C. Modified HA-60 at UW

A Varian HA-60 NMR Spectrometer modified by T. J. Scheffer,[26,27] in which the ^{19}F frequencies are derived from a frequency synthesizer and in which frequency sweeps of up to 100 kHz are possible, was used to record all the IF_7 spectra and also to carry out a saturation study in several samples.

For these measurements a Varian V-4331-THR Dewar Probe Insert containing a calibrated copper-constantan thermocouple was placed in the probe and carefully aligned with the spinner housing to help prevent breakage. Temperature regulation was achieved by passing nitrogen gas through the Dewar insert via an insulated connector. The nitrogen was obtained by boiling nitrogen gas at a variable rate out of a liquid nitrogen Dewar with a 25-ohm (Nichrome wire) heating element carrying a constant current supplied by a regulated dc power supply.

Temperatures were read directly from the thermocouple at frequent intervals with a Rubicon potentiometer. Samples were thermostated before running, as described in Sect. IVB.

The substitution method was again used to obtain a CCl_3F reference line; no sidebanding procedures were necessary for calibrations with this spectrometer. Samples were seldom spun when recording wide line spectra since spinning generally introduced "noise" at higher power levels.

HF ^{19}F spectra were recorded with the spectrometer in the 2-kHz field-modulation phase-sensitive detection mode, the Varian sweep system in operation, and the synthesizer set at approximately the sample resonance frequency. A CCl_3F sample was used to obtain a reference frequency and sweep-width calibrations. Chemical shifts in Hz from CCl_3F were calculated from relative line positions, the appropriate sweep calibration, and the respective synthesizer frequencies. Line widths of HF from these spectra were generally larger than from ANL spectra, due to the greater field inhomogeneity of the UW spectrometer.

The wider sweep widths required for IOF_5 (8 kHz) and IF_7 (16 kHz) spectra were obtained by placing the spectrometer in the frequency-sweep mode without 2-kHz field modulation. In this mode the synthesizer beat frequency was used to determine deviations from linearity of the sweep and to give an accurate frequency for at least one point in each individual spectrum. The exact frequency in Hz of any point in a given spectrum was then computed by interpolation. Frequencies for the NMR samples and the CCl_3F reference samples were determined in this way.

D. Saturation Study of IF_7 and IOF_5

A study of the dependence of the IF_7 and IOF_5 peak heights on the radiofrequency (rf) field strength H_1, as H_1 increased into the saturation range,[28,29] was carried out in an attempt to obtain an estimate of the longitudinal relaxation time T_1 in these compounds. Only the experimental procedure is described in this section; the treatment used to extract T_1 values from the peak-height data is given in Sect. VF.

The UW spectrometer was chosen for the saturation study because of its greater rf power range and because of the accessibility of this range to calibration, as described in Sect. IVE. The spectrometer was placed in the frequency-sweep mode without 2-kHz modulation.

Seven samples were selected and run at ambient probe temperature (29 ± 1°C) and at approximately -12°C. Each sample was allowed to equilibrate in the probe for about 10 min at high rf power level (at perhaps -10 db, corresponding to an H_1 of about 25 mG). The leakage was then minimized, and preliminary scans of the chosen line were made to find a 15-db rf power range which included several saturated traces as well as one which was not obviously saturated. An appropriate setting for signal amplification was also chosen.

After minimizing the leakage again, the line was recorded a few times at each of four or five H_1 settings in the chosen 15-db range, at constant signal amplification, beginning usually at the highest power level. A slow enough sweep was used to achieve maximal peak-height depressions.

In order to know the H_1 value corresponding to each rf power level setting as accurately as possible, the V-4311 attenuator buttons actually used were noted along with the corresponding V-4311 RF output voltage (see Sect. IVE).

An average maximum peak height A, measured in mm, was determined for IF_7 or IOF_5 at each rf power level setting; in a few cases, data for the IF_5 ν_A band were also available. These results are listed in Appendix I. The H_1 values shown were obtained by the procedure described in the next section.

E. Calibration of H_1

Radiofrequency field strengths H_1 were determined for the UW spectrometer at four high-power level settings of the V-4311 RF Unit by the sideband method of Anderson.[30] The calibration results were then used to calculate H_1 values for the lower power-level settings involved in the saturation study described in Sect. IVD.

In Anderson's method, the basic spectrometer frequency ω_s is modulated at some variable but well-known frequency ω_m, and the frequency separation between the modulation sidebands is studied as a function of ω_m for large, fixed rf field. A value of H_1 for this rf field can then be found in the following way. The applicable resonance condition for the sidebands produced is given by

$$\omega_m^2 = (\gamma H_0 - \omega_s)^2 + (\gamma H_1)^2, \tag{1}$$

where ω_s and ω_m are the spectrometer and modulation frequencies, respectively, in radian sec^{-1}, γ is the gyromagnetic ratio in radian sec^{-1} $gauss^{-1}$, H_0 is the static magnetic field strength in gauss, and H_1 is the rf field strength in gauss.

If the H_1 term in (1) is very small, as is usually the case in routine NMR work, the first modulation sidebands will appear as expected at $\pm\omega_m$ on either side of the center absorption band. For large H_1, however, the separation Δ of each sideband from the center absorption band will be reduced, as can be seen by rearranging (1) to give

$$\Delta^2 = (\gamma H_0 - \omega_s)^2 = \omega_m^2 - (\gamma H_1)^2. \tag{2}$$

Hence, for sufficiently large fixed rf power level, a plot of Δ^2 against ω_m^2, extrapolated to zero Δ^2, will yield $(\gamma H_1)^2$ as intercept. Note that since Δ^2 is extrapolated to zero, the sideband separation may be measured in any convenient arbitrary unit.

In practice, the sideband method is made feasible and accurate by detecting as well as modulating at ω_m, an approach which makes it possible to remove completely the strong center absorption band from the recorded spectrum. The sample chosen for this calibration procedure should, of course, have a simple one-line spectrum that does not saturate severely at the high rf power levels used.

Calibration of the UW spectrometer was carried out immediately before the saturation studies were begun, with the 5-mm Dewar probe insert already in place. A sealed 5-mm glass sample tube containing a pinch of NaF and about 2 atm of unpurified SiF_4 gas with an SiF_4 absorption-line half-width of 3.5 Hz was chosen for the calibration measurements.

The spectrometer was placed in the field-sweep mode and the usual 2-kHz modulation-detection system was replaced by the variable-frequency modulation and phase-sensitive detection system described by D. K. Hindermann.[31]

The rf field was calibrated at 5-, 7-, 10-, and 12-db nominal attenuation of the V-4311 RF Unit (preset for the standard 7-V rms output at 0-db attenuation). The actual attenuator buttons used and the corresponding rf output voltage (read from a panel meter) were noted for each power-level setting; the modulation frequencies ω_m were determined with a counter. The modulation index was maintained at a constant low value in order to avoid significant power loss to the sidebands. The phase of each sideband was adjusted individually to allow accurate determination of position. The four H_1 values obtained had an uncertainty of less than ±1%.

The high power levels required for the H_1 calibration were not used for the saturation studies, which were made, instead, in the vicinity of 40-db attenuation. Values of H_1 for the lower power-level settings were calculated from the calibrated H_1 values and a knowledge of the rf output voltages and attenuation factors for the attenuator buttons involved. Attenuation factors for three buttons (the 2-db, 3-db, and first 10-db buttons) were known directly from the current-H_1 calibration data. For the remaining buttons, attenuation factors were obtained from a previous calibration[32] or, in the case of the -20-db buttons, assumed to be given by their nominal value (0.10).

Values of H_1 calculated in this way generally had uncertainties of ±5-10%. Most of this was attributable to the relatively large uncertainties assigned to the attenuation factors taken from the earlier calibration which, although made at the same standard preset rf output voltage, involved a different probe insert and tuned capacitance.

CHAPTER V

EXPERIMENTAL RESULTS

A. General Data Treatment

This chapter contains all the NMR results obtained from the eight mixture systems, presented in graphical and condensed tabular forms. Except for IOF_5, all data were taken directly from conventional NMR traces; the customary experimental uncertainty based on a consideration of the accuracy of calibrations and peak locations was assigned. The use of computer-generated spectra to increase the accuracy of the IOF_5 results is described in Sect. VB.

Chemical shifts, as well as line half-widths and coupling constants, are given in Hz rather than parts per million because it was believed that this scale would provide the most lucid representation of their dependence on solute, concentration, and temperature. All results refer to liquid samples except where clearly marked otherwise. In certain figures, data from the two samples which were leaking slowly have been included and are marked with an "L."

The tables show the values obtained for each mixture component as a pure substance and in the limit of infinite dilution in certain solvents, at both the highest and lowest temperatures studied. Values at infinite dilution were chosen by graphical extrapolation of the pertinent experimental data.

Considerable difficulty was encountered in obtaining meaningful spectra from those samples exhibiting two liquid phases. Their spectra reflected a sensitivity to temperature gradients, spinning, and meniscus location. It was assumed that a lower liquid phase of less than 3-mm length, or an upper liquid phase above a 40-mm (or longer) lower phase could not affect or contribute to the observed spectrum. For samples with the phase boundary between these limits, however, the spectra obtained suggested that lines were often shifted and sometimes broadened by the presence of two different phases in the vicinity of the receiver coil; data from such samples were reluctantly discarded.

The assignment of the reliable spectra from two-phase samples to the upper or lower liquid phase is indicated in the figures by the filling-in of the corresponding portion of the symbol. Each such point is plotted against the bulk sample composition, which is believed to be close to although not exactly equal to the composition of the indicated (upper or lower) liquid phase.

B. Computer Programs for Fitting IOF_5 Spectra

Chemical shifts, intrinsic line widths, and ^{19}F-^{19}F spin-coupling constants for the IOF_5 multiplet components were obtained by fitting NMR traces with spectra generated by computer programs.

The fluorine nuclei in IOF_5 are an example of an AB_4 spin system possessing C_{4v} symmetry,[3-5,21,33] the general analysis of which is well known in high resolution NMR.[34-36] Fortunately, further splitting of the ^{19}F lines due to the ^{127}I (spin 5/2) nucleus is not observed because of the very rapid relaxation of the ^{127}I nuclear spin states via the nuclear quadrupole-coupling mechanism.[37]

A CDC 3600 computer was used for the numerical calculations, and punched output from it was then plotted by an IBM 1620 on-line Calcomp incremental plotter.

Stick Spectra. The expressions of Emsley, Feeney, and Sutcliffe for the AB_4 spin system[36] were used to calculate the relative positions and intensities of the 25 fluorine transitions, which are determined by the absolute value of the dimensionless ratio (RATIO) of the spin-spin coupling constant J_{FF} (in Hz) to the chemical shift

$$\nu_0\delta_{AB} = \nu_A - \nu_B$$

(where δ_{AB} is dimensionless) of the B-band center ν_B (Hz) from the A-band center ν_A (Hz).

From previously reported partially resolved IOF_5 spectra, this ratio was known to be about 0.13.[3,4,6] Spectra were calculated for several values of $(J_{FF}/\nu_0\delta_{AB})$ in this region by a program entitled AB4FIT and were plotted as stick spectra on a scale suitable for direct comparison with NMR sample traces. A typical trace and a matching stick spectrum are shown in Fig. 15.

An accurate assignment (to within ~1%) of the ratio for a given NMR trace could be made only for fairly well resolved spectra (line half-widths of 100 Hz or less). In most of these cases the ratio was found to be 0.136 ± 0.002, ranging from 0.134 ± 0.002 for the most concentrated solutions of IOF_5 in IF_5, to 0.138 ± 0.001 for dilute solutions of IOF_5 in IF_5 at temperatures below 0°C. In well-resolved spectra, the matching of stick spectra also provided an accurate means of locating ν_A and ν_B. From the ratio and $\nu_0\delta_{AB}$, values of J_{FF} were calculated. These results are given in Sect. VE.

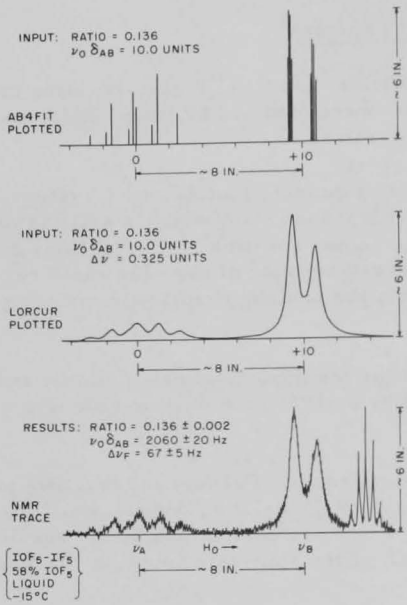

Fig. 15. Typical ^{19}F NMR Spectrum of IOF_5 Dissolved in IF_5, with Matching Computed Stick Spectrum and Matching Computed Spectral Envelope Curve. Symbols are defined in Sect. VB.

Spectral Envelope Curves. During the fitting of well-resolved NMR traces with stick spectra, which concentrated on correct line positions, it became apparent that the 25 lines in a given IOF_5 spectrum had nearly the same line width. Consequently, a program called LORCUR was written which calculated a spectral envelope from the appropriate stick-spectrum data by assuming that all 25 lines had a Lorentzian line shape[38] with the same intrinsic half-width at half-height $\Delta\nu$. The envelope was calculated by LORCUR at 500 points in the spectrum, and the punched output was plotted on a scale close to that of the NMR trace, as shown in Fig. 15.

For the fitting of well-resolved NMR spectra, the value of RATIO from the matching stick spectrum was chosen, of course; for all less well-resolved NMR spectra, the value of 0.136 ± 0.002 was assumed in the computation.

The computed curves were used to make a good choice of ν_A, ν_B, and the baseline for all the NMR traces of IOF_5; when a good fit of the two curves was achieved, the input half-width $\Delta\nu$ for the computed curve was noted and converted from the arbitrary program units to $\Delta\nu_F$ in Hz. Line widths and chemical shifts obtained in this manner are given in the next two sections of this chapter.

No difficulties were encountered in obtaining a good fit of the IOF_5 NMR traces with these computed curves for half-widths ranging from 300 Hz down to 25 Hz, where the well-resolved lines are particularly sensitive to a bad choice of line-shape function. Repeated scans with a digital storage unit (CAT) of very well-resolved ν_A bands, in which a few single transitions could be distinguished, gave further support to the assumption of a Lorentzian line shape for the multiplet components.

C. Chemical Shifts

All chemical shifts are presented in Hz from liquid CCl_3F or in Hz from pure liquid HF proton, determined by the straightforward substitution

methods described in Sects. IVB and IVC. A positive value of the chemical shift indicates a resonance which occurs at a frequency higher than that of the CCl_3F or HF proton line (i.e., at a lower field than the reference line). Note that this sign convention is the opposite of the sign convention customarily adopted when reporting chemical shifts in ppm.

There was no need to correct any of the data for a difference in static H_0 field between the CCl_3F reference line and the spectrum of interest, since both of the spectrometers employed are based on a frequency-sweep principle. (The Varian A56/60A uses field sweep only to produce sidebands, to produce small "sweep offsets" of up to 1 kHz, and to scan the chosen sweep width.)

To convert the ^{19}F data to ppm from CCl_3F, the frequency of the CCl_3F reference line must be known. This frequency is 56.4633 MHz for the ANL instrument and 56.4560 MHz for the UW spectrometer; the difference between the two static H_0 fields therefore amounts to 129 ± 2 ppm, which happens to be less than or of the same order of magnitude as the experimental uncertainties in the observed chemical shifts. Thus, all the chemical shifts reported here were measured at the same static H_0 field within experimental error. To obtain chemical shifts relative to some other reference, such as gaseous SiF_4, a correction for change of field such as is detailed by Alexakos and Cornwell[39] may be necessary. Hindermann and Cornwell have recently published a revised table of absolute shielding constants for ^{19}F, to which the results presented here can also be readily related.[40]

Chemical shifts of the ν_A and ν_B bands for IOF_5 were determined after fitting NMR traces with the computer-generated spectra described in Sect. VB. Extrapolated results for all five mixture systems containing IOF_5 are presented in Table IV. Since the data for IOF_5 in IOF_5-WF_6 and IOF_5-IF_7 solutions did not show any interesting dependence (within experimental error) on solute, concentration, or temperature, they are not plotted. Data for the other three mixture systems are shown in Fig. 16.

TABLE IV. Extrapolated Chemical Shifts for IOF_5

NMR of	In	T (°C)	ν_A[a]	ν_B[a]	$\nu_0\delta_{AB}$[b]
IOF_5	IOF_5	23 ± 2	6,005 ± 20	3,890 ± 10	2,115 ± 30
		11 ± 1	6,010 ± 20	3,895 ± 10	2,115 ± 30
	WF_6	36 ± 1	6,000 ± 30	3,890 ± 20	2,110 ± 50
		5 ± 1	6,000 ± 30	3,870 ± 30	2,130 ± 60
	IF_7	23 ± 1		3,820 ± 30	
		10 ± 1		3,820 ± 30	
	BrF_5	22 ± 2	6,005 ± 20	3,990 ± 10	2,015 ± 30
		-35 ± 3	5,982 ± 10	3,980 ± 10	2,000 ± 20
	IF_5	23 ± 2	6,050 ± 20	4,000 ± 10	2,050 ± 30
		-15 ± 1	6,020 ± 10	3,990 ± 10	2,030 ± 20
	HF[c]	31 ± 2	5,960 ± 50	3,890 ± 20	2,070 ± 70

[a]Chemical shift in Hz from CCl_3F, determined with the aid of computer programs (see Sect. VB).
[b]$\nu_0\delta_{AB} = \nu_A - \nu_B$; in Hz.
[c]Values listed are for lower liquid phase, IOF_5 saturated with HF (~50 m/o; see Fig. 16a). Data for extrapolation to infinite dilution in HF not available.

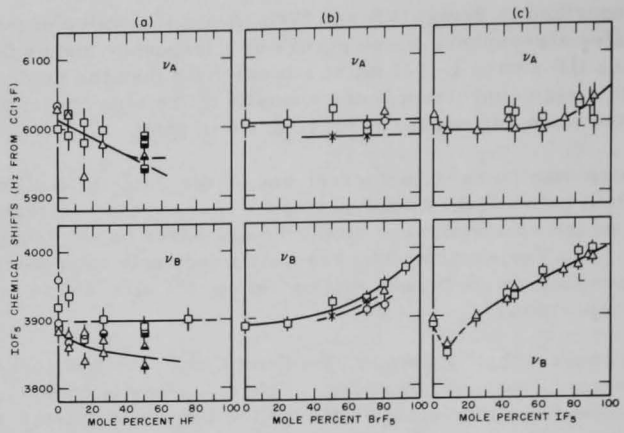

Fig. 16. Chemical Shifts for IOF_5 (ν_A and ν_B bands): a) in HF-IOF_5 Solutions, □ 31 ± 2°C, △ 22 ± 1°C, and ○ 10 ± 2°C. Half-filled symbol denotes a sample with two liquid phases. b) in IOF_5-BrF_5 Solutions, □ 22 ± 2°C, △ -15 ± 1°C, ○ -25 ± 2°C, and × -35 ± 3°C. c) in IOF_5-IF_5 Solutions (liquids only), □ 23 ± 2°C, and △ 11 ± 1°C. Data for solutions at -15 ± 1°C and -25 ± 2°C are very similar but are not shown.

Data obtained for IF_7 are characterized by the large uncertainties inherent in determining the center of its broad, unresolved doublet spectrum.[41,42] Chemical shifts are presented only in extrapolated tabular form (see Table VI). The spectrum of IF_7 in IF_5-IF_7 solutions was apparently the same as that of pure IF_7; unfortunately, no CCl_3F reference frequency was available for the NMR traces of IF_7 in these solutions, so that chemical shifts could not be computed.

The spectrum of IF_7 saturated with HF was also the same as that of pure IF_7, although probably shifted 300 ± 300 Hz to lower frequency.

Results for WF_6, in both solid and liquid samples, are presented in Fig. 17a and Table V. A value of the liquid-to-solid chemical shift of pure WF_6 at -3.5°C, given in Table VI, was measured directly from the spectrum of a sample observed to contain both solid and supercooled liquid WF_6. A value of the liquid-to-solid chemical shift for WF_6 at infinite dilution in IOF_5 was also obtained (see Table V) by assuming that the concentration dependence of the chemical shifts in liquid WF_6-IOF_5 solutions at -3.5°C would in fact parallel that observed at 11°C (see Fig. 17a).

HF proton data were obtained at only one temperature, 20°C, and are shown in Fig. 17b. Extrapolations to infinite dilution were not attempted. Data from samples with two liquid phases are plotted against bulk compositions, as actual phase concentrations were unknown. The phase assignments shown

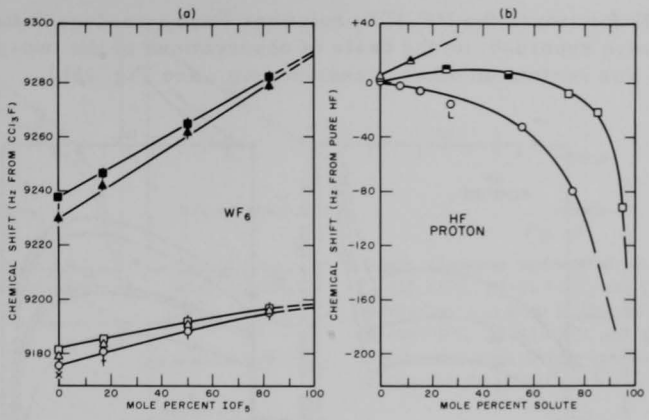

Fig. 17. a) ^{19}F Chemical Shift for WF_6 in IOF_5-WF_6 Solutions. Liquids: □ +36 ± 1°C, △ +23 ± 2°C, ○ +11 ± 1°C, + +5 ± 1°C, and × -3.5 ± 1°C (supercooled). Solids: ■ -3.5 ± 1°C and ▲ -12 ± 1°C. b) HF Proton Chemical Shift at 20 ± 1°C, △ HF-IF_7, □ HF-IOF_5, and ○ HF-BrF_5. Experimental errors in these data are smaller than the symbol size would indicate. Half-filled symbol denotes a sample with two liquid phases.

TABLE V. Liquid-to-Solid Chemical Shifts for WF_6 at -3.5 ± 1°C

WF_6	$\nu(s)^a$	$\nu(\ell)^a$	$\nu(s) - \nu(\ell)^b$	$\frac{\sigma(s) - \sigma(\ell)^c}{1 - \sigma_r}$
Pure	9,238 ± 2	9,172 ± 2	66 ± 4	-1.17 ± 0.07
In IOF_5	9,291 ± 2	9,195 ± 2[d]	96 ± 4	-1.70 ± 0.07

[a]Chemical shift of WF_6 in Hz from CCl_3F.
[b]In Hz.
[c]Difference in shielding constants, in ppm. σ_r for CCl_3F is given in Ref. 40.
[d]By inference from liquid solution data at 11 ± 1°C (see Fig. 17a).

TABLE VI. Extrapolated Chemical Shifts for IF_7, WF_6, and HF Fluorine

NMR of	In	T (°C)	Hz from CCl_3F	T (°C)	Hz from CCl_3F
IF_7	IF_7	30 ± 2	9,400 ± 400	10 ± 1	9,200 ± 200
	IOF_5	23 ± 1	9,100 ± 800	10 ± 1	9,100 ± 200
WF_6	WF_6	36 ± 1	9,182 ± 2	-3.5 ± 1	9,172 ± 2
	IOF_5	36 ± 1	9,198 ± 2	11 ± 1	9,197 ± 2
WF_6 (s)[a]	WF_6	-3.5 ± 1	9,238 ± 2	-12 ± 1	9,230 ± 2
	IOF_5	-3.5 ± 1	9,291 ± 2	-12 ± 1	9,290 ± 2
HF fluorine[b]	HF	15 ± 2	-11,230 ± 5	-40 ± 3	-11,077 ± 5

[a]Data from solid samples.
[b]Measured on Varian A56/60A at ANL.

in Fig. 17b for two of the HF-IOF_5 solutions were introduced after the spectra were recorded, on the basis of observations of the two-phase behavior of this system on other occasions (e.g., see Fig. 18b).

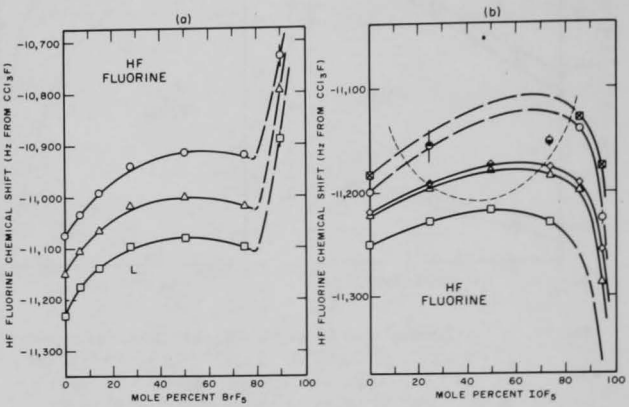

Fig. 18. HF Fluorine Chemical Shift: a) in HF-BrF_5 Solutions, □ +15 ± 1°C, △ -14 ± 1°C, and ○ -40 ± 3°C. b) in HF-IOF_5 Solutions, □ +30 ± 2°C, △ +22 ± 1°C, ◇ +21 ± 1°C, ○ +9 ± 1°C, and ⊠ +6 ± 1°C. Half-filled symbol denotes a sample having two liquid phases. A rough estimate of the liquid-liquid phase boundary for this mixture system has been sketched in (finely dashed line).

The single result for HF proton in HF-IF_7 mixtures was assigned to the upper of the two liquid phases, HF saturated with IF_7. No HF proton or HF fluorine signal was detected from the lower phase (IF_7 saturated with HF) in the other available sample in this mixture system.

The behavior shown here for the HF proton in HF-BrF_5 solutions (Fig. 17b) agrees very well with proton results obtained by R. Field.[43]

In the HF-BrF_5 mixture system, one sample (73 m/o HF) was known to be leaking slowly at the seal. This fact is reflected in the chemical shifts recorded for the proton as well as for all the fluorines in this sample (see Figs. 17b, 18a, and 19a), which indicate clearly that, as would be expected, the sample was losing more HF than BrF_5.

It has been established that in pure liquid HF the ^{19}F chemical shift varies linearly (within experimental error) with the temperature, shifting to higher field (i.e., lower frequency) as the temperature is raised from -50 to +30°C, at the rate of 2.7 ± 0.1 Hz per °C.[44] Chemical shifts for the HF fluorine in HF-BrF_5 and HF-IOF_5 solutions are presented in Figs. 18a and 18b, but do not appear in the tables because it was not possible to obtain reliable extrapolated values for either mixture system.

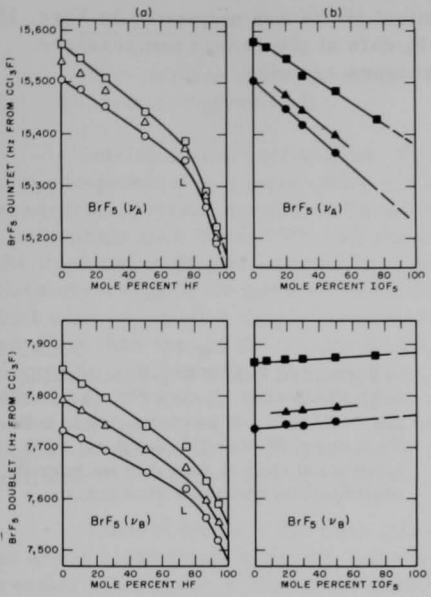

Fig. 19

a) BrF_5 Chemical Shifts in HF-BrF_5 Solutions, □ +16 ± 1°C, △ -14 ± 1°C, and ○ -38 ± 3°C.
b) BrF_5 Chemical Shifts in IOF_5-BrF_5 Solutions, ■ +22 ± 2°C, ▲ -23 ± 2°C, and ● -35 ± 3°C.
Experimental errors in these data are generally smaller than the symbol size would indicate.

Chemical shifts for the HF fluorine in HF-IOF_5 solutions at 9, 22, and 30°C were measured with the UW spectrometer and were consistently found to be about 25 Hz larger than the same shifts measured with the ANL instrument. To facilitate comparison, a 25-Hz correction was added to the UW data before they were plotted in Fig. 18b, since the principal point of interest here is the dependence on concentration.

The more reliable data from samples with two liquid phases are included in Fig. 18b, plotted against bulk compositions, which in this case should be fairly close to the concentrations in the assigned phases. It is possible to make a rough estimate of the liquid-liquid phase boundary for this system, as is also indicated in Fig. 18b.

An attempt is in progress to uncover the source of the 25-Hz systematic error. However, the outcome of this investigation cannot significantly affect the remainder of the UW chemical-shift data, since the latter are concerned with the relatively very wide lines of IF_7 and IOF_5.

The HF fluorine signal in mixtures with IF_7, like the proton signal in this same system, was detected in only one sample, 89 bulk m/o HF (two liquid phases). At both 9 and 22°C, it was assigned to the upper liquid phase (HF saturated with IF_7) and had a chemical shift similar to that of the HF fluorine in IOF_5 solutions in the same concentration region. These data are neither plotted nor tabulated.

Results for BrF_5 and IF_5 chemical shifts are presented in Figs. 19 and 20, and in Table VII. The IOF_5-IF_5 data at the lowest temperature probably include supercooled liquid mixture samples.

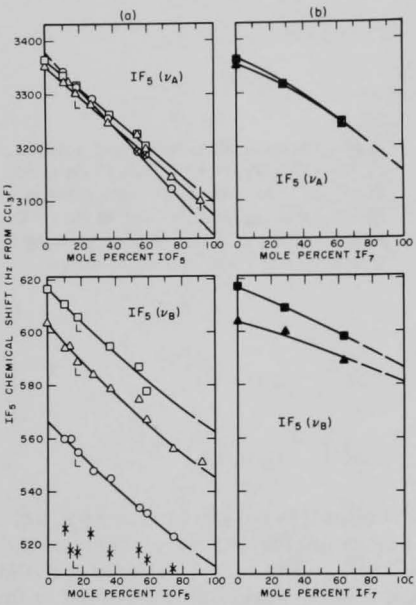

Fig. 20

a) IF_5 Chemical Shifts in IOF_5-IF_5 Solutions (liquids only), □ +23 ± 2°C, △ +11 ± 1°C, ○ -15 ± 1°C, and × -25 ± 2°C. b) IF_5 Chemical Shifts in IF_5-IF_7 Solutions, ■ +23 ± 2°C, and ▲ +11 ± 1°C. Experimental errors in these data are generally smaller than the symbol size would indicate.

TABLE VII. Extrapolated Chemical Shifts for BrF_5 and IF_5

NMR of	In	T (°C)	ν_A [a]	ν_B [a]	$\nu_0\delta_{AB}$ [b]
BrF_5	BrF_5	22 ± 2	15,580 ± 4	7,864 ± 10	7,716 ± 15
		-38 ± 3	15,505 ± 5	7,732 ± 5	7,773 ± 10
	HF	16 ± 1	15,160 ± 20	7,550 ± 10	7,610 ± 30
		-38 ± 3	15,130 ± 20	7,480 ± 10	7,650 ± 30
	IOF_5	22 ± 2	15,377 ± 5	7,882 ± 5	7,495 ± 10
		-35 ± 3	15,227 ± 15	7,763 ± 5	7,464 ± 20
IF_5	IF_5	23 ± 2	3,363 ± 5	616 ± 1	2,747 ± 6
		11 ± 1	3,352 ± 5	604 ± 1	2,748 ± 6
	IOF_5	23 ± 2	3,100 ± 10	563 ± 5	2,537 ± 15
		-15 ± 1	3,035 ± 10	512 ± 3	2,523 ± 13
	IF_7	23 ± 2	3,150 ± 20	586 ± 2	2,564 ± 22
		11 ± 1	3,150 ± 20	580 ± 5	2,570 ± 25

[a] Chemical shift in Hz from CCl_3F.
[b] $\nu_0\delta_{AB} = \nu_A - \nu_B$; in Hz.

D. Line Half-widths

This section contains results of the measurement of line half-widths, $\Delta\nu$. All data are given in Hz.

Intrinsic line half-widths, $\Delta\nu_F$, were determined for the IOF_5 multiplet components by successfully fitting the NMR traces with computer-generated spectral envelopes based on Lorentzian-shaped multiplet components (see Sect. VB). All the IOF_5 results presented here are for the ν_B-band multiplet components, as that band could be fitted most accurately owing to its greater intensity. In general, however, it was found that each ν_A-band multiplet components had an intrinsic half-width 15 ± 5% smaller than that of the ν_B-band multiplet components in the same spectrum. Some idea of this effect may be seen by a careful scrutiny of Fig. 15, in which the computed curve, based on a single value of the line width, provides a good fit for the ν_B band but is less resolved than the actual ν_A band. Signal-to-noise ratio problems with the ν_A band discouraged attempts at refining the results for the ν_A-band multiplet components any further.

Line-width data for pure IOF_5 were taken with the ANL instrument at about 4° intervals over the temperature range from -40 to +10°C, and the results are shown in Fig. 21a. (Line-width data obtained on other occasions were in good agreement and are included in Fig. 21a.) About 15 min of equilibration time was allowed at each temperature setting. In the vicinity of the expected melting point (4.6°C), the state of the sample was observed by eye immediately after recording each spectrum.

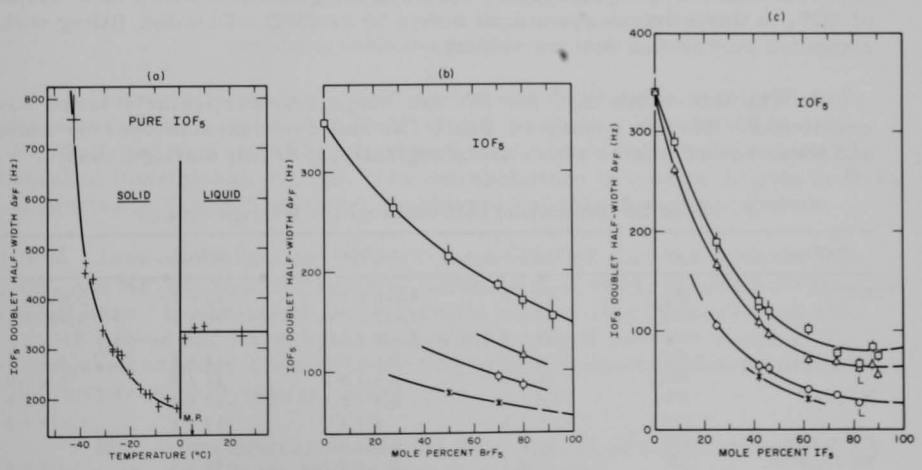

Fig. 21. IOF_5 Fitted Half-width $\Delta\nu_F$ (ν_B-band multiplet components only): a) in Pure IOF_5 as a Function of Temperature. b) in IOF_5-BrF_5 Solutions, □ 22 ± 2°C, △ -15 ± 1°C, ○ -25 ± 2°C, and × -40 ± 3°C. c) in IOF_5-IF_5 Solutions (liquids only), □ 23 ± 2°C, △ 11 ± 1°C, ○ -15 ± 1°C, and × -25 ± 2°C.

The IOF_5 line width (see Table VIII) was virtually unaffected by dissolution in WF_6, in solid as well as in liquid samples it may have been slightly increased by dilution in HF, as is indicated in Table VIII. Because of the smallness of the observed effects, the magnitude of the experimental uncertainties, and the difficulties of phase assignments in the HF-IOF_5 system, line-width data for IOF_5 in these two mixture systems are not plotted here.

TABLE VIII. Extrapolated Intrinsic Half-widths for the ν_B-band Multiplet Components for IOF_5[a]

NMR of	In	T (°C)	$\Delta\nu_F$ (Hz)	T (°C)	$\Delta\nu_F$ (Hz)
IOF_5	IOF_5	23 ± 2	325 ± 20	11 ± 1	340 ± 15
	IOF_5 (s)[b]	0 ± 2	180 ± 10	-43 ± 3	760 ± 50
	WF_6	36 ± 1	350 ± 30	5 ± 1	330 ± 30
	BrF_5	22 ± 2	147 ± 5	-40 ± 3	55 ± 5
	IF_5	23 ± 2	82 ± 5	-15 ± 1	27 ± 3
	HF[c]	25 ± 2	380 ± 40		

[a]Determined with the aid of computer programs (see Sect. VB).
[b]Data from solid sample.
[c]Value listed is for lower liquid phase, IOF_5 saturated with HF (~50 m/o; see Fig. 16a). Data for extrapolation to infinite dilution in HF not available.

Fitted half-widths for IOF_5 in IOF_5-BrF_5 and IOF_5-IF_5 solutions show marked solvent effects, as can be seen in Figs. 21a and 21b, and in Table VIII.

Data for IOF_5 in the IOF_5-IF_7 mixture system were obtained only with the UW spectrometer, using an 8-kHz or 16-kHz sweep width. There was no apparent narrowing or broadening effect of the gross measured band widths of IOF_5 in this mixture system, at either 10 or 23°C. Detailed fitting with computed curves was not carried out.

The line-width data for IF_7 are subject to particularly large uncertainties. Results appear in Table IX, and are characterized by solvent and temperature effects which are marginally, if at all, distinguishable.

TABLE IX. Extrapolated Half-widths for IF_7, WF_6, and Pure HF

NMR of	In	T (°C)	$\Delta\nu$ (Hz)	T (°C)	$\Delta\nu$ (Hz)
IF_7	IF_7	29 ± 2	4,000 ± 75	10 ± 1	3,800 ± 75
	IOF_5	23 ± 2	3,850 ± 150	10 ± 1	3,850 ± 150
	IF_5	29 ± 2	4,000 ± 150		
WF_6	WF_6	36 ± 1	0.6 ± 0.1	11 ± 1	0.5 ± 0.1
	IOF_5	36 ± 1	0.5 ± 0.1	11 ± 1	0.4 ± 0.1
WF_6 (s)[a]	WF_6	-3.5 ± 1	6.5 ± 0.5	-12 ± 1	14 ± 0.5
	IOF_5	-3.5 ± 1	8 ± 1	-12 ± 1	18 ± 2
HF proton	HF	20 ± 1	0.9 ± 0.1		
HF fluorine	HF	21 ± 1	0.5 ± 0.1	-40 ± 3	1.8 ± 0.1

[a]Data from solid samples.

Figure 22a shows WF_6 half-widths as a function of temperature in pure WF_6 and in IOF_5 solutions. The measurements extended into the solid-sample range (below 2.3°C, Ref. 45), where there is known to be a solid-solid phase transition in pure WF_6 at 8.2°C.[45] Extrapolated results are given in Table IX.

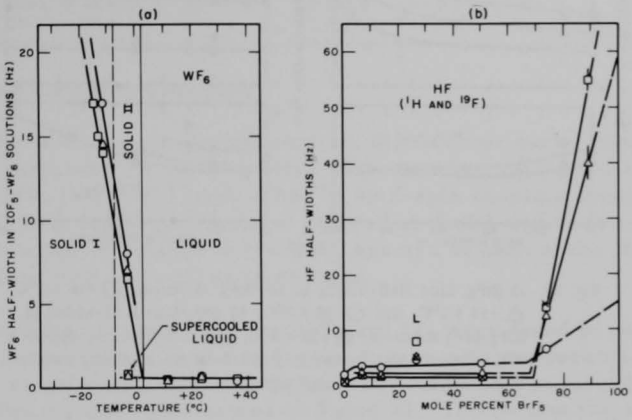

Fig. 22. a) WF_6 Line Half-width $\Delta\nu$ in IOF_5-WF_6 Solutions as a Function of Temperature, □ Pure WF_6 Sample, △ 16 and 50 m/o IOF_5 Solutions, and ○ 82 m/o IOF_5 Solution. b) HF Proton and Fluorine Line Half-widths in HF-BrF_5 Solutions, × Proton at +20 ± 1°C, □ Fluorine at +15 ± 1°C, △ Fluorine at -14 ± 1°C, and ○ Fluorine at -40 ± 3°C. Experimental errors in these data are generally smaller than the symbol size would indicate.

Line-width results for HF proton and HF fluorine in the HF-BrF_5 mixture system are found in Fig. 22b and Table IX. For the HF in each HF-BrF_5 solution at 20°C, proton half-widths were found to be essentially equal to fluorine half-widths. The extrapolations to infinite dilution in BrF_5 suggested in Fig. 22b were not considered reliable enough to tabulate.

Line-width data for both HF proton and HF fluorine from the HF-IOF_5 and HF-IF_7 mixture systems, although numerous, are not presented in detail here. In essentially every sample studied (see Figs. 17b and 18b), the HF proton and HF fluorine half-widths ranged between 1 and 2 Hz (compared to about 1 Hz for pure HF) with no well-defined dependence on the temperature or concentration.

Half-width measurements for BrF_5 and IF_5 in two mixture systems each are shown in Figs. 23 and 24 and in Table X.

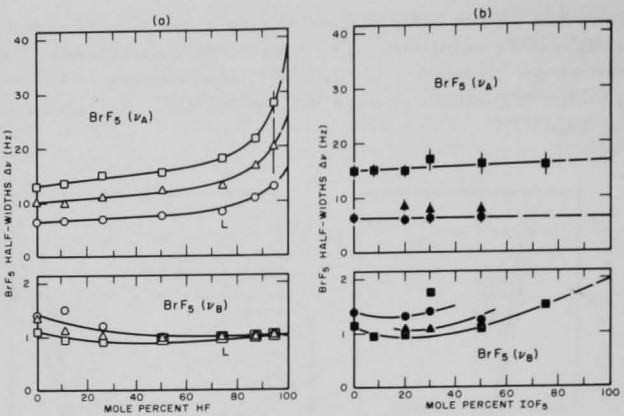

Fig. 23. a) BrF_5 Line Half-widths in HF-BrF_5 Solutions, □ +16 ± 1°C, △ -14 ± 1°C, and ○ -38 ± 3°C. b) BrF_5 Line Half-widths in IOF_5-BrF_5 Solutions, ■ +22 ± 2°C, ▲ -23 ± 2°C, and ● -35 ± 3°C. Experimental errors in these data are generally smaller than the symbol size would indicate.

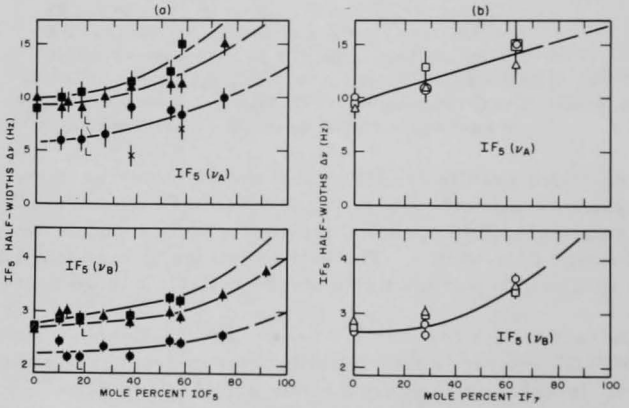

Fig. 24. a) IF_5 Line Half-widths in IOF_5-IF_5 Solutions (liquids only), ■ +23 ± 2°C, ▲ +11 ± 1°C, ● -15 ± 1°C, and × -25 ± 2°C. b) IF_5 Line Half-widths in IF_5-IF_7 Solutions, □ +23 ± 2°C, △ +20 ± 5°C, and ○ +11 ± 1°C.

TABLE X. Extrapolated Half-widths for BrF_5 and IF_5

NMR of	In	T (°C)	$\Delta\nu_A$ (Hz)	$\Delta\nu_B$ (Hz)	T (°C)	$\Delta\nu_A$ (Hz)	$\Delta\nu_B$ (Hz)
BrF_5	BrF_5	22 ± 2	15 ± 1	1.1_5 ± 0.1	-38 ± 3	6.4 ± 0.3	1.4 ± 0.1
	HF	16 ± 1	40 ± 5	1.0 ± 0.2	-38 ± 3	16 ± 3	1.0 ± 0.2
	IOF_5	22 ± 2	16 ± 2	2.0 ± 0.5	-35 ± 3	6 ± 1	
IF_5	IF_5	23 ± 2	10.0 ± 0.5	2.7_5 ± 0.1	11 ± 1	9.5 ± 0.5	2.7_5 ± 0.1
	IOF_5	23 ± 2	24 ± 5	4.7 ± 0.5	-15 ± 1	12.5 ± 2	3.0 ± 0.3
	IF_7	23 ± 2	17 ± 2	5 ± 1	11 ± 1	17 ± 2	5 ± 1

E. Spin-Spin Coupling Constants

In three of the compounds studied, the fluorine nuclei possess C_{4v} symmetry, and their ^{19}F NMR spectra are classified as of the AX_4 (for BrF_5 and IF_5) or AB_4 (for IOF_5) type. The ^{19}F spin-spin coupling constant J_{FF} for the coupling between the two sets of equivalent nuclei was measurable from resolved multiplet splittings in the NMR spectra of each of the three compounds in pure form as well as in solution.

Coupling constants J_{FF} for BrF_5 and IF_5 were found to vary with solute and concentration, and to a lesser degree with temperature. These variations, as exhibited by the BrF_5 and IF_5 doublet (ν_B band) splittings, are plotted in Fig. 25 and summarized in Table XI. The quintet (ν_A band) splittings are in agreement with the doublet data, but were not in general obtained to better than ±1 Hz. The J_{FF} values were taken directly from the doublet line separations in Hz, since both the line widths (see Table X) and the ratio of J_{FF} to $\nu_0\delta_{AB}$ (also shown in Table XI) remained small in all cases studied.

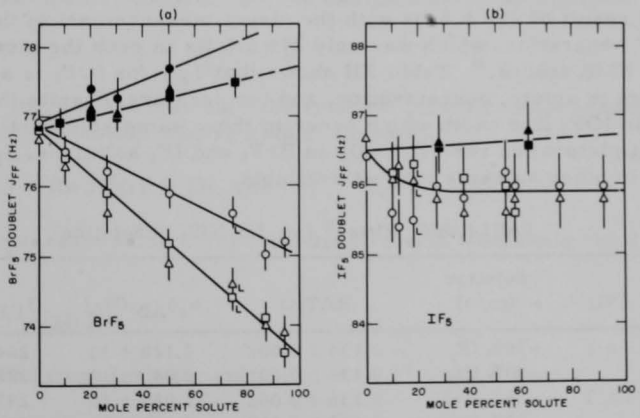

Fig. 25. a) Fluorine Spin-Spin Coupling Constant of the BrF_5 Doublet (ν_B) in HF-BrF_5 Solutions, □ +16 ± 1°C, △ -14 ± 1°C, and ○ -38 ± 3°C; and in IOF_5-BrF_5 Solutions, ■ +22 ± 2°C, ▲ -23 ± 2°C, and ● -35 ± 3°C. b) Fluorine Spin-Spin Coupling Constant of the IF_5 Doublet (ν_B) in IOF_5-IF_5 Solutions (liquids only), □ +23 ± 2°C, △ +11 ± 1°C, and ○ -15 ± 1°C; and in IF_5-IF_7 Solutions, ■ +23 ± 2°C and ▲ +11 ± 1°C.

TABLE XI. Extrapolated J_{FF} and Calculated RATIO Values for BrF_5 and IF_5 in Solution

NMR of	In	T (°C)	J_{FF} (Hz)	$\nu_0\delta_{AB}$ (Hz)[a]	RATIO x 10^2
BrF_5	BrF_5	22 ± 2	76.8 ± 0.2	7,716 ± 15	9.95 ± 0.05
		-35 ± 3	76.8 ± 0.2	7,773 ± 10	9.88 ± 0.04
	IOF_5	22 ± 2	77.7 ± 0.1	7,495 ± 10	10.37 ± 0.03
		-35 ± 3	78.4 ± 0.3	7,464 ± 20	10.50 ± 0.07
	HF	16 ± 1	73.6 ± 0.1	7,610 ± 30	9.67 ± 0.05
		-35 ± 3	75.0 ± 0.2	7,650 ± 30	9.80 ± 0.07
IF_5	IF_5	23 ± 1	86.5 ± 0.4	2,747 ± 6	31.5 ± 0.2
		11 ± 1	86.5 ± 0.2	2,748 ± 6	31.5 ± 0.1
	IF_7	23 ± 1	86.7 ± 0.2	2,564 ± 22	33.8 ± 0.3
		11 ± 1	86.7 ± 0.3	2,570 ± 25	33.7 ± 0.4
	IOF_5	23 ± 1	85.9 ± 0.2	2,537 ± 15	33.9 ± 0.3
		-15 ± 1	85.9 ± 0.3	2,523 ± 13	34.0 ± 0.3

[a]These are extrapolated values of $\nu_A - \nu_B$ and appear first in Table VII.

The J_{FF} data shown in Fig. 25a for the HF-BrF_5 system at 16°C include a correction of +1%, which was needed to bring the J_{FF} value obtained for pure BrF_5 into line with other data for pure BrF_5. The original source of this error probably lies in an incorrect calibration of the 250-Hz sweep width for that day.

Table XII presents J_{FF} results for IOF_5 obtained by fitting well-resolved NMR spectra with computer-generated curves. That the computer approach described in Sect. VB was necessary is clear when one compares the fitted result of 284 ± 5 Hz with the direct measurement of the ν_B-band "doublet" separation, which was only 275 ± 5 Hz in even the most well-resolved NMR traces.[46] Table XII shows that J_{FF} for IOF_5 is apparently insensitive to solute, concentration, and temperature, despite the significant changes in IOF_5 line width which occur in these same solutions. Since the IOF_5 multiplets were resolved only in BrF_5 and IF_5 solutions, J_{FF} results for IOF_5 in other solvents are not available.

TABLE XII. Fitted[a] J_{FF} for IOF_5 in Solution

T (°C)	Solution (m/o)	RATIO	$\nu_0\delta_{AB}$ (Hz)	J_{FF} (Hz)
-15 ± 1	~10% IF_5	0.134 ± 0.002	2,120 ± 30	284 ± 5
	~90% IF_5	0.138 ± 0.001	2,040 ± 30	282 ± 5
-35 ± 3	50% BrF_5	0.136 ± 0.002	2,080 ± 20	283 ± 5
	70% BrF_5	0.138 ± 0.002	2,060 ± 20	284 ± 5

[a]Values of RATIO and $\nu_0\delta_{AB}$ were determined for resolved IOF_5 spectra with the aid of computer programs (see Sect. VB).

F. Longitudinal Relaxation Times in IF_7 and IOF_5

The "progressive saturation" method of determining a longitudinal relaxation time T_1 was first suggested by Bloembergen, Purcell, and Pound (BPP) in 1948.[28,29] In the original paper, this method was applied to simple spin-$\frac{1}{2}$ systems whose longitudinal relaxation rate could be characterized by the single time constant T_1 and whose transverse relaxation time T_2 determined the Lorentzian shape of its unsaturated absorption spectrum. Evaluation of T_1 depended on a knowledge of T_2 (taken from the width of unsaturated lines) and of how the peak height changed as the rf field strength H_1 was increased into the saturation range.

It would be desirable to have available a more general expression for the entire line shape which would include the possibility of saturation (i.e., of nonthermal-equilibrium populations) and yet was not restricted to a Lorentzian line-shape function. It is shown here that such a relationship was, in fact, implicit in the BPP formulation. For clarity, the derivation will be presented in some detail; portions of it will follow closely the development chosen also by Slichter.[47]

It is then argued that this approach is suitable for the extraction of T_1 values from a saturation study (see Sect. IVE) of the more complex spin systems, IF_7 and IOF_5. Lastly, T_1 results are given for the seven samples studied; they were generally of the order of 1 sec.

Derivation. Let us make the customary assumption that the effective rotating rf field is actually produced by a linearly polarized homogeneous field in the laboratory y-direction. In complex notation this field is[28,48,49]

$$H_y^c(t) = 2H_1 e^{i\omega t}; \qquad H_x^c(t) = 0,$$

where $\omega = \gamma H_0$, the nuclear Larmor frequency in the static magnetic field H_0. In standard notation, the rf field is given by

$$H_y(t) = \mathrm{Re}\, H_y^c(t) = 2H_1 \cos \omega t; \qquad H_x(t) = 0. \tag{1}$$

The corresponding complex magnetization induced in the sample will then be

$$M_y^c(t) = \chi H_y^c(t),$$

where χ is the complex susceptibility: $\chi = \chi' - i\chi''$. Thus,

$$M_y(t) = \mathrm{Re}\, M_y^c(t) = 2H_1(\chi' \cos \omega t + \chi'' \sin \omega t). \tag{2}$$

The signal voltage induced in a receiver coil in the y-direction by $M_y(t)$ will be given by Faraday's law[50]

$$S_y(\omega) = -k_1(dM_y/dt),$$

so that

$$\mathrm{Re}\, S_y(\omega) = 2k_1\omega H_1(\chi' \sin \omega t - \chi'' \cos \omega t),$$

where k_1 is a geometric factor. If phase-sensitive detection is used to select only the component which is in phase with $H_y(t)$, then the signal displayed will have an amplitude equal to

$$A(\omega) = 2k_2\omega H_1\chi'', \tag{3}$$

where k_2 includes instrument factors.

A suitable expression for χ'' can be obtained in the usual manner, by equating two different expressions for the mean rate at which the spin system absorbs rf energy. From general principles on the one hand, this rate (erg $cm^{-3}sec^{-1}$) must be[48,51,52]

$$\overline{(dE/dt)} = -\overline{(M_y)(dH_y/dt)}.$$

If $H_y(t)$ is given by (1) above, then it follows that

$$\overline{(dE/dt)} = 4H_1^2(\chi' \overline{\sin \omega t \cos \omega t} + \chi'' \overline{\sin^2 \omega t}) = 2H_1^2\chi''. \tag{4}$$

Taking, on the other hand, a more microscopic point of view, one can relate the absorption rate to the time rate of change of the spin state populations,[28,51,53,54] that is,

$$\overline{(dE/dt)} = \sum_{E_a > E_b} n_{ab}(\hbar\omega_{ab})W_{ab}(\nu), \tag{5}$$

where the sum is over all pairs of spin states $|a\rangle$ and $|b\rangle$ for which

$$(E_a - E_b) = \hbar\omega_{ab} > 0,$$

and where n_{ab} is the steady-state population difference between the states. In (5), $W_{ab}(\nu)$ is the probability per unit time that the perturbation V [caused by $H_y(t)$] will induce that particular transition

$$W_{ab}(\nu) = (2\pi/\hbar)|\langle a|V|b\rangle|^2 g(\nu),$$

and $g(\nu)$ is a normalized shape function for the transition and does not contain any V dependence.

Equation (5) is clearly analogous to Eq. (6) of BPP,[28] except that (6) has been restricted to a population distribution corresponding to thermal equilibrium. The parallel with Slichter's Eqs. (11) and (7) (Sect. 2.10) is also apparent,[51] except that Slichter's expressions are not limited to steady-state experimental conditions (i.e., the population differences may still contain some time dependence). Slichter also prefers to use a δ-function for the line shape.

For the case of a system of identical, independent spin-$\frac{1}{2}$ nuclei (i.e., of a two-level system), the sum in (5) is reduced to a single term and the transition probability is given by[28,54]

$$W(\nu) = (\tfrac{1}{4})\gamma^2 H_1^2 g(\nu). \tag{6}$$

If this two-level system is such that, in the absence of a transition-inducing rf field, any arbitrary population distribution would in fact approach the thermal-equilibrium (Boltzmann) population difference n_0 with a single (and hence exponential) time constant T_1, then the steady-state solution for n in the presence of a rf field would be [28,53]

$$n = n_0/[1 + 2W(\nu)T_1].$$

This condition on the approach to equilibrium is equivalent to assuming either of the following:[55] that the spin system of interest can be described by a spin temperature, or that the decay of the longitudinal magnetization is dependent, at least to first order, on a single relaxation mechanism.

The second expression for the rate of energy absorption is thus

$$\overline{(dE/dt)} = n\hbar\omega W(\nu) = \frac{n_0\hbar\omega W(\nu)}{1 + 2W(\nu)T_1}. \tag{7}$$

Equating the right-hand sides of (4) and (7), and inserting (6) for $W(\nu)$, one obtains

$$\chi'' = (n_0\hbar\gamma^2/8) = \frac{g(\nu)}{1 + (\frac{1}{2})\gamma^2 H_1^2 T_1 g(\nu)},$$

in which case the desired general expression for the NMR signal amplitude is

$$A(\nu) = A(\omega/2\pi) = \frac{kH_1 g(\nu)}{1 + (\frac{1}{2})\gamma^2 H_1^2 T_1 g(\nu)}, \tag{8}$$

where k is a "constant" containing both numerical and instrumental factors. For the case of a Lorentzian line shape, that is, when[47,56]

$$g(\nu) = \frac{2T_2}{1 + 4\pi^2(\nu_0 - \nu)^2 T_2^2}, \tag{9}$$

Eq. (8) becomes the familiar Bloch expression[48,52]

$$A(\nu) = \frac{k'H_1T_2}{1 + 4\pi^2(\nu_0 - \nu)^2 T_2^2 + \gamma^2H_1^2T_1T_2}. \tag{10}$$

The equivalence of (8) and (10) for a Lorentzian line is particularly clear at the peak, where $g(\nu_0) = 2T_2$ [from (9)], and (10) reduces to

$$A \equiv A(\nu_0) = \frac{k'H_1T_2}{1 + \gamma^2H_1^2T_1T_2}. \tag{11}$$

The denominator in (11) or (8) is frequently called the saturation factor.

Applicability. To justify application of (8) or (11) to the ^{19}F NMR spectra of IF_7 or IOF_5, it must first be shown that these complex spin systems are well approximated by the above two-level model.

The first complication to be examined is the presence of the ^{127}I spin-$\frac{5}{2}$ nucleus. If the lifetimes of the ^{127}I spin states were sufficiently long, each ^{19}F spin state and transition would be split into a sextet; the absorption lines would have a separation equal to the ^{127}I-^{19}F spin-spin coupling constant J_{IF}.[57] Such splittings are, in fact, not observed, because a strong quadrupolar relaxation mechanism is effective in shortening the ^{127}I lifetimes in both IF_7 and IOF_5.[37,57,58]

An estimate of the rate of the iodine relaxation is available from recent studies of these compounds. The calculation, described in detail in Sect. VIA, yields a rate $(1/T_1)_I$ of the order of 10 kHz in pure IF_7 and of 100 kHz or more in IOF_5, which, it should be noted, is much greater than the $(1/T_1)_F$ expected (and indeed found) for the fluorine nuclei. Such large rates indicate that the ^{127}I nuclei are always able to maintain their thermal-equilibrium (Boltzmann) spin-state populations. In other words, the ^{127}I nucleus is so strongly coupled to the lattice (compared to the ^{19}F nuclei) that it may be considered to be part of it.

Although relegated to the lattice, the iodine nucleus still has a relevant effect on the fluorine spectra. The ^{127}I relaxation rate can make a contribution to both the transverse and longitudinal relaxation rates of the ^{19}F nuclei via a "scalar coupling mechanism of the second kind,"[59] accounting in the present cases for essentially all the observed transverse

relaxation but, fortunately for the immediate purpose, making a contribution of only 10^{-3} sec^{-1} or less to $(1/T_1)_F$. (The calculation is given in more detail in Sect. VIB.) Another way of expressing this is to say that in IF_7 and in IOF_5 the scalar coupling with the ^{127}I broadens (or dephases) each of the fluorine energy levels [by contributing significantly to $(1/T_2)_F$] but is not a significant source of transitions among the levels [that is contributes negligibly to $(1/T_1)_F$].

It is now possible to make a good case for applying Eq. (8) to IF_7 spectra. It can be assumed that on the time scale involved in an NMR measurement all seven fluorines in IF_7 are equivalent,[42] which means that they will exhibit the behavior of a single spin-$\frac{1}{2}$ ^{19}F nucleus, having effectively only two levels and necessarily only one longitudinal relaxation rate constant T_1. Since IF_7 does not have a Lorentzian line shape, nor a known or well-defined T_2, it is necessary to use the more general relationship (8) in treating the saturation data.

The case for applicability to IOF_5 is less clear-cut. The most important point to note is that the energy-level scheme is actually very close to the first-order AX_4 case in which the eigenfunctions are simple products of a pure A state and a symmetrized X_4 spin-product function state.[60] To this approximation, the IOF_5 ν_A- and ν_B-band components may be viewed as arising from different spin systems composed of one and four equivalent fluorines, respectively, which interact only adiabatically. All that remains is to make the usual assumption that a set of equivalent nuclei will exhibit a first-order longitudinal relaxation rate.

It is conceded that the above arguments have oversimplified the problem, at least from a theoretical standpoint. Even so, detailed theoretical considerations in several analogous cases have led us to expect only minor deviations from a first-order longitudinal relaxation process. To choose an example, Hubbard[61,62] predicts that the effects of motional correlations (which are present among the nuclei of the IOF_5 molecule, but are probably destroyed in IF_7 by the rapid internal fluorine rearrangement[6]) will be so small that they will be difficult to observe experimentally. Some empirical evidence is also available from recent pulsed-NMR measurements of CF_4, SiF_4, SF_6, and CHF_3, in each of which the fluorine longitudinal relaxation is found to be first order to within experimental error.[63]

An important test of the validity of these arguments for the present applications would be provided by a study of transient and steady-state Overhauser effects in a double irradiation experiment with IF_7 and IOF_5.[64] In the interim, it may be noted that the saturation data for these substances do appear to have the required H_1 dependence, and in the case of IOF_5 yield nearly equal T_1 values for all portions of its spectrum studied (see Tables XIV and XVI).

Extraction of T_1 Values. The actual treatment of saturated signal-height data to obtain T_1 from Eq. (8) can be carried out in more than one way. A graphical method rather than a direct point-by-point calculation was chosen here in hopes of reducing the effects of the theoretical and experimental uncertainties.

Rearrangement of the basic relationship (8) gives

$$\frac{H_1}{A(\nu)} = \frac{1}{kg(\nu)} + \left(\frac{\gamma^2 T_1}{2k}\right) H_1^2,$$

from which it can be seen that a plot of $[H_1/A(\nu)]$ vs. H_1^2, at some fixed frequency ν (such as at the signal maximum) and at constant signal amplification, would have a slope of $(\gamma^2 T_1/2k)$ and an intercept (at $H_1^2 = 0$) of $[1/kg(\nu)]$. Taking the ratio of slope to intercept eliminates k, and solving for T_1 (sec) yields

$$T_1 = \left(\frac{\text{slope}}{\text{intercept}}\right) \frac{2}{\gamma^2 g(\nu)}. \tag{12}$$

Note that since the ratio of the slope to the intercept will have the units of $(H_1^2)^{-1}$, the signal height $A(\nu)$ may be measured in arbitrary units. Of course, H_1 must have units compatible with those of the gyromagnetic ratio γ. (For H_1 in mgauss, $\gamma_F = 25.176$ rad $\sec^{-1}$mgauss^{-1}.)

To complete the calculation of T_1, $g(\nu)$ must be known. In the general case of a non-Lorentzian-shaped line, $g(\nu)$ can be evaluated from a knowledge of the unsaturated line shape. For an unsaturated line, $\gamma^2 H_1^2 T_1/2g(\nu)$ is negligible compared to unity, and it is easy to show [using (8) twice] that

$$g(\nu) = \frac{A(\nu)}{\int_0^\infty A(\nu)d\nu} = \frac{\text{signal height at } \nu}{\text{signal area}}. \tag{13}$$

The numerical value obtained for $g(\nu)$ at a given ν will depend on the unit of length chosen. It can be shown (for example, by examining the case of a Lorentzian-shaped line) that in order to be compatible with (12), the height and area must be converted into units of Hz and Hz^2, respectively, which is conveniently done using the spectrometer sweep-width calibration (in Hz per unit length) for the unsaturated trace.

For the special case of a Lorentzian line [Eq. (9)], $g(\nu)$ at any frequency can be evaluated from a knowledge of T_2 (sec), which is readily obtained by measuring the half-width at half-height $\Delta\nu$ (Hz) of an unsaturated trace

$$T_2 = (1/2\pi\Delta\nu). \tag{14}$$

Signal-height data for IF_7 and IOF_5, and in a few cases for IF_5, were obtained only at the signal maxima, where the effect of saturation is the most pronounced. An average value of A for each H_1 was determined; these peak-height data are tabulated in Appendix I and are included in the thesis because of the uncertainties involved in the treatment given them here. Not all of the data have been converted into T_1 values. (Applicability of this treatment to IF_5 data is covered by the arguments presented above for IOF_5.)

From a plot of H_1/A against H_1^2, a slope and intercept were chosen and uncertainties assigned to them by inspection of the plot. Uncertainties were often of the order of 10% in the slope and of 5% in the intercept; a few were higher.

It was encouraging to note that the data for IF_7 produced a clearly linear plot at both temperatures, 29 and -10°C. Values of $g(\nu)$ for IF_7 at its signal maxima were determined from unsaturated traces, using a polar planimeter to measure signal areas; $g(\nu)$ and the resulting T_1 values are given in Table XIII.

TABLE XIII. Longitudinal Relaxation Times T_1 in Pure IF_7 from a Saturation Study

T (°C)	State	Line Shape	$g(\nu)$ (Hz^{-1})	T_1 (sec)
+29 ± 2	(ℓ)	Broad symmetrical doublet	$1.25 \pm 0.05 \times 10^{-4}$	0.7 ± 0.2
-10 ± 2	(s)	Broad singlet	$1.72 \pm 0.07 \times 10^{-4}$	1.7 ± 0.3

Well-resolved as well as unresolved IOF_5 spectra were included among the six other samples. The peak-height data were not corrected for the effects of the overlap of the multiplet components. This correction would probably significantly affect the resulting ratio of slope to intercept only in the cases of a partially resolved IOF_5 ν_B band; such cases are clearly marked in the tables of T_1 results.

At the IOF_5 signal maxima it was assumed that $g(\nu) = T_2 = 1/2\pi\Delta\nu$. This assertion is based on the fact that peaks in the completely unresolved and well-resolved IOF_5 spectra, in addition to being very well approximated by a superposition of several Lorentzian components, are nearly Lorentzian in shape themselves, with a half-width only slightly larger (5-10%) than the individual component half-widths. Thus, the approximation involved was in most cases as accurate as a signal-area approach for these wide lines would have been.

For each liquid sample, a T_2 was taken from fitted multiplet-component half-widths $\Delta\nu_F$ of unsaturated ν_B-band NMR traces (obtained at ANL and extrapolated when necessary to the appropriate temperature). For the two samples which were solid at -12°C, T_2 was calculated from ν_B-band half-widths which had to be estimated from the less accurate spectra (8-kHz rather than 5-kHz sweep width) obtained on the UW spectrometer in the course of the saturation study.

Resulting T_2 and T_1 values for the IOF_5 ν_B band are given in Tables XIV and XV. For resolved IOF_5 spectra, only the results for the more intense of the two signal maxima are listed. Results for the less-intense ν_B-band maximum were generally slightly smaller (~10%), a discrepancy which could probably have been removed by making overlap corrections to the peak-height data. At the lower temperature (see Table XV), more scatter was present in the peak-height data, due to increased sensitivity (especially of the line width) to small temperature fluctuations (±2°C).

TABLE XIV. Longitudinal Relaxation Times T_1 for the IOF_5 ν_B Band in Several Liquid Samples at 29 ± 2°C, from a Saturation Study[a]

Sample	Spectrum	T_2 (msec)[b]	T_1 (sec)[c]
Pure IOF_5	Unresolved	0.49 ± 0.03	0.37 ± 0.05
75.1% IOF_5 in IF_5	Unresolved	0.76 ± 0.05	0.50 ± 0.06
57.7% IOF_5 in IF_5	Partially resolved	1.14 ± 0.04	0.86 ± 0.09
37.8% IOF_5 in IF_5	Partially resolved	1.45 ± 0.07	1.14 ± 0.15
9.8% IOF_5 in IF_5	Well-resolved	1.9 ± 0.1	1.53 ± 0.25
29.8% IOF_5 in BrF_5	Partially resolved	0.80 ± 0.05	1.04 ± 0.20

[a]Peak-height data (see Appendix I) have not been corrected for overlap of multiplet components. This effect may be important in partially resolved spectra.

[b]From fitted half-widths of ANL traces, extrapolated to 29°C.

[c]T_1 value for partially or well-resolved spectra is based only on data for more intense of two peak maxima.

TABLE XV. Longitudinal Relaxation Times T_1 for the IOF_5 ν_B Band in Several Samples at -12 ± 2°C from a Saturation Study[a]

Sample	Spectrum and State	T_2 (nsec)	T_1 (sec)[c]
Pure IOF_5	Partially resolved (s)	0.80 ± 0.05[b]	1.35 ± 0.30
57.7% IOF_5 in IF_5	Well-resolved (s)	1.83 ± 0.10[d]	1.10 ± 0.40
37.8% IOF_5 in IF_5	Well-resolved (ℓ)	3.2 ± 0.3[b]	1.7 ± 0.7
9.8% IOF_5 in IF_5	Well-resolved (s)	2.7 ± 0.2[d]	1.7 ± 0.3

[a]Peak-height data (see Appendix I) have not been corrected for overlap of multiplet components, which may be important in partially resolved spectra.
[b]From fitted half-widths of ANL traces, extrapolated to -12°C.
[c]T_1 value is based only on data for the more intense of the two peak maxima.
[d]From estimates of component half-widths of UW traces.

Results for the IOF_5 ν_A-band maximum are given in Table XVI along with a few results for the IF_5 ν_A band, recorded simultaneously. The half-width of IOF_5 ν_A-band components was assumed to be 15 ± 5% less than that of the corresponding ν_B band, in accordance with observations noted above in Sect. IVD. The value of T_2 for the IF_5 ν_A band at 29°C was taken from available line-width data (shown in Fig. 24a). Peak-height data for the IF_5 ν_A band in these samples were also obtained at -12°C. Suitable line-width data for the two solid samples involved were not available, however; the remaining liquid sample (37.8% IOF_5 in IF_5) yielded a result at -12°C approximately equal to the 29°C result.

TABLE XVI. Longitudinal Relaxation Times T_1 for the IOF_5 and IF_5 ν_A Bands in Several Samples at 29 ± 2°C from a Saturation Study

Sample	IOF_5 ν_A Band		IF_5 ν_A Band	
	T_2[a] (msec)	T_1 (sec)	T_2[c] (msec)	T_1[b] (sec)
Pure IOF_5	0.58 ± 0.06	0.4 ± 0.1[b]		
75.1% IOF_5 in IF_5	0.89 ± 0.09	0.2 ± 0.1[b]		
57.7% IOF_5 in IF_5	1.34 ± 0.10	0.6 ± 0.2[b]	11.4 ± 1.0	1.5 ± 0.5
37.8% IOF_5 in IF_5	1.71 ± 0.15	0.5 ± 0.1[b]	13.3 ± 1.0	0.9 ± 0.4
9.8% IOF_5 in IF_5	2.2 ± 0.2	0.5 ± 0.1[d]	15.9 ± 1.6	0.5 ± 0.1
29.8% IOF_5 in BrF_5	0.94 ± 0.09	0.9 ± 0.2[b]		

[a]From half-widths, assumed to be 15 ± 5% smaller than corresponding ν_B-band-fitted half-width.
[b]Unresolved or poorly resolved ν_A-band spectrum.
[c]From measured half-widths (see Fig. 24a) extrapolated to 29°C.
[d]Well-resolved ν_A-band spectrum.

It is claimed that a more accurate or painstaking treatment of the IOF_5 data is not justified in view of the experimental error present and the state of our knowledge about the actual relationships among the levels of the IOF_5 spin system.

Chapter VI is concerned with an attempt to account theoretically for the magnitude of the results presented here.

G. Samples of Solid IOF_5-IF_5 Mixtures

Three features of the IOF_5-IF_5 mixtures in the solid state which deserve special mention are described briefly in this section: a significant freezing-point depression, the unexpected appearance of an IF_5 spectrum from apparently solid samples, and the evidence provided by their spectra for a solid-solution phase of limited solubility.

A crude check was made for a noticeable freezing-point depression in three other mixture systems which freeze near ice point, with negative results: IOF_5-IF_7, IF_5-IF_7, and IOF_5-WF_6. A few NMR results from solid samples in the latter system have already been presented (see Figs. 17a and 22a).

Although the findings reported in this section for solid IOF_5-IF_5 samples are interesting, they are unfortunately not exhaustive enough to allow the construction of a complete phase diagram. It is believed that this mixture system merits more extensive investigation, involving other kinds of physicochemical measurements. A knowledge of the crystal structure of both pure components would be particularly valuable.[65]

Freezing-point Depression. During the NMR measurements, some of the IOF_5-IF_5 samples remained liquid even at -20°C, representing a large depression below the normal freezing points of 4.6°C for pure IOF_5 (Refs. 20 and 37) and 9.4°C for pure IF_5.[66]

An attempt was made to observe the initial freezing points and final melting points of the eleven samples involved in this mixture system, by suspending the samples in a variable-temperature bath. Excellent visibility was achieved by using a clear glass Dewar filled with 95% ethanol; a single loop of 3/8-in. copper tubing served as heat exchanger when hot or cold nitrogen gas was passed through it; an electric stirrer was used. The bath temperature was indicated to ±0.1°C by a platinum resistance thermometer sensor attached to a Princeton Applied Research Digital Thermometer Controller DTC-1. The Kel-F sample tubes were suspended directly in the bath liquid in such a way that they could be tapped, shaken, or inverted without removal from the bath.

Two cooling and two warming runs were performed, between -30°C, where all samples were solid, and +10°C, where all samples were liquid. The temperature was changed very slowly (< 1°C per 5 min) and provision was made for reversing its direction of change at any time.

During cooling runs, the temperature at which crystals first formed in each tube was noted. Samples containing more than 50 m/o IOF_5 were characterized by the slow growth of transparent crystals from the liquid surface downwards, while those samples containing more than 50 m/o IF_5 had a proclivity to supercooling followed by rapid freezing to an opaque white mass.

During warming runs, some difficulty with mixing within the samples was encountered in the early stages of melting, although the tubes were repeatedly inverted. Despite a considerable effort, reproducible "warming" data were not obtained for the crucial center portion of the concentration range.

The results of this study are shown in Fig. 26. The initial slopes of the melting-point curves, although reasonably well-defined by the data (to about ±7%), were not considered suitable for a calculation of the heats of fusion of pure IOF_5 and pure IF_5 because of the evidence, given below, for the likelihood of solid-solution formation in this system. (There is also the possibility that IOF_5, in analogy with some of the hexafluorides,[67] may have more than one solid-state modification.)

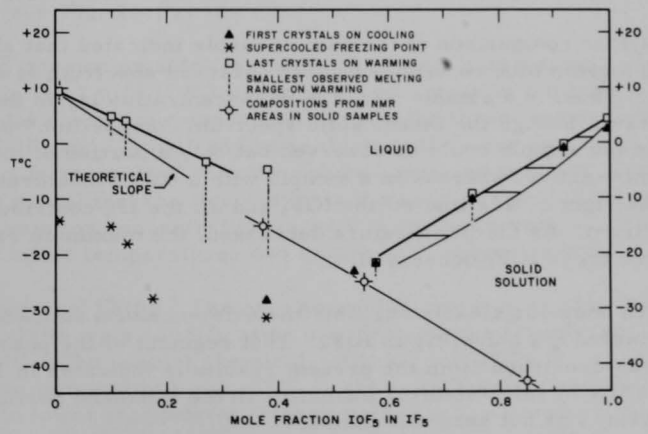

Fig. 26. Melting-point Data, Spectral-area Ratios, and Partial Phase Diagram for the IOF_5-IF_5 Mixture System

A recent calorimetric determination of the latent heat of fusion of pure IF_5 (Ref. 68) (ΔH_f = 2680.5 ± 0.5 cal/mole) provided the theoretical

initial slope of the melting-point curve shown in the left-hand portion of Fig. 26; in the calculation, it was assumed that the liquid phase was an ideal solution and that the solid phase formed was pure IF_5. It would not be surprising if the discrepancy between the theoretical slope and the slope of the observed melting-point curve were attributable to the formation of solid solutions in this region of the phase diagram.

Relative Spectral Areas. Signal areas were measured with a polar planimeter on NMR charts obtained from IOF_5-IF_5 samples over a temperature range from 23 to -43°C, in an attempt to elucidate the behavior of this system at low temperatures.

Pure IF_5 exhibited a detectable (high-resolution) NMR spectrum only at temperatures where the sample remained liquid. In mixtures of IF_5 and IOF_5, however, an IF_5 spectrum resembling that of pure IF_5 liquid was observed at all temperatures studied, even down to -43°C, at which all the mixture samples were apparently solid. Area measurements revealed that in spectra from liquid samples the relative peak areas for IOF_5 and IF_5 were, as expected, in roughly the same ratio as the number of moles of each component in the sample tube, whereas in spectra from solid samples the observed ratios of IF_5 to IOF_5 peak areas were constant at a given temperature (except for certain IOF_5-rich samples in which the ratio was smaller, in accordance with the explanation in the next paragraph). Area ratios from two solid samples at -15 ± 1°C, four solid samples at -25 ± 2°C, and eight solid samples at -43 ± 3°C yielded the three "solid spectrum composition" points plotted in Fig. 26 as a function of temperature.

Further comparison of the data available indicated that all the IOF_5 present in a given tube contributed to the observed spectrum at all temperatures. Thus, in a sample whose bulk concentration lay to the left of the line drawn through the three "solid spectrum composition" points, all the IOF_5 in the sample could be observed but only a portion of the available IF_5 was NMR-active, whereas in a sample with a bulk concentration lying on or to the right of this line all the IOF_5 and all the IF_5 contributed to the NMR spectrum. As the temperature decreased, the maximum ratio of NMR-active IF_5 to IOF_5 decreased.

Such behavior clearly suggests the existence of a solid-solution phase of limited IF_5 solubility in IOF_5. That segment of the phase boundary which can be construed from the present results is indicated in Fig. 26. The possibility of solid-solution formation in the left-hand portion of the phase diagram has not been eliminated.

Line Widths. Measurements of area and line widths were made with the same set of NMR traces. Line-width data for IOF_5 and IF_5 in solid samples were not inconsistent with the above interpretation of the area

ratios, in that the half-widths in all samples whose bulk concentration lay to the left of the "solid spectrum composition" line (see Fig. 26) were also quite constant for a given temperature. Table XVII gives the half-widths found for the IOF_5 and IF_5 ν_B (doublet) bands in these samples. The uncertainties shown were based on the range of $\Delta\nu$ values observed at the given temperature; some of the scatter was caused by sensitivity to small temperature fluctuations.

TABLE XVII. Half-widths of IOF_5 and IF_5 ν_B (doublet) Bands in IOF_5-IF_5 Mixtures in the Solid-sample Temperature Range

T (°C)	State	IOF_5[a] $\Delta\nu_F$ (Hz)	No. of Samples Observed	IF_5 $\Delta\nu$ (Hz)	No. of Samples Observed
-15 ± 1	(ℓ)	f (conc.)[b]	6	2.5 ± 0.5[c]	8
-25 ± 2	(ℓ)	37 ± 7, 53 ± 7[b,d]	2	7 ± 2[d]	6
	(s)	65 ± 15	6	10 ± 2	5
-43 ± 3	(s)	215 ± 20	9	110 ± 10	9

[a]Based on fitted half-widths (see Sect. VB).
[b]Shown in Fig. 21c.
[c]Shown in Fig. 24a.
[d]Some samples may have been supercooled.

The NMR-active ν_B band of IF_5 is strongly broadened in the solid, particularly at the lowest temperature; where the less intense ν_A band was observable, it was comparably broadened. On the other hand, IOF_5 lines in these solid mixtures are considerably narrower than in pure IOF_5 (see Fig. 21a) and slightly broader than in liquid mixtures at the same temperature (see Fig. 21c, at -25°C).

An interesting sidelight to the line-width data was provided by the one sample (91.7 m/o IOF_5) whose bulk concentration fell well to the right of the "solid spectrum composition" line at the three temperatures studied. Both the IOF_5 and IF_5 half-widths in this sample were substantially greater (by about a factor of two) than the values appearing in Table XVII, which served to reveal that the line widths in the solid are actually a function of the solid-solution concentration as well as the temperature, tending to increase at lower temperatures and smaller IF_5 concentrations.

Chemical Shifts. The only appreciable change in IOF_5 and IF_5 chemical shifts upon solidification occurred for the IF_5 ν_B band (doublet) below -25°C. The doublet chemical shift in liquid IOF_5-IF_5 mixtures between room temperature and -25°C is shown in Fig. 20a and tends monotonically to lower frequencies (higher fields) as the temperature is lowered; a discernable difference in solid and liquid chemical shifts was not observed at either -15 or -25°C. In contrast, doublet data for solid IF_5 at -43°C produced a curve (not shown in any figure) parallel to and falling between the curves for liquid mixtures at 11 and -15°C (see Fig. 20a). The significance of this change in trend is not immediately apparent.

CHAPTER VI

RELAXATION MECHANISMS IN LIQUID IF_7 AND IOF_5

A theoretical account of the relaxation phenomena observed in liquid IF_7 and IOF_5 is presented in this chapter. Section VIA reviews what is currently known about the ^{127}I relaxation in these compounds and outlines the approach taken to calculate a correlation time for molecular reorientation.

In Sect. VIB this correlation time is combined with conventional relaxation theory in an analysis of the fluorine longitudinal relaxation times reported in Sect. VF for IF_7 and IOF_5. The insight gained is interpreted in Sect. VIC in terms of molecular rotation in the liquid.

Values of the nuclear properties of ^{127}I and ^{19}F which were used in these calculations can be found in Appendix II.

A. Relaxation of the ^{127}I Nucleus

The ^{19}F NMR spectra of IF_7 and IOF_5 are characterized by unusually broad lines, which indicate efficient (i.e., rapid) transverse relaxation of the fluorines in these molecules. It has been suggested in both cases that the magnitude and temperature dependence of the fluorine line widths are related to the rapid relaxation of the central, quadrupolar ^{127}I (spin-$\frac{5}{2}$) nuclear spin states.[42,43] In this interpretation, the broad IF_7 ^{19}F doublet is viewed as a partially collapsed sextet, corresponding to an intermediate rate of ^{127}I relaxation; each of the 25 multiplet components of the IOF_5 ^{19}F spectrum is regarded as a well-collapsed sextet, corresponding to the more rapid ^{127}I relaxation rate expected from a molecule with relatively less electrical symmetry at the ^{127}I site.[57]

The relaxation of the ^{127}I nucleus itself is a result of the time-dependent nature of the interaction between the nuclear quadrupole moment and the molecular electric field gradient; the field-gradient orientation fluctuates with time as the molecule undergoes reorientation. The induced ^{127}I transition rate among its six m_I states depends on the magnitude of the quadrupole moment, on the magnitude and asymmetry of the field-gradient tensor components, and on the correlation time τ_c characterizing the random reorientation of the field gradient at the nucleus.[57,70]

Recently, progress has been made in determining some of the parameters for the coupling of the iodine nucleus to both the molecular motion and to the fluorines in IF_7 and IOF_5. The first step was the determination of the ^{127}I-^{19}F spin-spin coupling constant J_{IF}. It was assumed that the entire IF_7 fluorine line width is due to quadrupolar broadening. Then, by virtue of the non-Lorentzian shape of the resonance, Pierce and

Cornwell[37] were able to deduce both a shape parameter α and a value of J_{IF} = 1525 ± 200 Hz from the fitting of IF_7 ^{19}F spectra with computer-generated curves based on the equations of Suzuki and Kubo[69] for intermediate quadrupolar relaxation rates. The value J_{IF} = 2100 ± 200 Hz was obtained previously in an analogous manner by Gillespie and Quail.[58]

The dependence of the relaxation rate of the ^{127}I nucleus on the molecular motion is given by[69,70]

$$(1/T_1)_I = \frac{3(2I+3)}{40I^2(2I-1)} (e^2qQ/\hbar)^2\tau_c. \qquad (1)$$

Here, I is the iodine spin, $(e^2qQ/\hbar)$ is the quadrupole coupling constant for the molecule in rad sec^{-1}, and τ_c is the correlation time for reorientation of the field gradient at the nucleus. The equation applies in the extreme narrowing limit ($\omega_I\tau_c << 1$), and to the case for which the field gradient has axial symmetry.

Suzuki and Kubo have expressed (1) in terms of the parameter α for the resulting fluorine line shape:[69]

$$(1/T_1)_I = \frac{3(2I+3)}{40I^2(2I-1)} 2\pi J_{IF}\alpha, \qquad (2)$$

which thus allows this rate to be determined with a minimum of information. By means of Pierce's value of α and J_{IF},[37] the iodine relaxation rate in IF_7 was obtained. It appears in Table XVIII.

TABLE XVIII. Parameters for the ^{127}I Relaxation in IF_7 and IOF_5. Assumed values are in parentheses.

Item	Pure IF_7 at ~30°C	Pure IOF_5 at 29°C	9.8 m/o IOF_5 in IF_5 (liquid) at 29°C	9.8 m/o IOF_5 in IF_5 (liquid) at -15°C
J_{IF} (Hz)	1525 ± 200	(1525)		
$\Delta\nu_F$ (Hz)	-	325 ± 15	75 ± 5	27 ± 3
$(1/T_1)_I$ (sec^{-1})	1.7×10^4	1.3×10^5	5.7×10^5	1.6×10^6
τ_c(sec)	(0.5×10^{-12})	0.45×10^{-12}	2.0×10^{-12}	5.5×10^{-12}
$(e^2qQ/\hbar)$ (MHz)	190 ± 20	552.9 ± 0.6		

Because an α cannot be determined by inspection in the limiting case of Lorentzian-shaped lines, a different approach was necessary to

obtain $(1/T_1)_I$ in IOF_5. It was assumed that the entire IOF_5 line width is due to quadrupolar broadening and that J_{IF} in IOF_5 is approximately equal to J_{IF} in IF_7. The appropriate basic relationship between the fluorine line width and the rate of the iodine relaxation, which is an example of scalar coupling "of the second kind,"[59] is

$$(1/T_2)_F = 4\pi^2 J_{IF}^2 [I(I+1)/3](T_1)_I. \tag{3}$$

(The first term in Abragam's equation (127), which depends on $(T_2)_I$, is negligible compared to the second term.[59]) Rearranging (3) and inserting

$$(1/T_2)_F = 2\pi\Delta\nu_F,$$

where $\Delta\nu_F$ is the fitted half-width of the Lorentzian-shaped IOF_5 components, one obtains the ^{127}I relaxation rates $(1/T_1)_I$ shown in Table XVIII for IOF_5.

Since the IOF_5 quadrupole coupling constant was recently measured by microwave spectroscopy,[33] knowledge of the ^{127}I relaxation rate permitted a calculation of the correlation time τ_c for molecular reorientation in IOF_5 directly from (1). The correlation times obtained (Table XVIII) are of the order of 10^{-12} sec, not unlike correlation times determined from quadrupole effects in chlorine-, nitrogen-, deuterium-, and boron-containing compounds.[71]

The quadrupole coupling constant in IF_7 has not been measured, but Pierce and Cornwell[37] obtained an estimate from Eq. (1): $(e^2qQ/\hbar) = 190 \pm 20$ MHz, by assuming that the correlation time in pure IF_7 is about the same as in <u>pure</u> IOF_5 (both at 29°C).

Table XVIII summarizes the calculations discussed in this section, and illustrates the dependence of the fluorine line width and the ^{127}I relaxation rate on the correlation time.

It can be shown that, in the extreme narrowing limit (which applies throughout this work), the molecular motion which induces longitudinal relaxation in a quadrupolar nucleus will make an equal contribution to the transverse relaxation,[70] that is,

$$(1/T_2)_I = (1/T_1)_I,$$

for this mechanism of relaxation. It has been assumed here that this mechanism is the only one which makes a significant contribution to the iodine relaxation in IF_7 and IOF_5. The calculations outlined in the next section, which are for the fluorine nuclei, support such a view, since the results of similar calculations for the ^{127}I nucleus would invariably be even smaller, often because of its smaller gyromagnetic ratio.

B. Fluorine Relaxation

The experimental results of Ch. V indicate that the fluorines in IF_7 and IOF_5 undergo rather rapid transverse relaxation but much slower longitudinal relaxation. In Sect. VIA it was assumed that all the transverse relaxation (i.e., the fluorine line width) was due to a coupling with the rapidly relaxing ^{127}I nucleus. In this section theoretical estimates are made of the contributions from a number of other mechanisms to $(1/T_2)_{F,exp}$ and to $(1/T_1)_{F,exp}$. The purpose is twofold: to account for the magnitude of $(1/T_1)_{F,exp}$ and to demonstrate that all contributions to $(1/T_2)_{F,exp}$ other than the ^{127}I-^{19}F spin-spin coupling are indeed negligible.

The theory of nuclear relaxation in liquids has been summarized in detail by Abragam[72] in terms of the general quantum-mechanical density-matrix formulation of relaxation, as developed by Redfield[73] from foundations laid by the work of BPP,[28] Wangsness, and Bloch.[74,75] In view of the readability of this and other accounts of the theory,[72,76,77] practical results of the theory will be utilized below without further introduction. (Recently, Deutch and Oppenheim have claimed that linear response theory provides an approach of equivalent generality.[78])

For the present calculation, each relaxation mechanism chosen is considered independently of all others (i.e., cross relaxation terms are assumed to be negligible) and differential equations of motion of the system of the following (macroscopic, operator) form are sought for each mechanism:[79,80]

$$d\langle S_z\rangle/dt = -(1/T_1)(\langle S_z\rangle - S_0);$$

$$d\langle S_y\rangle/dt = -(1/T_2)\langle S_y\rangle, \tag{4}$$

where $\langle S_z\rangle$ and $\langle S_y\rangle$ are the average expectation values of the longitudinal and transverse components, respectively, of the macroscopic fluorine magnetization, and $(1/T_1)$ and $(1/T_2)$ are the first-order rate constants for the decay of the longitudinal and transverse magnetizations back to their equilibrium values of S_0 and zero, respectively. The relaxation rates in turn can be evaluated from expressions involving the spectral densities (which are Fourier transforms of correlation functions) appropriate to a given mechanism.[81]

It should be stated that for some mechanisms the equations of motions are not of as simple a form as (4). Exceptions to (4) will be noted as they are encountered. Also, since we are always in the extreme narrowing limit ($\omega\tau_c \ll 1$), the spectral densities are no longer a function of ω, and expressions for $(1/T_1)$ and $(1/T_2)$ are greatly simplified over those for the general case.

The random motions which modulate the interactions, and are the source of the correlation functions and their spectral densities, are characterized by a correlation time. For several of the mechanisms, the correlation times obtained in Sect. VIA are used in the calculation of $(1/T_1)_F$ contributions.

Scalar Coupling to ^{127}I. The scalar ^{127}I-^{19}F spin-spin coupling, first considered in Sect. VIA [see Eq. (3)] was assumed to account for all the transverse fluorine relaxation (line width) in IF_7 and IOF_5, that is, this mechanism made a large contribution to $(1/T_2)_F$. The corresponding contribution of this scalar coupling "of the second kind" to $(1/T_1)_F$ is given by[59]

$$(1/T_1) = \frac{4\pi^2 J_{IF}^2[2I(I+1)/3](T_2)_I}{1 + (\omega_I - \omega_S)^2(T_2)_I^2}, \tag{5}$$

where I is the iodine spin, ω_I and ω_S are the iodine and fluorine Larmor frequencies (see Appendix II), respectively, and $(T_2)_I$ is assumed equal to $(T_1)_I$ (given in Table XVIII). The contribution to $(1/T_1)_F$ is very small and is listed in the last row of Table XIX.

TABLE XIX. Calculated Contributions to $(1/T_1)_F$ and $(1/T_2)_F$ for IF_7 and IOF_5

Interaction Mechanism	Contribution to $(1/T_1)_F$ (sec^{-1}) in:			
	Pure IF_7 at 29°C	Pure[a] IOF_5 at 29°C	9.8 m/o IOF_5 in IF_5 at 29°C	9.8 m/o IOF_5 in IF_5 at -15°C (ℓ)
Spin rotation[a,b]	1.63	1.13	2.5×10^{-1}	7.8×10^{-2}
F-F dipole-dipole under translation[b]	2.0×10^{-2}	1.5×10^{-2}	1.5×10^{-2}	$\geq 1.5 \times 10^{-2}$
F-F dipole-dipole under rotation[b]	1.1×10^{-2}	0.43×10^{-2}	1.9×10^{-2}	5.3×10^{-2}
Shielding anisotropy[a,c]	3.8×10^{-3}	2.1×10^{-3}	0.93×10^{-2}	2.6×10^{-2}
F-I dipole-dipole under translation[d]	1.0×10^{-3}	1.0×10^{-3}	1.0×10^{-3}	$\geq 1.0 \times 10^{-3}$
F-I dipole-dipole under rotation[d]	3.2×10^{-3}	3.7×10^{-3}	1.6×10^{-2}	4.5×10^{-2}
Scalar coupling to ^{127}I relaxation[e]	1.2×10^{-4}	0.89×10^{-3}	3.9×10^{-3}	1.1×10^{-2}

[a]Calculated for the IOF ν_B band only.
[b]For this mechanism, $1/T_2 = 1/T_1$.
[c]For this mechanism, $1/T_2 = (7/6)(1/T_1)$.
[d]For this mechanism in IF_7 and IOF_5, $1/T_2 \cong 1/T_1$; see text.
[e]For this mechanism, $1/T_2 \gg 1/T_1$.

It might be noted that this mechanism is unique among those examined here in that, in the extreme narrowing limit, it alone is capable of making very unequal contributions to the transverse and longitudinal rates of fluorine relaxation.

^{19}F-^{19}F Dipole-Dipole Interaction under Reorientation. The intramolecular dipole-dipole interaction modulated by molecular reorientation is a more important relaxation mechanism than the intermolecular dipole-dipole interaction under reorientation, and is calculated here. For IF_7 and IOF_5, this contribution to $(1/T_1)_F$ is[81]

$$1/T_1 = 2\gamma_F^4 \hbar^2 S(S+1)\, \tau_c \sum_{F-F} (1/b)^6, \tag{6}$$

where S is the fluorine spin, τ_c is the correlation time for the molecular reorientation, b is a ^{19}F-^{19}F distance in the molecule, and the sum is over the distances from one fluorine to all (six or five) others.

For IF_7, distances between fluorines were taken directly from X-ray data;[82] the above sum was computed for each of the seven fluorines, and the largest value (3.3×10^{46} cm^{-6}) was used in the calculation of (6). For IOF_5, a 90° F_A-I-F_B angle was assumed, with bond lengths of 1.75×10^{-8} cm and 1.86×10^{-8} cm, respectively;[13] the axial fluorine was used as the reference fluorine in the sum.

The correlation times for molecular reorientation were assumed to be the same as the correlation times for reorientation of the field gradient at the ^{127}I nucleus (shown in Table XVIII). Contributions from this mechanism are listed in Table XIX.

^{19}F-^{19}F Dipole-Dipole Interaction with Diffusion. This is the only intermolecular mechanism included in these calculations. The contribution to $(1/T_1)_F$ may be estimated[83,84] from

$$(1/T_1) = \gamma_F^4 \hbar^2 S(S+1)(4\pi N/15aD), \tag{7}$$

where S is the fluorine spin, N is the number of fluorine nuclei per cc, a is the effective molecular radius, and D is the translational diffusion coefficient.

Diffusion coefficients for liquid WF_6, MoF_6, and UF_6 have recently been measured at several temperatures by a spin echo technique.[85] In the absence of measured translational diffusion coefficients for IF_7 and IOF_5, the diffusion coefficient for WF_6 at 15°C (3.2×10^{-5} cm^2-sec^{-1}) was used in the calculation of (7). Liquid densities were taken from Ref. 17; a was assumed to be 1.9×10^{-8} cm.[13,82] Results are shown in Table XIX.

Equation (7) carefully avoids the use of Stokes' expression relating the diffusion coefficient to the coefficient of bulk viscosity. Although the latter approach has fallen into disrepute in NMR work,[85,86] an entirely satisfactory alternative has not yet been found. For example, Chaffin and

Hubbard have recently reported that (7) predicts too small a contribution to $(1/T_1)_F$ in liquid CHF_3.[64]

^{19}F-^{127}I Dipole-Dipole Interactions. In contrast to dipole-dipole interactions between like spins, this mechanism involves a coupled equation for two unlike spins, of the form[87]

$$d\langle S_z\rangle/dt = -(1/T_1)_{SS}(\langle S_z\rangle - S_0) - (1/T_1)_{SI}(\langle I_z\rangle - I_0), \tag{8}$$

where the ^{19}F nuclei are denoted by S and the iodines by I. Different subscripts have been placed on the two "rate constants" to distinguish them.

As with the like-spin interactions, both inter- and intramolecular interactions must be considered, which involve diffusion and reorientation, respectively.

Fortunately, it was found that for IF_7 and IOF_5 the second constant $(1/T_1)_{SI}$ is always smaller by at least an order of magnitude than the first. Hence, only the first term will be reported here.

The exact expressions for $(1/T_1)_{SS}$ under reorientation and diffusion are quite similar to (6) and (7) above.[81,83,87] However, there would be only one term in the sum in (6), which should contain the shortest I-F bond distance. The same assumptions were made for τ_c, a, D, and the liquid densities. Results of the calculations appear in Table XIX.

It should also be noted that in the extreme narrowing limit $(1/T_2) = (1/T_1)_{SS}$ for this mechanism.

Shielding Anisotropy and Molecular Reorientation. Reorientation of the molecule can also cause relaxation of a nucleus in an anisotropic shielding environment by introducing time dependence into the effective magnetic field at the nuclear spin. The theoretical contribution to the longitudinal relaxation is given by[88]

$$(1/T_1) = (3/10)\gamma_F^2 H_0^2 \delta_z^2 (1 + \eta^2/3)\, \tau_c. \tag{9}$$

The anisotropy parameter δ_z and the asymmetry parameter η, as well as the shielding constant σ and a quantity usually called the "anisotropy" $\Delta\sigma$, are all defined in terms of the components of the shielding tensor, $\underline{\underline{\sigma}}$:

$$\sigma = (1/3)\mathrm{Tr}\, \underline{\underline{\sigma}};$$

$$\eta = (\sigma_{xx} - \sigma_{yy})/(\sigma_{zz} - \sigma);$$

$$\Delta\sigma = \sigma_{zz} - (1/2)(\sigma_{xx} + \sigma_{yy}) = (2/3)\delta_z;$$

$$\delta_z = \sigma_{zz} - \sigma. \tag{10}$$

In lieu of measured values of shielding-tensor components in IF_7 and IOF_5, estimates of η and δ_z were obtained in the following manner. The observed chemical shifts, in Hz from CCl_3F, were converted into ppm from SiF_4 and placed on the scale of absolute ^{19}F shielding constants recently published by Cornwell and Hindermann.[40] The resulting shielding constants are shown in Table XX.

TABLE XX. Quantities Used in Theoretical Calculations of Relaxation Rates

Quantity	IF_7	IOF_5 (ν_B)	IOF_5 (ν_A)
$\sigma_{F,abs}$ (ppm)	+22 ± 7	+120.0 ± 0.5	+82.5 ± 0.5
C_F (Hz)	-5015	-4212	-4662
$I_M(10^{-40}$ g cm$^2)$	430	400	400

With the fluorine nucleus taken as origin and the F-I bond axis as the z-axis, it was assumed that the magnetic shielding in IF_7 and IOF_5 would be symmetric about that axis, in which case $\eta = 0$. It was further assumed that the shielding along the bond axis would be approximately equal to the (diamagnetic) shielding of a fluorine atom. (This assumption is also used in the following discussion of the spin-rotation interaction, where it is explained in somewhat more detail.) Hence,[89]

$$\sigma_{zz} = \sigma^d(F^\circ) = 470.7 \text{ ppm},$$

and δ_z was calculated from the observed shielding constants.

Contributions from this mechanism to $(1/T_1)_F$ were calculated from (9) using the correlation times deduced in Sect. VIA for molecular reorientation. Results appear in Table XIX.

Spin-rotation Interaction and Molecular Motion. The interaction between a nuclear spin and the field produced at the nucleus by the overall rotation (in rotational state $|Jm_J\rangle$) of the other charged particles in the molecule is interrupted and changed in magnitude by collisions. Although the details of the statistical model for this process are still a matter for discussion,[84,85,90,91] Green and Powles[91] have pointed out that the equation given by Hubbard[84] for $1/T_1$ should retain its validity regardless of which of the microscopic models is preferred.

The contribution to $(1/T_1)_F$ is given by[84]

$$1/T_1 = (8\pi^2 I_M kT/3\hbar^2)\tau_{sr}(2C_{xx}^2 + C_{zz}^2), \tag{11}$$

where I_M is the moment of inertia, k is the Boltzmann constant, T is the absolute temperature, τ_{sr} is the appropriate correlation time for fluctuations in the angular momentum vector of the molecule, and C_{zz} and C_{xx} are components of the spin-rotation interaction tensor $\underline{\underline{C}}$ (in Hz) which are parallel and perpendicular, respectively, to the z-axis. Also, Hubbard has shown that[84]

$$\tau_{sr} = (I_M/6kT)\tau_c^{-1}, \tag{12}$$

where τ_c is the correlation time involved in the dipole-dipole and scalar spin-spin couplings. Thus, the contribution from the spin-rotation mechanism is the only one which is <u>inversely</u> proportional to τ_c. Values of τ_c were taken from Sect. VIA; the moments of inertia used appear in Table XX. Components of $\underline{\underline{C}}$ were obtained as described below, from their relationship to $\underline{\underline{\sigma}}$ components.

For a polyatomic spherical top, it has been shown that, for choice of origin at the nucleus of interest[92,93]

$$\underline{\underline{\sigma}}^p = (m_p/2m_e gB)\underline{\underline{C}} - \sum_i{}' (r_e Z_i/2R_i^3)(R_i^2\underline{\underline{1}} - \underline{R}_i \cdot \underline{R}_i), \tag{13}$$

where $\underline{\underline{\sigma}}^p$ is the paramagnetic contribution to the shielding, m_p and m_e are the proton and electron rest masses, g is the nuclear g-factor (see Appendix II), B is the rotational constant in the same units as $\underline{\underline{C}}$ ($B = \hbar/4\pi I_M$), r_e is e^2/mc^2, Z_i is the atomic number of the ith nucleus, $\underline{R}_i$ is the vector from the nucleus of interest to nucleus i, and the sum is over all other nuclei in the molecule.

To proceed further, it is necessary to make an assumption. The shielding tensor, again with origin at the nucleus of interest, may be broken down into the following terms:

$$\underline{\underline{\sigma}} = \underline{\underline{\sigma}}^{d1} + \underline{\underline{\sigma}}^{d2} + \underline{\underline{\sigma}}^p, \tag{14}$$

where $\underline{\underline{\sigma}}^{d1}$ is the diamagnetic contribution from the electrons on the nucleus of interest and $\underline{\underline{\sigma}}^{d2}$ is the diamagnetic contribution to the shielding from electrons on other nuclei. Cornwell[94] has pointed out that since $\underline{\underline{\sigma}}^{d2}$ is well approximated by the second term on the right in (13), it follows that

$$(m_p/2m_e gB)\underline{\underline{C}} = \underline{\underline{\sigma}}^p + \underline{\underline{\sigma}}^{d2} = \underline{\underline{\sigma}} - \underline{\underline{\sigma}}^{d1}. \tag{15}$$

If one now makes the very reasonable assumptions that $\underline{\underline{\sigma}}^{d1}$ is isotropic and is equal to the shielding of a free atom [$\sigma^d(F^\circ) = 470.7$ ppm],[89] the following <u>tensor</u> equation for $\underline{\underline{C}}$ is obtained (specialized to fluorides):

$$\underline{\underline{C}} = (2m_e gB/m_P)(\underline{\underline{\sigma}} - 470.7 \times 10^{-6}). \tag{16}$$

The spin-rotation interaction constant is then given by

$$C = (1/3)\mathrm{Tr}\underline{\underline{C}} = (2m_e gB/m_P)(\sigma - 470.7 \times 10^{-6}). \tag{17}$$

If the z-axis is again chosen parallel to the F-I bond in IF_7 and IOF_5, it is consistent with the present development[94] to assume that

$$(\underline{\underline{\sigma}}^p + \underline{\underline{\sigma}}^{d2})_{zz} = 0, \tag{18}$$

from which it follows that

$$C_{zz} = 0;$$
$$C_{xx} = (3/2)C. \tag{19}$$

In Table XX, the values of σ, I_M, and C which were used in computing (11) are listed. The resulting contributions to $(1/T_1)_F$ are given in Table XIX, and the values of τ_{sr} appear in Table XXI where they are contrasted with τ_c.

TABLE XXI. Comparison of Calculated Relaxation Times with Experimental Relaxation Times[a]

	IF_7 at 29°C	IOF_5 at 29°C	9.8 m/o IOF_5-IF_5 at 29°C	9.8 m/o IOF_5-IF_5 at -15°C
$(1/T_2)_{F,exp}$ (sec^{-1})[b]	Not defined	2042 ± 100	471 ± 30	170 ± 20
$(1/T_1)_{F,exp}$ (sec^{-1})[c]	1.4 ± 0.4	2.7 ± 0.4	0.65 ± 0.10	≤0.59[d]
τ_c $(\times 10^{-12}$ sec)[e]	0.5	0.45	2.0	5.5
τ_{sr} $(\times 10^{-13}$ sec)	3.4	3.6	0.80	0.29
$(1/T_1)_{F,th}$ (sec^{-1})[f]	1.67	1.16	0.31	0.23
Dominant mechanism(s)	Spin-rotation	Spin-rotation	Spin-rotation	Spin-rotation, dipole-dipole

[a]For IOF_5 ν_B band only.
[b]Calculated from line widths, $1/T_2 = 2\pi\Delta\nu_F$.
[c]Obtained in saturation study; see Sect. VF.
[d]Estimated from results in Table XV.
[e]Also appears in Table XVIII.
[f]Sum of all contributions listed in Table XIX.

C. Conclusions and Interpretation of Narrowing in IOF_5

Results of the calculations discussed in Sect. VIB are summarized in Table XIX, which lists contributions to $(1/T_1)_F$ and indicates the corresponding contributions to $(1/T_2)_F$.

A comparison with the experimentally determined relaxation rates is presented in Table XXI. Insofar as the mechanisms considered are

independent and obey the equations of motion (4), the predicted relaxation rate is the simple sum of the contributions listed in Table XIX. This sum appears as $(1/T_1)_{F,th}$ in Table XXI; the mechanism(s) making the most significant contribution(s) is noted just below it.

Several conclusions can be drawn:

1) The assumption made in Sect. VIA that the rapid transverse fluorine relaxation rates in IF_7 and IOF_5 were due entirely to scalar spin-spin coupling with the ^{127}I nucleus is seen to be internally consistent, since all of the other mechanisms examined yield contributions which are insignificant (see Table XIX) compared to $(1/T_1)_{F,exp}$. Consequently, the correlation times obtained can be regarded with increased confidence.

2) For pure IF_7 and pure IOF_5 liquids at 29°C, the spin-rotation interaction mechanism is clearly the dominant source of longitudinal fluorine relaxation (see Table XIX), and the order of magnitude of $(1/T_1)_{F,exp}$ is accounted for by the theory employed (see Table XXI). This result adds IF_7 and IOF_5 to the growing number of fluorine-containing compounds for which it has recently been demonstrated that the spin-rotation interaction mechanism plays an important role in the fluorine relaxation.[64,85,90,91,94]

The fact that a single mechanism is predominant in the longitudinal fluorine relaxation of IF_7 and IOF_5 provides further justification for the assumption of first-order relaxation rates made during the treatment of the saturation data (see Sect. VF).

3) The narrowing of the IOF_5 lines observed in the other sample included in Tables XIX and XXI (9.8 m/o IOF_5 in IF_5) is to be associated with an increase in the correlation time τ_c for molecular reorientation as IOF_5 becomes more dilute in IOF_5, and as the temperature is lowered. Implied by this increase in τ_c is a decrease in the correlation time τ_{sr} describing the fluctuations associated with the spin-rotation interaction mechanism.

As a consequence of these changes, the spin-rotation interaction mechanism is less important in the mixture sample, and the dipole-dipole contributions are greater.

These theoretical results predict the same direction of change in $(1/T_1)_F$ with concentration and temperature as was observed for this sample (see Table XXI), although the values are in only fair agreement. The calculations underestimate $(1/T_1)_F$ in IOF_5 in general by a factor of about two. However, the results in no way weaken the assumption made in Sect. VF of overall first-order relaxation behavior.

4) Hence, the narrowing of IOF_5 lines which occurs in both IF_5 and BrF_5 solutions is related to less frequent molecular reorientation and more frequent changes in the angular momentum state. This suggests an interpretation in terms of rotation in the liquid, in which pure IF_7 and pure IOF_5 are viewed as being relatively free of barriers or hindrances to rotation, at least compared to solids and very viscous, less spherical, or highly polar liquids. Each uninterrupted period of rotation (probably about 1 rad on the average) changes the orientation coordinates, while collisions are effective in changing both the orientation and the angular momentum state; the situation is such that $\tau_c \cong \tau_{sr}$.

In mixtures with IF_5 and BrF_5, the IOF_5 is less free to rotate, and changes in the angular momentum are more frequent, so frequent, in fact, that the orientation is much less efficiently altered by rotations ($\tau_c \gg \tau_{sr}$).

Relaxation of IOF_5 in the liquid state thus seems amenable to a fairly straightforward characterization. It would, of course, be interesting to pursue the line width and the longitudinal relaxation rate over a range of temperatures, using more accurate measuring techniques (e.g., see Ref. 64). Among other things, a detailed temperature study of the dilute IOF_5 solutions might determine which mechanism was actually dominant (see Table XIX) and perhaps provide experimental evidence for the existence, not yet experimentally verified,[1,90] of the shielding-anisotropy interaction mechanism.

CHAPTER VII

SUMMARY

A. General

In most cases, the NMR data presented in Ch. V exhibit relatively small and gradual changes with solvent, concentration, and temperature. With a few exceptions, there is little indication of strong, specific interactions in these binary mixtures of inorganic fluorides.

As was also noted by Evans,[96] it was found here that changes in ^{19}F chemical shifts in mixtures generally exceeded bulk magnetic-susceptibility effects; however, no attempt was made to correct the data for these effects.

The observed variety in the magnitude, direction, and temperature dependence of the changes in chemical shifts, J_{FF} coupling constants, and especially line widths is very intriguing, but usually could not be readily understood in terms of events at the molecular level, a problem common to solvent-effect studies in general.

Rather than give a detailed listing of all the trends observed, many of which are best grasped by studying and comparing the figures in Ch. V, this chapter will be constructed around three topics which include the most interesting findings and which involve more than one mixture system. Tentative explanations are put forth, and suggestions for further work are made.

It is not inconceivable that explanations or at least acceptable arguments may eventually be found for many of the solvent effects observed in mixtures of diamagnetic inorganic fluorides. As a preliminary study, the present work has revealed a variety of effects and has illustrated the value of including measurements of longitudinal relaxation rates.

B. IOF_5 Solutions and Molecular Rotation

IOF_5 is a quasi-spherical molecule with a small dipole moment,[33] and its volatile liquid phase was found to form miscible solutions with solutes of varying degrees of polarity, ranging from WF_6 (nonpolar and octahedral) to IF_5 (pyramidal and polar). Miscibility with HF, which was observed here above room temperature (see Fig. 18b), becomes easier to understand when one remembers that HF is a highly polymerized liquid[9a] and probably is not as "polar" a medium as a monomeric HF liquid would be. There are limits, however; the solubility of IF_7 in HF, and vice versa, was observed to be very limited (see Table III).

As a solvent, IOF_5 produced only minor effects on the NMR spectra of the nonpolar solutes WF_6 and IF_7 (see Figs. 17a and 22a), and slightly

stronger effects on dilute BrF_5 and IF_5 (see Figs. 19b, 23b, 20b, 24b, and 25). Dilute solutions of HF in IOF_5 showed an interesting concentration dependence; both proton and fluorine were shifted towards the corresponding monomer HF resonances,[97] without appreciable broadening (see Figs. 27b and 28b, and text in Sect. VD).

On the other hand, dilute IOF_5 in these same mixtures showed almost no signs of interaction (see Fig. 16, and Tables IV and VIII) except for a striking effect on the IOF_5 line width in the two polar solvents IF_5 and BrF_5 (see Figs. 21b and 21c, and Table XII), which was stronger at lower temperatures and was also found to extend into solid mixtures (see Table XVII, Sect. VG).

Chapter VI has described how the IOF_5 (and IF_7) line-width data can be combined with the measured longitudinal relaxation rates (see Sect. VF) to show that this narrowing of IOF_5 lines in IF_5 and BrF_5 is associated with a relative decrease in the freedom of rotational motion in the liquid. Details of that argument will not be repeated here.

In an attempt to find the source of this hindering of molecular rotation, two models might be considered. The interaction may simply be due to ordinary dipole-dipole forces, or there may be a very weak, but dynamic, interaction between the oxygen on IOF_5 and the lone pair on the IF_5 or BrF_5 molecule.

The observation that the narrowing effect is relatively stronger in the IF_5 solution may be a point in favor of the second model, in which the greater symmetry of the IF_5-IOF_5 couple over BrF_5-IOF_5 might produce the difference in narrowing. Or the difference may be related to the fact that IF_5 is believed to be a more associated liquid than BrF_5.[98] Difficulties encountered in synthesizing BrF_7 could also be relevant. In any case, the nature of the intermolecular forces is weak and dynamic, fluctuating faster than 10^{12} sec^{-1}. It must be noted that a small shift of the IOF_5 equatorial fluorines (see Table IV) accompanies the narrowing in IF_5 and BrF_5 solution.

Initially, IF_7 was included in the current study in an attempt to find a narrowing effect on <u>its</u> spectrum. It is probably pertinent that none was detected and that IF_7 does not have an oxygen atom, nor a net dipole moment on the time scale of an NMR measurement.

The plausibility of these speculations could be tested by examining the NMR spectra of other pairs of molecules for analogous effects, including various combinations of lone pair donors, oxygen donors, polar and nonpolar molecules, and spherical and nonspherical geometries.

These insights into molecular motion in liquid IOF_5 and some of its solutions may also have value in analyses of solid-phase NMR spectra in the same systems. For example, the fact that pure IOF_5 has a minimum in its line width just below the melting point may indicate rotation in the solid (see Fig. 21a). Also, the line widths of IOF_5 and IF_5 in the IOF_5-IF_5 "solid solutions" examined in Sect. VG were each substantially less than in the pure solids at the same temperature (see Table XVII).

Again, the spectrum of solid IF_7 at -12°C consisted of a broad singlet, rather than the very broad doublet observed in the liquid phase (see Table XIII); in its high-temperature solid phase WF_6 should also be examined more carefully for onset of rotation.

It is clear that the current efforts constitute only a preliminary study of relaxation effects in binary mixtures of inorganic fluorides. Measurements should be extended into solid, liquid, dilute solution, and gas phases, using more accurate and sophisticated measuring techniques.[64]

C. Line Widths in Three AB_4 Spin Systems

It seems worth pointing out that the line widths of BrF_5, IF_5, and even IOF_5 indicate that further investigation of relaxation phenomena in these substances would be of considerable interest.

Each of the pure liquids exhibits a different width for axial and equatorial fluorines, as is summarized below in Table XXII. The variation in temperature dependence observed in pure and mixed samples is also reviewed in Table XXII. Except for the IOF_5 ν_A band, the line-width data appear in more detail in Figs. 21, 23, and 24, and in Tables VIII and X.

TABLE XXII. Line Widths in Three AB_4 Spin Systems

NMR of	$\Delta\nu_A:\Delta\nu_B$ (Room temp)	As T Decreases, Pure Liquid	As T Decreases, Fixed Solute Concentration
BrF_5	13:1	$\Delta\nu_A$ decreases $\Delta\nu_B$ increases	$\Delta\nu_A$ decreases $\Delta\nu_B$ ~ constant
IF_5	3.5:1	Both constant	Both decrease
IOF_5	0.85:1	Both ~ constant	Both decrease

Each of these molecules contains a central quadrupolar nucleus, so that the quadrupole relaxation is expected to contribute something to the transverse fluorine relaxation. Since in normal liquids the quadrupole coupling mechanism and the spin-rotation interaction mechanism both predict a

decrease in line width with decreasing temperature,[57,84] the observed temperature dependence (see Table XXII) alone cannot indicate which of these two mechanisms is the more important in BrF_5 and IF_5 line widths.

A detailed theoretical interpretation of line widths and longitudinal relaxation rates in terms of relaxation mechanisms is expected to be more difficult in general for BrF_5 and IF_5 than for IOF_5. Whereas the latter is very nearly a spherical top, BrF_5 and IF_5 are true symmetric tops in which the axial fluorine may well possess a different shielding tensor, J_{IS} coupling constant, and correlation time than do the equatorial fluorines.

Relaxation phenomena in these compounds should also be explored further in the solid state, especially for IF_5 in solid IOF_5-IF_5 mixtures (see Table XVII).

D. HF Spectra in Dilute Solution

HF was included in the present study because it was hoped that changes in the NMR spectrum of dilute HF would yield some information about the changes occurring in its polymeric liquid structure with progressive dilution in a given solvent. HF was studied in IOF_5 (a slightly polar solvent) and in BrF_5 (a polar solvent), with quite different results. (The HF-IF_7 mixtures prepared had such limited solubility ranges that almost no information was obtained for this system.)

Changes in the HF proton and fluorine chemical shifts and line widths in IOF_5 and BrF_5 solutions are shown in Figs. 17b, 18, and 22b. On the scales used in the figures, the gaseous HF-monomer proton resonance would occur at about -400 Hz and the ^{19}F resonance at about -1200 Hz (for 30°C).[97] Interestingly enough, at HF concentrations below about 25 m/o, the HF proton and fluorine lines in HF-IOF_5 solutions are shifted towards the monomer resonances without appreciable broadening, while the HF fluorine line in HF-BrF_5 solutions is shifted rapidly away from the monomer resonance and both HF lines are (apparently equally) broadened. There is also a change in the temperature coefficient of the latter line widths.

Before attempting to interpret these differences, the spectra of the IOF_5 and BrF_5 in these same solutions should be considered. Although changes in the IOF_5 spectrum are quite small over the entire concentration range (see Fig. 16 and Tables IV and VIII), the BrF_5 in concentrated HF solution (below about 25 m/o BrF_5) exhibits marked changes in the equatorial fluorine chemical shift, in the J_{FF} coupling constant, and probably in the axial fluorine line width (see Figs. 19, 23, and 25a, and Tables VII, X, and XI). It should be noted that effects on the BrF_5 spectrum in HF-BrF_5 mixtures are generally greater than in IOF_5-BrF_5 mixtures (see the same set of figures and tables), indicating that IOF_5 is a more inert solvent for BrF_5 than is HF.

From the NMR results presented here, it is surmised that intermolecular interactions in HF-IOF_5 solutions are of a relatively nonspecific nature, leading to a gradual breakdown of the original polymeric structure, whereas stronger and more specific interactions are in evidence at both ends of the concentration range in HF-BrF_5 solutions. There is no NMR evidence for rapid exchange of fluorines.

The HF-BrF_5 system has been the subject of a number of other investigations.[98,99] Previous NMR studies have also noted the absence of fluorine exchange, in distinct contrast to other mixtures of inorganic fluorides in HF (e.g., HF-IF_5).[16] Measurements of the conductivity of HF-BrF_5 solutions indicated limited ionization with a maximum in conductivity at 72 m/o HF.

It is consistent with all these results to propose that a limited degree of proton transfer occurs in HF-BrF_5 solutions according to the equation

$$BrF_5 + (HF)_{n+1} \rightleftharpoons HBrF_5^+ + (H_nF_{n+1})^-,$$

where the structure of the HF polymers is not specified. The structure of charged and uncharged polymers need not be the same.

It is clear that NMR studies can provide valuable information about interactions in HF solutions. In one limiting case, rapid exchange of fluorines can be detected (as in HF-IF_5 and HF-BrF_3 mixtures) and, in the other extreme, more subtle effects can be distinguished, ranging from little or no interaction (e.g., as in mixtures of HF and IF_7 or in solutions of HF and IOF_5) through simple dipole-dipole effects, to a significant degree of proton transfer.

APPENDIX I

Saturation Data

The following tables contain the average peak-height data obtained from the saturation measurements described in Sect. IVD. The rf field-strength values (H_1) were taken from the calibration described in Sect. IVE. The state of the sample during the recording of its NMR spectrum is noted as liquid (ℓ) or solid (s). Treatment of portions of these data to extract T_1 values is discussed in Sect. VF.

For IF_7 at 29°C, the maximum heights of both sides of the broad doublet were averaged to obtain the values listed in Table XXIII.

TABLE XXIII. Peak Height as a Function of RF Field Strength for Pure IF_7

T (°C) and State	Shape of Spectrum	H_1 (mG)	Average Peak[a] Height A (mm)
29 ± 1	Broad doublet	8.5 ± 0.5	35 ± 3
(ℓ)		4.76 ± 0.15	38 ± 2
		2.70 ± 0.20	29 ± 1
		1.58 ± 0.12	19.3 ± 0.5
-11 ± 2	Broad singlet	6.1 ± 0.5	44 ± 5
(s)		3.73 ± 0.25	53 ± 2
		2.70 ± 0.20	52 ± 5
		1.24 ± 0.12	37 ± 2
		0.92 ± 0.09	26 ± 1
		0.482 ± 0.025	15 ± 1
		0.278 ± 0.025	10 ± 1

[a]At constant (or standardized) signal amplification.

When the IOF_5 spectrum was resolved, the heights of both peaks in the ν_B band were measured; the first value reported in Table XXIV is for the more intense peak, which always occurs at the higher frequency (i.e., closer to the ν_A band).

The values reported for the ν_A bands of IOF_5 and IF_5 are for the center peak in the quintet. For unresolved IOF_5 ν_A bands, the observed average band maximum is tabulated.

TABLE XXIV. Peak Height as a Function of RF Field Strength for IOF_5 in Various Samples

Sample	T (°C) and State	H_1 (mG)	Average Peak Height A (mm)			
			IOF_5 (ν_B)		IOF_5 (ν_A)	IF_5 (ν_A)
Pure IOF_5	29 ± 1	4.76 ± 0.15	105 ± 3		57 ± 3	
	(ℓ)	3.73 ± 0.25	164 ± 3		48 ± 3	
		2.70 ± 0.20	172 ± 3		44 ± 2	
		2.03 ± 0.20	173 ± 4		39 ± 2	
		1.58 ± 0.12	146 ± 2		37 ± 2	
		1.24 ± 0.12	126 ± 2		34 ± 2	
		0.92 ± 0.09	95 ± 1		25 ± 1	
		0.482 ± 0.025	57 ± 1.5		15 ± 1	
		0.278 ± 0.025	32 ± 1		9.0 ± 0.5	
	-15 ± 2	1.58 ± 0.12	77 ± 1	73 ± 1	37 ± 2	
	(s)	0.92 ± 0.09	79 ± 1	73 ± 1	30 ± 2	
		0.482 ± 0.025	53 ± 1	46 ± 1	15 ± 1	
		0.404 ± 0.040	48 ± 1	42 ± 1	11 ± 1	
		0.278 ± 0.025	35 ± 1	30 ± 1	9.5 ± 1	
75.1% IOF_5 in IF_5	29 ± 1	4.76 ± 0.15	58 ± 2		32 ± 2	
	(ℓ)	2.70 ± 0.20	86 ± 1		34 ± 1	
		1.58 ± 0.12	90 ± 1		31 ± 1	
		1.24 ± 0.12	81 ± 1		23 ± 1	
		0.92 ± 0.09	68 ± 1		15 ± 1	
		0.482 ± 0.025	43 ± 1		10 ± 1	
		0.093 ± 0.008	9 ± 1		3 ± 1	
29.8% IOF_5 in BrF_5	29 ± 1	1.58 ± 0.12	92 ± 2		25 ± 2	
	(ℓ)	1.24 ± 0.12	86 ± 1		27 ± 2	
		0.92 ± 0.09	82 ± 2		23 ± 1	
		0.482 ± 0.025	59 ± 1	51 ± 1	17 ± 1	
		0.404 ± 0.040	50 ± 1	41 ± 1	9 ± 1	
		0.278 ± 0.025	36 ± 1	30 ± 1	7 ± 1	
57.7% IOF_5 in IF_5	29 ± 1	4.76 ± 0.15	45 ± 5		20 ± 3	
	(ℓ)	1.58 ± 0.12	84 ± 1	83 ± 1	25 ± 1	11 ± 1
		1.24 ± 0.12	85 ± 1	82 ± 1	23 ± 1	14 ± 1
		0.92 ± 0.09	80 ± 1	73 ± 1	19 ± 1	19 ± 1
		0.482 ± 0.025	61 ± 1	52 ± 1	15 ± 1	28 ± 1
		0.278 ± 0.025	36 ± 1	30 ± 1	10 ± 1	29 ± 1
	-12 ± 2	0.482 ± 0.025	70 ± 3	58 ± 4		26 ± 5
	(s)	0.404 ± 0.040	60 ± 1	46 ± 2		32 ± 1
		0.278 ± 0.025	48 ± 2	37 ± 2		34 ± 3
37.8% IOF_5 in IF_5	29 ± 1	1.58 ± 0.12	117 ± 3	107 ± 3	35 ± 5	
	(ℓ)	0.92 ± 0.09	125 ± 2	105 ± 2	31 ± 3	65 ± 2
		0.64 ± 0.05	118 ± 2	98 ± 2	30 ± 2	68 ± 3
		0.482 ± 0.025	102 ± 1	80 ± 1	25 ± 2	90 ± 3
		0.404 ± 0.040	90 ± 1	73 ± 1	21 ± 1	97 ± 2
	-10 ± 2	0.92 ± 0.09	55 ± 5	52 ± 5		37 ± 4
	(ℓ)	0.482 ± 0.025	66 ± 2	59 ± 2		70 ± 10
		0.404 ± 0.040	68 ± 2	53 ± 2		84 ± 5
		0.278 ± 0.025	56 ± 2	43 ± 2		84 ± 5
		0.162 ± 0.013	34 ± 1	25 ± 1		64 ± 3
		0.136 ± 0.014	29 ± 1	21 ± 1		56 ± 3
9.8% IOF_5 in IF_5	29 ± 1	1.58 ± 0.12	63 ± 1	59 ± 1	19 ± 2	118 ± 3
	(ℓ)	1.24 ± 0.12	72 ± 1	67 ± 1	19 ± 2	142 ± 5
		0.92 ± 0.09	74 ± 1	66 ± 1	16 ± 1	190 ± 5
		0.482 ± 0.025	75 ± 1	62 ± 1	15 ± 1	
		0.278 ± 0.025	56 ± 1	40 ± 1	9 ± 1	
		0.162 ± 0.013	32 ± 1	24 ± 1	5 ± 1	
		0.92 ± 0.09	49 ± 4	43 ± 4		41 ± 5
		0.482 ± 0.025	49 ± 5	43 ± 5		47 ± 5
		0.404 ± 0.040	47 ± 3	37 ± 2		56 ± 5
		0.278 ± 0.025	39 ± 2	32 ± 2		58 ± 3
		0.162 ± 0.013	26 ± 1	20 ± 2		40 ± 2

APPENDIX II

Nuclear Properties

TABLE XXV. Some Useful Nuclear Properties

Description[a,b]		^{127}I	^{19}F
Spin	I or S	5/2	1/2
Magnetic moment, nuclear magnetons	μ/μ_0	2.7939	2.62728
Magnetic moment, erg gauss^{-1}	$\mu = \mu_0 gI$	14.110×10^{-24}	13.269×10^{-24}
Gyromagnetic ratio, rad sec^{-1} gauss^{-1}	$\gamma = \mu/\hbar I$	5.354×10^3	25.176×10^3
Larmor frequency in a standard 14.7-kgauss field, rad sec^{-1}	$\omega = \gamma H_0$	75.45×10^6	354.75×10^6
Larmor frequency, Hz	$\nu = \omega/2\pi$	12.008×10^6	56.46×10^6

[a]The values listed are either taken from or derived from values given in Ref. 29, p. 480.

[b]Reference 35 contains very clear definitions of these properties and their relationships to one another.

ACKNOWLEDGMENTS

I wish to thank Dr. C. Daniel Cornwell for constant and patient support of this endeavor, for numerous enlightening discussions, and for several astute suggestions which proved vital to the completion of the thesis.

I am also very grateful for the direction and assistance of Dr. Herbert H. Hyman of Argonne National Laboratory, particularly during the experimental phases of this work.

My introduction to fluorine chemistry at ANL was greatly facilitated by generous contributions of time and interest from many people in the Chemistry Division. I wish particularly to mention Irving Sheft and Lloyd Quarterman, who were on hand in the early stages, and also Dr. H. D. Frame and Dr. Felix Schreiner, who gave valuable assistance later on. The very excellent services of the Chemistry Division Shop, the Instrument Shop, and other technical offices are acknowledged with pleasure.

I am indebted to Dr. J. J. Katz for patience and concern during the use of equipment in his NMR laboratory at ANL.

At The University of Wisconsin, special thanks are due my colleagues Terry Scheffer and Charles Dickinson, whose cooperation greatly expedited the measurements made there.

At times, this work has enjoyed the support of the Wisconsin Alumni Research Foundation, the National Science Foundation, and the E. I. Du Pont de Nemours and Co., Inc. An AEC fellowship at Argonne National Laboratory, administered by Associated Midwest Universities, Inc., is very much appreciated.

REFERENCES

1. P. Laszlo, also H. G. Hertz, in *Progress in Magnetic Resonance Spectroscopy*, Vol. III, J. W. Emsley, J. Feeney, and L. H. Sutcliffe, eds., Pergamon Press, London, 1967.
2. J. W. Emsley, J. Feeney, and L. H. Sutcliffe, *High Resolution Nuclear Magnetic Resonance Spectroscopy*, Vol. I and II, Pergamon Press, London, 1965.
3. R. J. Gillespie and J. W. Quail, Proc. Chem. Soc. (London) *278* (1963).
4. L. G. Alexakos, C. D. Cornwell, and S. B. Pierce, Proc. Chem. Soc. (London) *341* (1963).
5. N. Bartlett and L. E. Levchuk, Proc. Chem. Soc. (London) *342* (1963).
6. N. Bartlett, S. Beaton, L. W. Reeves, and E. J. Wells, Can. J. Chem. *42*, 2531 (1964).
7. I. Sheft and D. J. Lind, Rev. Sci. Inst. *37*, 1272 (1966).
8. I. Sheft, Rev. Sci. Inst. *37*, 767 (1966).
9. a) H. H. Hyman and J. J. Katz in *Nonaqueous Solvent Systems*, T. C. Waddington, ed., Academic Press, New York, 1965.

   b) J. H. Canterford and T. A. O'Donnell, "Manipulation of Volatile Fluorides and Other Corrosive Compounds," in *Technique of Inorganic Chemistry*, Vol. VII, H. B. Jonassen and A. Weissberger, eds., Interscience Publishers, New York, 1968.
10. Much of the equipment used for fluorine chemistry at ANL was developed in the Chemistry Division Shop, currently under the direction of E. Klocek. The late John Pickhardt contributed many of the early Kel-F designs; more recent developments have involved several of the Chem. Div. staff members, including I. Sheft and L. Quarterman. The assistance of the Plastics Shop, under G. Lobell, was also important.
11. H. D. Frame, private communication.
12. Currently, the purity of liquid HF is being assessed at ANL by two criteria: a specific conductivity of about 10^{-6} mho (Ref. 9a), and the absence of fluorescence in the Raman spectrum.
13. G. M. Begun, W. H. Fletcher, and D. F. Smith, J. Chem. Phys. *42*, 2236 (1965).
14. T. G. Burke, D. F. Smith, and A. H. Nielsen, J. Chem. Phys. *20*, 447 (1951).
15. J. Gaunt, Trans. Far. Soc. *49*, 1122 (1953).
16. L. Stein, *Physical and Chemical Properties of Halogen Fluorides*, Vol. I of *Halogen Chemistry*, V. Gutmann, ed., Academic Press, New York, 1967.
17. This method was also chosen by H. Selig, C. W. Williams, and G. J. Moody, J. Phys. Chem. *71*, 2739 (1967).
18. For a list of IF_7 IR band frequencies, see Ref. 5.
19. A good example of the IF_7 IR spectrum was provided by H. H. Claassen of ANL.

20. S. P. Beaton, Thesis, University of British Columbia, 1966.

21. D. F. Smith and G. M. Begun, J. Chem. Phys. *43*, 2001 (1965).

22. For IR spectrum of SiF_4, see J. Heicklen and V. Knight, Spectrochim. Acta *20*, 295 (1964).

23. See Ref. 17.

24. M. T. Rogers, J. L. Speirs, H. B. Thompson, and M. B. Panish, J. Am. Chem. Soc. *76*, 4843 (1954).

25. G. H. Cady and G. B. Hargreaves, J. Chem. Soc. (London) *1563* (1961).

26. A detailed description will appear in the Ph.D. Thesis of T. J. Scheffer, The University of Wisconsin.

27. A brief description appears in D. K. Hindermann and C. D. Cornwell, J. Chem. Phys. *48*, 2017 (1968).

28. N. Bloembergen, E. M. Purcell, and R. V. Pound, Phys. Rev. *73*, 679 (1948).

29. See also J. A. Pople, W. G. Schneider, and H. J. Bernstein, *High Resolution Nuclear Magnetic Resonance*, McGraw-Hill Book Co., Inc., New York, 1959, p. 82.

30. W. A. Anderson, Phys. Rev. *102*, 151 (1956).

31. D. K. Hindermann, Thesis, The University of Wisconsin, 1967.

32. L. C. Dickinson, U.W., private communication.

33. S. B. Pierce and C. D. Cornwell, J. Chem. Phys. *47*, 1731 (1967).

34. H. M. McConnell, A. D. McLean, and C. A. Reilly, J. Chem. Phys. *23*, 1152 (1955).

35. P. L. Corio, *Structure of High Resolution NMR Spectra*, Academic Press, New York, 1967, p. 224.

36. See Ref. 2, p. 339.

37. S. B. Pierce, Thesis, The University of Wisconsin, 1967.

38. For shape function, see Ref. 29, p. 37, among others.

39. L. G. Alexakos and C. D. Cornwell, J. Chem. Phys. *41*, 2098 (1964).

40. D. K. Hindermann and C. D. Cornwell, J. Chem. Phys. *48*, 4148 (1968).

41. See Ref. 4 and Ref. 6, Fig. 3.

42. E. L. Muetterties and K. J. Packer, J. Am. Chem. Soc. *86*, 293 (1964).

43. R. Field and H. H. Hyman, ANL, private communication.

44. R. Field, H. D. Frame, and H. H. Hyman, ANL, private communication.

45. E. J. Barber and G. H. Cady, J. Phys. Chem. *60*, 505 (1956).

46. A value of J_{FF} = 280 cps (no uncertainty was given) was reported in Ref. 6.

47. C. P. Slichter, *Principles of Magnetic Resonance*, Harper and Row, New York, 1963.

48. A. Abragam, *The Principles of Nuclear Magnetism*, Oxford University Press, London, 1961, pp. 41 ff.

49. Ref. 47, p. 31.

50. Ref. 29, p. 38.

51. Ref. 47, pp. 40-42.

52. Ref. 29, p. 36.

53. Ref. 47, pp. 5-8.

54. Ref. 48, p. 28.

55. Ref. 47, pp. 115-121.

56. Ref. 28, Eq. (15).

57. J. A. Pople, Mol. Phys. *1*, 168 (1958).

58. R. J. Gillespie and J. W. Quail, Can. J. Chem. *42*, 2671 (1964).

59. Ref. 48, pp. 306-312.

60. In Ref. 2, compare the spin-product functions (see Table 8.18) with the eigenfunctions formed from them (see Table 8.19) for the case of large Q's.

61. P. S. Hubbard, Phys. Rev. *109*, 1153 (1958).

62. Ref. 48, pp. 293-294.

63. G. B. Matson, Thesis, The University of Wisconsin, 1967.

64. This approach is well-illustrated by J. H. Chaffin III and P. S. Hubbard, J. Chem. Phys. *46*, 1511 (1967).

65. Partial crystallographic results have been obtained by R. D. Burbank and F. N. Bensey, Jr., J. Chem. Phys. *27*, 982 (1957).

66. M. T. Rogers, J. L. Speirs, M. B. Panish, and H. B. Thompson, J. Am. Chem. Soc. *78*, 936 (1956).

67. R. Blinc, E. Pirkmajer, J. Slivnik, and I. Zupancic, J. Chem. Phys. *45*, 1488 (1966).

68. D. W. Osborne, F. Schreiner, and H. Selig, *Abstracts of the 155th National Meeting of the Am. Chem. Soc.*, San Francisco, Calif., April 1968.

69. M. Suzuki and R. Kubo, Mol. Phys. *7*, 201 (1963).

70. Ref. 48, pp. 313-315.

71. a) D. E. O'Reilly and G. E. Schacher, J. Chem. Phys. *39*, 1768 (1963).

    b) W. B. Moniz and H. S. Gutowsky, J. Chem. Phys. *38*, 1155 (1963).

    c) D. E. Woessner, J. Chem. Phys. *40*, 2341 (1964).

    d) R. L. Vold and H. S. Gutowsky, J. Chem. Phys. *47*, 4782 (1967).

72. Ref. 48, Ch. VIII, Sect. II.

73. A. G. Redfield, IBM J. Res. Develop. *1*, 19 (1957).

74. R. K. Wangsness and F. Bloch, Phys. Rev. *89*, 728 (1953).

75. F. Bloch, Phys. Rev. *102*, 104 (1956).

76. Slichter provides an excellent introduction to the theory in Ref. 47, Sect. 5.4-5.8.

77. A. G. Redfield in *Advances in Magnetic Resonance*, Vol. I, J. S. Waugh, ed., Academic Press, New York, 1965.

78. J. M. Deutch and I. Oppenheim in Ref. 77, Vol. III, 1968.

79. Ref. 47, pp. 143, 150, 152.

80. Ref. 48, pp. 290-291.

81. For a clear example of this sequence of steps, see Ref. 48, pp. 298-300.

82. R. D. Burbank and F. N. Bensey, J. Chem. Phys. *27*, 981 (1957).

83. Ref. 48, p. 302.

84. P. S. Hubbard, Phys. Rev. *131*, 1155 (1963).

85. P. Rigny and J. Virlet, J. Chem. Phys. *47*, 4645 (1967).

86. Ref. 64, and references therein.

87. Ref. 48, pp. 294-297.

88. Ref. 48, pp. 315-316.

89. G. Malli and S. Fraga, Theoretical Chemica Acta (Berlin) *5*, 275 (1966).

90. R. J. C. Brown, H. S. Gutowsky, and K. Shimomura, J. Chem. Phys. *38*, 76 (1963).

91. D. K. Green and J. G. Powles, Proc. Phys. Soc. (London) *85*, 87 (1965).

92. W. H. Flygare, J. Chem. Phys. *41*, 793 (1964).

93. S. I. Chan, M. R. Baker, and N. F. Ramsey, Phys. Rev. *136*, A1224 (1964).

94. C. D. Cornwell, private communication.

95. H. S. Gutowsky, I. J. Lawrenson, and K. Shimomura, Phys. Rev. Letters *6*, 349 (1961).

96. D. F. Evans, J. Chem. Soc. *877* (1960).

97. HF monomer shifts (gas, P = 0) are given in Ref. 27.

98. M. T. Rogers, AECU-4720.

99. See Ref. 16, pp. 170, 173-174, and references therein.

ARGONNE NATIONAL LAB WEST
3 4444 00008197 6
ARGONNE NATIONAL LAB WEST
3 4444 00008197 6
ARGONNE NATIONAL LAB WEST
3 4444 00008197 6
ARGONNE NATIONAL LAB WEST
3 4444 00008197 6
ARGONNE NATIONAL LAB WEST
3 4444 00008197 6
ARGONNE NATIONAL LAB WEST
3 4444 00008197 6
ARGONNE NATIONAL LAB WEST
3 4444 00008197 6
ARGONNE NATIONAL LAB WEST
3 4444 00008197 6
ARGONNE NATIONAL LAB WEST
3 4444 00008197 6
ARGONNE NATIONAL LAB WEST
3 4444 00008197 6
ARGONNE NATIONAL LAB WEST
ARGONNE NATIONAL LAB WEST